Diverse Actions of Synaptotagmin Isoforms in Neuronal Physiology and Development

By

David A. Ruhl

A dissertation submitted in partial fulfillment of the requirements for the degree

Doctor of Philosophy

(Neuroscience)

at the

UNIVERSITY OF WISCONSIN-MADISON

2018

Date of final oral examination: 12/12/2017

This dissertation has been submitted for approval by the following members of the Final Oral Committee:

Edwin R. Chapman, Neuroscience
Meyer B. Jackson, Neuroscience
Anjon Audhya, Biomolecular Chemistry
Robert Fettiplace, Neuroscience
Xin Huang, Neuroscience
Vaishali Bakshi, Psychology

Acknowledgements

First, I must acknowledge my dissertation advisor and scientific mentor, Dr. Edwin Chapman. I consciously sought a doctoral advisor who would be strict and hold my feet to the fire. Dr. Chapman certainly fit that bill, and in my time in his lab I learned more from him than he will ever know. Next, I must acknowledge my collaborators and fellow travelers in the Chapman lab, without whom much of this work would not have been possible. Dr. Chantell Evans performed the biochemistry experiments in Chapter 2 and Figure 13 of Chapter 3 of this dissertation. With Dr. Evans and Dr. Chapman, I wrote Evans, Ruhl[1], and Chapman (2015), portions of which (in modified form) comprise Chapter 2 of this dissertation. Dr. Ewa Bomba-Warzak made the initial anecdotal observation that overexpressing syt-17 may alter neuronal morphology, and contributed data to Figures 17, 18, and 28. The RT-PCR in Figure 15 was performed by Lindsay Schneider in Alan Attie's laboratory. All members of the Chapman lab provided invaluable advice during the course of these projects, Dr. Joseph Briguglio in particular. While many members (current and former) of this laboratory and others provided training in particular methodologies at one point or another, I wish to single out Dr. Renhao Xue, Dr. Joel Britten, Dr. Jon Gaffaney, Dr. Ewa Bomba-Warzak, Dr. Lindsey Roper, Annette Figueroa-Bernier, Sarah Brodnick, and Mark Perkins for their technical assistance early in my graduate career.

One of the projects in this dissertation, on the mechanism of syt-1 function, is squarely within the Chapman lab's traditional area of expertise, and I was fortunate to work under the world's expert on this topic. The other project, however, on syt-17, was

[1] Co-first authors

more of an intellectual journey. Unexpected and unusual (for a synaptotagmin) phenotypes pushed me in directions outside the traditional purview of the lab, both methodologically and in terms of biological subject matter. As I left this familiar territory, I benefitted enormously from the critical input of other faculty and students in the department, in particular Dr. Anjon Audhya. Invaluable advice and outside perspectives were provided by my dissertation committee: Dr. Audhya, Dr. Meyer Jackson, Dr. Robert Fettiplace, Dr. Vaishali Bakshi, and Dr. Xin Huang.

On a personal level, I am most grateful to my parents, Thomas and Carolyn Ruhl. The support I received from them growing up is what led me to believe that spending a life pursuing intellectual curiosities was a noble – and viable – path.

Finally, I must acknowledge the funding sources that made my graduate work possible. I was fortunate to obtain a National Science Foundation Graduate Research Fellowship (DGE-1256259) that funded much of my time in graduate school. Additional funding and merit fellowships from the Neuroscience Training Program at the University of Wisconsin-Madison (Grant: T32-GM007507) funded most of the remainder of my graduate education. Within the lab, my work itself was supported by Dr. Chapman's NIH Grant MH061876, and the Howard Hughes Medical Institute.

Table of Contents

Abstract…….....1

Chapter 1: General background and significance

1.1 Synaptic Transmission and the Synaptic Vesicle Cycle in Neurons……..2

1.2 Synaptotagmin 1 – A Ca^{2+} Sensor for Neurotransmitter Release……..4

1.3 Synaptotagmin Isoforms in Neurons……...5

1.4 Figures……...14

Chapter 2: An Engineered Metal Sensor Tunes the Kinetics of Synaptic Transmission

2.1 Introduction……...16

2.2 Materials and Methods……17

2.3 Results……...25

2.4 Discussion……31

2.5 Figures……...34

Chapter 3: Synaptotagmin 17 Controls Neuronal Development and Physiology Through Multiple Cellular Pathways

3.1 Introduction……...44

3.2 Materials and Methods……49

3.3 Results……...57

3.4 Discussion……67

3.5 Figures……...69

Chapter 4: Perspectives & Future Directions……85

References……..90

Abbreviations

AMPA - α-amino-3-hydroxy-5-methyl-4-isoxazolepropionic acid

AMPAR – AMPA-sensitive glutamate receptor

APV - D-(-)-2-Amino-5-phosphonopentanoic acid (NMDA-receptor antagonist)

BDNF – brain-derived neurotrophic factor

C2AB – cytosolic domain of a syt isoform, containing C2A and C2B domains

Ca^{2+} - calcium

CNQX - 6-Cyano-7-nitroquinoxaline-2,3-dione (AMPAR antagonist)

DIV – days *in vitro*

EPSC – excitatory postsynaptic current

ER – endoplasmic reticulum

GluR – AMPA-type glutamate receptor subunit

KO – knockout

mEPSC – miniature EPSC, the response to the release of a single quantum

PKA – protein kinase A

Rab – Ras-related protein in brain

RRP – Readily-releasable pool of synaptic vesicles

shRNA – short hairpin RNA

siRNA – short interfering RNA

SNAP-25 – Synaptosomal-associated protein 25

SNARE – soluble N-ethyl maleimide-sensitive factor attachment protein receptor

Sr^{2+} - strontium

SV – synaptic vesicle

SYT – synaptotagmin

t-SNARE – target membrane SNARE

TTX – tetrodotoxin

v-SNARE – vesicular SNARE protein

VAMP – vesicle-associated membrane protein

WT – wildtype

Abstract:

The synaptotagmins (syts) are a family of proteins most known for playing a role in the release of neurotransmitters or hormones in neural and neuroendocrine cells. In my graduate work, I have characterized the biophysical role of synaptotagmin 1 (syt-1) in determining the timecourse of glutamate release in hippocampal neurons, and assigned the first functions to a largely-unstudied isoform, synaptotagmin 17 (syt-17). In the first part of my presentation, I show that the intrinsic kinetics of syt-1's interactions with membranes controls the kinetics of excitatory neurotransmission, using a "chimeric" presynaptic Ca^{2+} sensor containing structural elements of syt-1 (the fastest syt isoform) and synaptotagmin 7 (the slowest syt isoform). Further, this chimera displayed the novel property of being activated in response to Sr^{2+}, a cation not present in cells. I exploit this property to show that membrane penetration by syt-1 is a key step in exocytosis.

In the second part of my presentation, I characterize the first knockout of syt-17, a biochemically-unusual syt isoform of no known function. I find that syt-17 is expressed in the golgi of central neurons, where it mediates secretory trafficking. Impairment of protein synthesis/processing in syt-17 knockouts is associated with a severe impairment in neurite outgrowth, leading to morphological abnormalities in mature neurons. I also find that a second pool of syt-17 is present on rab5-positive early endosomes in neurites. Loss of syt17 leads to pathological accumulation of excess AMPA receptors in the plasma membrane of dendrites, resulting in a substantial increase in excitatory neurotransmission. Syt-17 thus controls neuronal development and postsynaptic glutamate receptor trafficking through multiple cellular pathways.

Chapter 1: General Background and Significance

1.1 Synaptic Transmission and the Synaptic Vesicle Cycle in Neurons

Most interneuronal communication takes the form of synaptic transmission, in which chemical neurotransmitters released from one neuron (the presynaptic neuron) are detected by receptors on the surface of another (the postsynaptic neuron). When an action potential is fired in the presynaptic neuron and propagated down an axon, the depolarization of the plasma membrane in synaptic boutons triggers influx of Ca^{2+} ions through voltage-gated Ca^{2+} channels. This Ca^{2+} spike serves as the signal to trigger release of neurotransmitter. Neurotransmitter molecules are packages into small (~40nm) vesicles (synaptic vesicles, SVs) that cluster in presynaptic boutons near the plasma membrane. Upon Ca^{2+} influx, a subset of these SVs fuse with the plasma membrane (a process known as *exocytosis*). The subset of SVs that are able to undergo exocytosis are referred to as the *Readily-Releasable Pool* of synaptic vesicles (RRP; Rosenmund & Stevens, 1996). This RRP consists of vesicles that are *docked* at the plasma membrane and have undergone *priming*, an additional pre-exocytosis preparatory step whose mechanism is only partially understood; (Kaeser & Regehr, 2014). Immediately after (or, as the final step of) exocytosis, the SVs neurotransmitter cargo (a *quantum*) is released into the extracellular space, where it diffuses across the synaptic cleft (the ~40nm space between presynaptic boutons and postsynapses) and activates receptors on the postsynaptic membrane. The SVs, are subsequently retrieved from the plasma membrane (i.e., endocytosed), and recycled for subsequent reuse. The SV cycle is diagrammed in Figure 1A.

Fusion of synaptic vesicles with the plasma membrane is mediated by the SNARE (soluble N-ethyl maleimide-sensitive factor attachment protein receptor) proteins: VAMP-2 on the vesicle membrane (a v-SNARE), syntaxin-1 and SNAP-25 on the plasma membrane (t-SNARES; Chen & Scheller, 2001). "Zippering" of the α-helical cytosolic domains of SNARE proteins into a single, tightly-wound SNARE complex, is thought to bring the vesicle membrane in close apposition to the plasma membrane, thus lowering the energy barrier to membrane fusion (Jackson & Chapman, 2006).

SV exocytosis can conceptually be divided into three modes: evoked synchronous release, evoked asynchronous release, and spontaneous quantal release. These modes are illustrated in Figure 1B. Synchronous and asynchronous release are "evoked" in the sense that they occur subsequent to an action potential, whereas spontaneous quantal release (a.k.a. "miniature" release) is the release of a single synaptic vesicle in the absence of an action potential. Additionally, synchronous and asynchronous release involve the release of multiple quanta within a specified time window. Synchronously-released quanta fuse very quickly following the opening of Ca^{2+} channels (tens of milliseconds, in excitatory hippocampal neurons), approximately following the timecourse of the presynaptic Ca^{2+} current (Kaeser & Regehr, 2014). Asynchronously-released quanta fuse within a substantially wider time window (generally hundreds of milliseconds, depending on the synapse) and is regulated by molecular mechanisms distinct from synchronous release (ex., Yao et al., 2012).

1.2 Synaptotagmin 1 – A Ca^{2+} Sensor for Neurotransmitter Release

In neurons, the exocytosis of synaptic vesicles with the plasma membrane is tightly-coupled to Ca^{2+} levels in the presynapse – some factor must serve as a Ca^{2+} sensor to catalyze fusion. Synaptotagmin-1 (syt-1, originally dubbed P65, Matthew et al., 1981; Perin et al., 1990) has been identified as the major Ca^{2+} sensor triggering synchronous SV release in most central neuron synapses (reviewed in Chapman, 2008). Syt-1 is a SV protein consisting of a transmembrane domain and two C2 domains, denoted C2A (the domain more proximal to the vesicle) and C2B, which are joined by a flexible linker (Figure 2A). Knockout of syt-1 selectively eliminates the synchronous phase of synaptic transmission, while leaving asynchronous release intact (DiAntonio and Schwarz, 1994; Geppert et al., 1994; Littleton et al., 1994; Mackler et al., 2002; Nishiki and Augustine, 2004). Importantly, the effect of syt-1 KO on synchronous release has been shown to be due to intrinsic changes in the release machinery. Burgalossi et al. (2010) loaded cultured hippocampal neurons with "caged" Ca^{2+}. A brief flash of UV light liberated the Ca^{2+} within nerve terminals, bypassing Ca^{2+} channels and stimulating the release machinery directly. The authors found that the Ca^{2+} dependence of exocytosis was significantly reduced in neurons lacking syt-1, providing possibly the most convincing evidence to date that syt-1 serves as a Ca^{2+} sensor for exocytosis in neurons.

Syt-1, along with the SNARE proteins VAMP2, SNAP-25, and syntaxin-1, can be thought of as a single "fusion machine" mediating exocytosis of SVs with the plasma membrane. A number of important mechanistic insights have been gleaned from reconstituting this fusion machine into liposomes. Using this purely reconstituted

approach (described and diagrammed in detail in Chapter 2 of this dissertation), our laboratory has established that Ca^{2+}*syt-1 accelerates the rate of SNARE-catalyzed fusion *in vitro* (Tucker et al., 2004) and that syt-1 must "fold" the soluble domain of SNAP-25 onto that of syntaxin-1 in order to trigger fusion (Bhalla et al., 2006). Despite considerable progress, the precise mechanism by which syt-1 triggers fusion of SVs with the plasma membrane remains elusive.

1.3 The Synaptotagmin Family in Neurons

The synaptotgmin protein family consists of seventeen isoforms, 1-17. Each possess two C2 domains separated by a short linker, and all except syt-17 (the subject of the second part of this dissertation) include a transmembrane domain (Figure 2B). The isoforms capable of triggering *in vitro* membrane fusion (Bhalla et al., 2008) exhibit a wide range of Ca^{2+} binding affinities (Bhalla et al., 2005) and membrane binding kinetics (Hui et al., 2005). Here I review the known and proposed functions of synaptotagmin isoforms, focusing (a) on loss-of-function studies or those that characterized endogenous function of the protein, (b) on functions in neurons (syt function in mast cells, spermatozoa, pituitary cells, etc are not considered), and (c) on the relevance of these isoforms for synchronous neurotransmitter release (if applicable).

The prototypical and best studied synaptotagmin is syt-1, whose role as a Ca^{2+} sensor for synchronous neurotransmitter release is discussed in the preceding section. However, syt-1 plays multiple roles in nerve terminals apart from its role as the synchronous Ca^{2+} sensor. It has been observed that neurons lacking syt-1, while deficient in evoked neurotransmitter release, nonetheless exhibit a substantial increase

in spontaneous miniature release (Chika et al., 2008; Liu et al., 2009). This led to the suggestion that syt-1 serves as a "clamp" of spontaneous release (Chika et al., 2008). Our laboratory (Liu et al., 2014; Bai et al., 2016) has generated mutant syt-1 variants that are able to rescue this clamping function (i.e., restore the normally-low rate of miniature release in syt-1 KO neurons) without rescuing evoked release, and conversely mutants that rescue evoked release without affecting the clamping defect (i.e., neurons expressing this mutant exhibit the synchronous release characteristic of wildtype neurons, but the elevated miniature release frequency characteristic of syt-1 KO neurons), demonstrating that the role of syt-1 in these processes can be dissociated. Specifically, the flexible linker between C2A and C2B of syt-1 was replaced with a proline rod, and since proline residues form such rods with known periodicity, it was possible to systematically control the relative orientation of the C2A and C2B domains (Bai et al., 2016). Holding the two C2 domains parallel permitted robust synchronous neurotransmitter release, but disrupted the clamping function, whereas affixing the two C2 domains in a staggered orientation restored the clamping function of syt-1 but failed to rescue evoked release. Different states of syt-1 (based on the relative orientation of the two C2 domains) thus control two modes of exocytosis (synchronous and spontaneous). Syt-1 has also been established to regulate the size of the readily-releasable pool of vesicles (RRP). Syt-1 knockout neurons exhibit a dramatic reduction (by 50% or more) of both the total number of SVs, and the fraction that are able to fuse with the plasma membrane in response to Ca^{2+} influx (Liu et al., 2009; Bai et al., 2016). The mechanism by which syt-1 maintains the neuronal RRP is murkier than is the case for exocytosis – to my knowledge no mutant has been identified which can dissociate

syt-1's role in RRP maintenance from other functions in the presynapse – but I will note that in other systems syt-1 has been shown to play a role in docking/priming of vesicles for release (Mohrmann et al., 2010; Lai et al., 2015). Additionally, multiple laboratories have identified a role for syt-1 in the endocytosis of synaptic vesicles (Poskanzer et al., 2003; Yao et al., 2011). Syt-1 has thus be implicated in virtually every step in the synaptic vesicle cycle: maintaining the RRP, docking/priming (in chromaffin cells), spontaneous release, action potential-evoked release, and SV endocytosis. Unsurprisingly, this functional promiscuity of syt-1, has complicated efforts to precisely define the molecular mechanisms of syt-1 action.

Syt-2 appears to serve a similar role as syt-1 – serving as a Ca^{2+} sensor for synchronous neurotransmitter release – but does so in a separate set of synapses. Syt-2 serves as the synchronous release sensor at the calyx of Held (Pang et al., 2006), cerebellar basket cell to Purkinje cell synapses (Chen et al., 2017a), and potentially other central synapses. It has been noticed that syt-2 is highly-expressed in Parvalbumin-positive GABAergic neurons (Sommeijer & Levelt, 2012), where it is proposed to mediate some synaptic release (Bouhours et al., 2017). Interestingly, while syt-1 has faster kinetics *in vitro*, syt-2 appears to mediate release with faster kinetics in cells, at least at some synapses. In a purely reconstituted system in which the dissociation kinetics of syt isoforms from Ca^{2+} & liposomes was monitored upon injection of a Ca^{2+} chelator, syt-1 exhibited the fastest kinetics of all isoforms (Hui et al., 2005). Syt-1 also mediates vesicle fusion with faster kinetics than syt-2 in chromaffin cells (Nagy et al., 2006). However, in a recent study in which either syt-1 or syt-2 were used to rescue fast release at the cerebellar basket cell to Purkinje cell synapses of syt-

2 knockout mice, EPSCs mediated by syt-2 exhibited faster decay kinetics than EPSCs mediated by syt-1 (Chen et al, 2017a). Further, when exogenously expressed in syt-1 knockout cultured cortical neurons, syt-2 supports EPSCs with faster kinetics than syt-1 (Xu et al., 2007). The relative speed of syt action is thus context-dependent, with syt1 or syt2 seemingly “optimized” to mediate fast release in particular synapses. The relative importance of membrane lipid composition versus SNARE composition for this synapse/syt specificity is unknown. Further, whether syt-2 can mediate some of the non-exocytic functions of syt-1 (RRP maintainance, SV endocytosis, etc.) is also largely unknown.

Syt-4 is localized to BDNF-harboring vesicles in hippocampal neurons, where it regulates exocytosis of these granules in both axons and dendrites (Dean et al., 2009) work. Syt-4 acts to repress BDNF release (pre- and postsynaptically), and knockout of syt-4 results in increased synaptic strength and long-term potentiation (LTP, the persistent increase in synaptic strength following specific amounts or patterns of neural activity; reviewed in Nicoll, 2017) secondary to augmented BDNF release. This function of syt-4 was subsequently replicated by an independent laboratory using an siRNA approach rather than a knockout (Wong et al., 2015). Interestingly, knockout of syt-4 also disrupts the structure of the golgi complex in cultured hippocampal neurons (Arthur et al., 2010). The golgi is abnormally large in syt-4 knockouts, and a large number of small clear vesicles (presumably axonal transport vesicles) tended to accumulate near the trans-golgi network. No mechanistic explanation for this golgi phenotype has been explored, but the result highlights the need to explore non-synaptic functions of syt isoforms in neurons.

While syt-6 is expressed in brain (Mittelsteadt et al., 2009), only a single study has examined syt-6 function in neuronal cells. Wong et al. (2006) report that exogenously-applied BDNF (labelled by a quantum dot to permit monitoring with fluorescent microscopy) becomes internalized into early (EEA1-positive) endosomes in neuronal dendrites, and that these endosomes then re-release this BDNF in an activity-dependent manner. This re-release of internalized BDNF (but not the initial uptake) was impaired in neurons when syt-6 was knocked down with siRNA. Knockdown of syts 4, 11, or 12 had no such effect. The authors concluded that syt-6 is a Ca^{2+} sensor for release of internalized BDNF from endosomes during high periods of neuronal activity.

The function of syt-7 is a contentious topic, currently under vigorous debate. Syt-7 knockouts were initially reported to have no exocytosis phenotype (Maximov et al., 2008). Later reports concluded that syt-7 is a Ca^{2+} sensor specific for asynchronous neurotransmitter release at the zebrafish neuromuscular junction (Wen et al., 2010), in cultured mouse neurons (Bacaj et al., 2013; Weber et al., 2014), at the calyx of Held (Lou et al., 2017), and for delayed asynchronous release at ribbon synapses in the mouse retina (Lou et al., 2015). A study from our laboratory identified syt-7 as a Ca^{2+} sensor mediating the replenishment of synaptic vesicles following high-frequency stimulation (i.e., recovery from synaptic depression is slowed in the knockout), and did not find any effect of syt-7 knockout on asynchronous release (Liu et al., 2014). This replenishment phenotype has subsequently been disputed by other laboratories using different preparations (Lou et al., 2015; Turecek et al., 2017). Finally, another laboratory has proposed syt-7 is a Ca^{2+} sensor for short-term synaptic facilitation (Jackson et al.,

2016; Turecek et al., 2017), a contention which, again, is contradicted by data from other laboratories in different preparations (Liu et al., 2014; Lou et al., 2017)

Interpretation of these divergent results on syt-7 is complicated by the use of different synaptic preparations and genetic backgrounds by different laboratories, and the fact that laboratories employ divergent definitions of “asynchronous release” (reviewed in Kaeser & Regehr, 2014). However, these three proposed functions of syt-7 (asynchronous release following stimulus trains, replenishment of the vesicle pool following prolonged stimulus trains, and facilitation of the synaptic response upon multiple stimulations) can be thought of as manifestations of a more general trend: all laboratories that examined the effect of syt-7 deletion on exocytosis report that the knockout evinces no changes in release for a single action potential (Liu et al., 2014, Bacaj et al., 2013, Jackman et al., 2017, Wen et al., 2010), and all agree that following multiple action potentials, fewer quanta are available for release in the knockout. Laboratories disagree as to whether this difference is best operationally-defined as a defect in “asynchronous release”, “replenishment”, “lack of facilitation”, or some other parameter. However one can safely generalize from the published studies that, in many situations, syt-7 is required to maintain synaptic efficacy during/after extended trains of action potentials. Indeed, a recent study (Chen et al., 2017b) at the cerebellar basket cell to Purkinje cell synapse finds that syt-7 mediates all three of these functions (vesicle replenishment, asynchronous release, synaptic facilitation) to a certain extent, and concludes that the overall function of syt-7 is to main efficient high-amplitude release, independent of presynaptic firing frequency. Interestingly, apart from whatever role(s) syt-7 may play in neurotransmitter release at particular synapses, a parallel

literature has identified syt-7 as a regulator of lysosomal fusion to the plasma membrane in fibroblasts and neurons (Martinez et al., 2000; Padamsey et al., 2017). Whether this role in exocytosis of lysosomes is mechanistically related to the synaptic transmission phenotypes observed in syt-7 knockouts has not been explored.

Syt-9[1] is another Ca^{2+}-triggered (Hui et al., 2005) isoform that has been the subject of considerable study. Whether syt-9 can mediate fast glutamate release is a matter of debate. A study in cultured neurons (Xu et al., 2007) exogenous expressed syts 1, 2, 3, 5, 6, 7, 9, and 10 in syt-1 knockout neurons, to determine which isoforms could rescue synchronous release. Besides syt-1 and syt-2 which (unsurprisingly) supported synchronous release, only syt-9 was able to restore fast neurotransmitter release in syt-1 knockout neurons. A subsequent study failed to replicate this finding that syt-9 can restore synchronous release in syt-1 knockouts (Dean et al., 2012). Working in the calyx of Held, where syt-2 is the chief Ca^{2+} sensor for fast exocytosis, Kochubey et al. (2016) found that viral expression of syt-9 can partially (~50%) rescue the loss of synchronous release in syt-2 knockouts. Thus no consensus exists on whether syt-9 can support synchronous release in neurons. Apart from the question of whether syt-9 can mediate synchronous release when exogenously expressed, only a single study has attempted to address the physiological role of endogenous syt-9 in central neurons (though extensive work has been done in other cell types). Genetic deletion of syt-9 reduced (by ~60%) evoked currents in cultured striatal neurons without altering the size of the RRP (measured with hypertonic sucrose), leading to the suggestion that syt-9 serves as a Ca^{2+} sensor for fast release in striatial neurons (Xu et

[1] Please note that due to a terminological disagreement, some groups refer to syt-9 as syt-5 (ex., Craxton, 2010), though this is not the case for any of the studies discuss herein.

al., 2007). However, this study did not measure the Ca^{2+} dependence of release in neurons lacking syt-9 (which presumably would be altered if syt-9 were serving as a fast release Ca^{2+} sensor) or the amplitude of quantal responses in neurons lacking syt-9 (a necessary control to ensure that reduced evoked current amplitude is not due to an alteration in postsynaptic efficacy or vesicular transmitter content). As such, the conclusion that syt-9 serves as a Ca^{2+} sensor for release in striatal neurons should be considered preliminary.

Two studies have sought a potential function of syt-10. The protein has been found to be a Ca^{2+} sensor mediating somatodendritic release of IGF-1 from olfactory bulb neurons (Cao et al., 2010). Knockout of syt-10 impaired activity-dependent exocytosis of IGF-1, resulting in stunted neuronal growth. A subsequent study from the same group (Cao et al., 2013) found that this effect of syt-10 on IGF-1 is mediated by complexin (a SNARE-binding protein that plays a modulatory role in exocytosis; Trimbuch & Rosenmund, 2016). While these studies focused on the olfactory bulb, syt-10 mRNA is also enriched in the dentate gyrus of the hippocampus (Mittelsteadt et al., 2009). Future studies are needed to determine the role of syt-10 in hippocampus.

Syt-11 has recently been reported to be a negative regulator of endocytosis (both Clathrin-dependent and –independent) in hippocampal and dorsal root ganglion neurons (Wang et al., 2016). Knockdown of syt-11 impaired endocytosis (assayed with pHluorin-tagged fusion proteins, uptake of stryl dyes, or uptake of fluorescently-tagged Transferrin) in a dynamin-dependent manner, and overexpressed myc-syt-11 localized with elements of the endocytic machinery (Clathrin, AP-2, and dynamin). However, conflicting reports on whether syt-11 expression in brain is chiefly neuronal (Yeo et al.,

2012) or glial (Mittelsteadt et al., 2009; Du et al., 2017) raise questions about whether the observed effect of syt-11 knockdown on endocytosis is direct or indirect (potentially through glia-to-neuron signaling). Replication and further study is warranted.

Only two studies (from a single laboratory) have examined the function of endogenous syt-12. Both report that syt-12 is a synaptic vesicle protein, which does not bind Ca^{2+}, in central glutamatergic synapses, whose phosphorylation state determines parameters of neurotransmitter release. In the first (Maximov et al., 2007), syt-12 is proposed to be a direct inhibitor of syt-1 that reduces spontaneous neurotransmitter release without affecting evoked transmission or short-term plasticity. In the second (Kaeser-Woo et al., 2013), syt-12 was suggested to be critical for presynaptic long-term potentiation in the mossy fiber pathway of the dentate gyrus (the main output from dentate granule cells to the CA3 subfields). Both of these phenotypes are reported to depend on cAMP-dependent phosphorylation of syt-12 (at the 97th amino acid) by protein kinase A (PKA). These results are provocative, and merit replication and further exploration.

The synaptotagmin isoforms not discussed so far (syt-3, syt-8, and syts 13-17) have not been subject to systematic phenotypic characterization in neurons. In sum, the functions of syt-1 and syt-2 as Ca^{2+} sensors for synchronous neurotransmitter release is uncontroversial, and a consensus is emerging that syt-4 regulates BDNF release - although the precise mechanisms in both cases are matters of debate. But for all other synaptotagmins, either few studies in neurons have been conducted (often by a single laboratory), no neuronal function has been assigned, or the assigned function is contested.

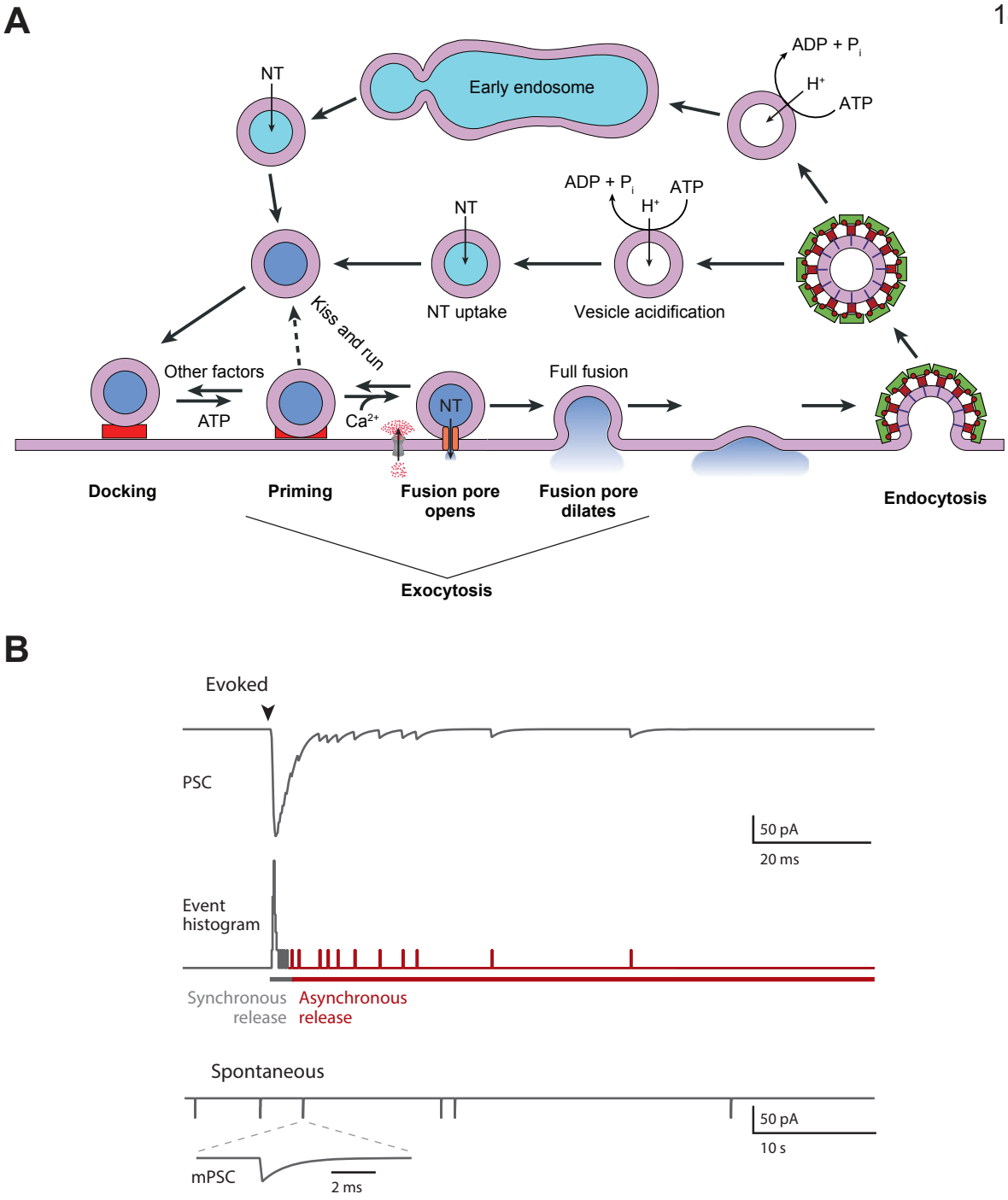

Figure 1. Basic concepts in synaptic vesicle cycling and exocytosis
(A) Diagram of basic steps in the synaptic vesicle cycle. This figure is (minimally) modified from Chapman, 2008. **(B)** Conceptual illustration of three modes of exocytosis, based on simulated data. This figure is adapted from Kaeser & Regehr, 2014.

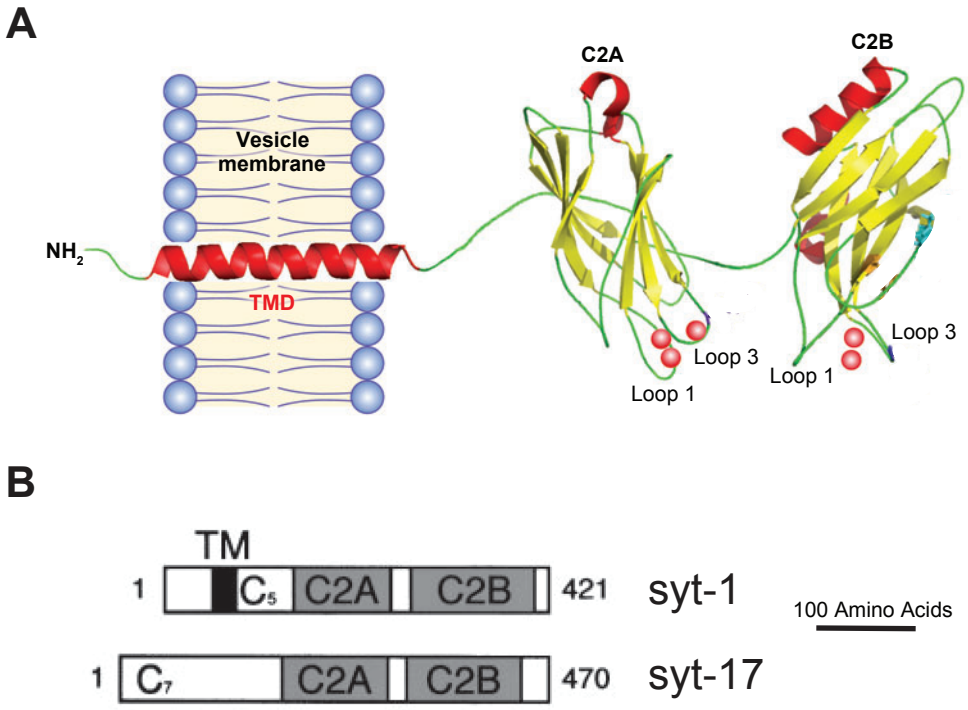

Figure 2. Synapotagmins 1 & 17. (A) Domain structure of syt-1, highlighting the putative Ca2+ binding loops on each C2 domain. Ca2+ ions are depicted as red spheres. Figure modified from Chapman, 2008. **(B)** Schematic representation of mouse syt-1and syt-17. Amino acid numbers are given on both sides. TM indicates the transmembrane domain, C# indicates a cystine cluster of the given number of residues. Figure modified from Fukuda & Mikoshiba, 2001.

Chapter 2:

An Engineered Metal Sensor Tunes the Kinetics of Synaptic Transmission

2.1 Introduction

As described in Chapter 1 of this dissertation, there are 17 known isoforms of syt (Dean et al., 2012) that exhibit divergent biochemical properties. Whether differences in intrinsic kinetics of membrane fusion have functional consequences in cells is not known.

The nonphysiological divalent cation Sr^{2+} has been used to probe the kinetics of neurotransmitter release, because replacement of extracellular Ca^{2+} with equimolar Sr^{2+} yields substantially reduced EPSCs with a largely asynchronous time course (Goda and Stevens, 1994; Rumpel and Behrends, 1999; Xu-Friedman and Regehr, 2000; Lau and Bi, 2005). Sr^{2+} readily enters presynaptic boutons through voltage-gated channels, but endogenous Ca^{2+} binding proteins are largely ineffective at buffering Sr^{2+}, resulting in a Sr^{2+} transient that can persist for seconds (Rumpel and Behrends, 1999; Xu-Friedman and Regehr, 2000; Babai et al., 2014).

The goal of this study was twofold: first, to determine whether the intrinsic kinetics of syt-1 determine the rate of neurotransmitter release, and second, to use a novel chemical genetic approach to engineer a sensor that responds to Sr^{2+}. Therefore, a chimera between the fastest syt isoform (syt-1) and a slower isoform, which responds to Sr^{2+}, (syt-7) was generated. This chimera exhibited slower intrinsic membrane binding kinetics and slowed the rate of neurotransmitter release in neurons, arguing that EPSC decay kinetics are partially governed by the intrinsic kinetics of the presynaptic

Ca^{2+} sensor. Furthermore, our modifications conferred upon syt-1 the ability to both penetrate membranes *in vitro* and trigger synchronous release *in vivo* in response to Sr^{2+}, consistent with the notion that penetration of the target membrane by syt-1 is a key step in SV exocytosis. Additionally, we dissociate evoked exocytosis from spontaneous single vesicle fusion, identifying a role for the metal binding loops of syt-1 in suppressing "miniature" release. Finally, we show that slowing the kinetics of syt*membrane interactions slowes the preferred frequency of at least some forms of population-level oscillations *in vitro*.

2.2 Materials and Methods

Materials

The following lipids were purchased from Avanti Polar Lipids: 1-palmitoyl-2-oleoyl-*sn*-glycero-3-phosphoethanolamine [phosphati-dylethanolamine (PE)]; 1,2-dioleoyl-*sn*-glycero-3-phospho-l-serine [phosphatidylserine (PS)]; 1-palmitoyl-2-oleoyl-*sn*-glycero-3-phos-phocholine [phosphatidylcholine (PC)]; 1,2-dipalmitoyl-*sn*-glycero-3-phospho-ethanolamine-*N*-(7-nitro-2–1,3-benzoxadiazol-4-yl) (NBD-PE); *N*-(lissamine rhodamine B sulfonyl)-1,2-dipalmitoyl-*sn*-glycero-3- phosphoethanolamine (rhodamine-PE); and 1,2-dioleoyl-sn-glycero-3- phosphoethanolamine-*N*-(5-dimethylamino-1-naphthalenesulfonyl) (dansyl-PE). *N*,*N* -dimethyl-*N*-(iodoacetyl)-*N* -(7-nitrobenz-2-oxa-1,3-diazol-4-yl)ethylenediamine (IANBD-amide) was purchased from Invitrogen. Accudenz was purchased from Accurate Chemical & Scientific Corporation. Glutathione Sepharose and Ni2 Sepharose High Performance affinity media were obtained from GE Healthcare Bio-Sciences.

Recombinant proteins and protein purification

cDNA encoding the cytoplasmic domain (denoted C2AB) of rat syt-1 (residues 96–421; the amino acid residues for all other syt constructs below are indicated in parentheses) was provided by T. C. Sudhof (Department of Molecular and Cellular Physiology, Howard Hughes Medical Institute, Stanford University, Stanford, CA); the D374 mutation was corrected by replacement with a glycine. cDNA for syt-2 (C2AB, 139–423), syt-6 (C2AB, 143–426), syt-7 (C2AB, 134–403), and syt-9 (C2AB, 104–386) were provided by M. Fukuda (Department of Developmental Biology and Neurosciences, Tohoku University, Sendai, Miyagi, Japan). cDNA encoding syt-3 (C2AB, 290–569) was provided by S. Seino (Department of Physiology and Cell Biology, Kobe University Graduate School of Medicine, Kobe, Japan). W. A. Catterall (Department of Pharmacology, University of Washington, Seattle, WA) provided 1B-synprint in a pTrcHis vector.

Syt-1 C2AB was subcloned into pGEX vectors to generate GST-tagged fusion proteins. Syt-2, syt-6, syt-7 and syt-9 C2AB were subcloned into a pTrcHis vector, and syt-3 C2AB was subcloned into a pET28a vector, to generate His6-tagged fusion proteins. Chimeras and cysteine mutant forms of syt-1 and chimera$_{1,3}$ were generated using PCR and a QuikChange Site-Directed Mutagenesis Kit (Stratagene). Chimeras were generated by grafting the metal binding loops of syt-7 C2A (loop 1, 162–172; loop 2, 192–198; loop 3, 225–233) onto syt-1 C2B. For cysteine mutants, first the lone native cysteine, C277, was mutated to an alanine. Then, a single cysteine was introduced at

M173 and F234 of C2A and V304 and I367 of C2B for syt-1 and M173 and F234 of C2A and F304 and F367 of C2B for chimera$_{1,3}$.

cDNA for SNAP-25B was provided by M. C. Wilson (Department of Neurosciences, University of New Mexico School of Medicine, Albuquerque, NM). Full-length synaptobrevin-2 (syb) and syntaxin-1A (syx) were provided by J. E. Rothman (Department of Cell Biology, School of Medicine, Yale University, New Haven, CT). All individual SNARE proteins were subcloned into pTrcHis vectors to generate His6 fusion proteins. Full-length SNAP-25B and syx were subcloned into a pRSFDuet vector to generate His6-tagged t-SNARE heterodimers (Chicka et al., 2008). All GST and His6-tagged fusion proteins were expressed in *Escherichia coli* and purified as described previously (Liu et al., 2014).

Full-length syt-1 and chimera$_{1,3}$ were subcloned into pLox Syn-DsRed-Syn-GFP lentiviral vector (provided by F. Gomez-Scholl, Facultad de Medicina, Departamento de Fisiología Médica y Biofísica, Universidad de Sevilla, Sevilla, Spain) for electrophysiological recordings. Proteins were inserted with BamH1-Not1 to replace the existing DsRed, and GFP was left intact to visualize transfected cells.

Vesicle preparation

Protein-free liposomes were prepared as described previously (Liu et al., 2014). Lipid compositions were 15% PS, 30% PE, and 55% PC for penetration assays; 25% PS, 30% PE, and 55% PC for cosedimentation assays; and 25% PS, 25% PE, 5% dansyl-PE, and 45% PC for stopped-flow rapid-mixing assays. SNARE-bearing vesicles were prepared as described previously (Chicka et al., 2008). Lipid compositions for the

vesicles used in the *in vitro* fusion assays were as follows: 15% PS, 27% PE, 55% PC, 1.5% NBD-PE, and 1.5% rhodamine-PE for v-SNARE vesicles; 15% PS, 30% PE, and 55% PC for heterodimer t-SNARE vesicles; and 25% PS, 30% PE, and 45% PC for syx-only t-SNARE vesicles. For coflotation assays, t-SNARE heterodimer vesicles were made from a lipid composition of 30% PE and 70% PC.

In vitro fusion assays

Fusion, between v-SNARE vesicles and heterodimer, or syx-only t-SNARE, vesicles was monitored using a Synergy HT multidetection microplate reader (Bio-Tek) as described previously (Chicka et al., 2008; Liu et al., 2014). For standard assays, 1M cytoplasmic domain (C2AB) of the indicated syt isoform or chimera was also used, and for split t-SNARE assays, 7M soluble SNAP-25B was also used. During each run, 1mM or the indicated final free [cation] was added and the reaction was monitored for an additional 60 or 120 min. Traces were normalized to the first time point and the maximum fluorescence signal, determined from the addition of *n*-dodecyl-D- maltoside, to determine the $\%F_{max}$.

Penetration assays

The cysteine mutant forms of syt-1 or $chimera_{1,3}$ were labeled with IANBD-amide as described previously (Hui et al., 2011). NBD-labeled proteins (0.3 M) were combined with liposomes (0.1 mM total lipid) in 50 mM HEPES-NaOH, 100 mM NaCl, pH 7.4, buffer plus 0.2 mM EGTA or 1 mM free cation. Fluorescence measurements were performed using a QM-1 fluorometer (Photon Technology International). NBD was

excited at 470 nm, and emission spectra were acquired from 490 to 630 nm. Spectra were corrected by subtracting the background; all spectra were normalized to the signal in EGTA.

Coflotation assays

The ability of syt-1 or chimera$_{1,3}$ to bind to t-SNAREs was monitored via a coflotation assay using an Optima L-90K ultracentrifuge (Beckman Coulter), as described previously (Tucker et al., 2004). The cytoplasmic domains of syt-1 or chimera$_{1,3}$ (10M) were incubated with PS-free t-SNARE heterodimer vesicles in the presence of Ca^{2+} or Sr^{2+} (1 mM), or EGTA (0.2 mM). After 60 min at room temperature, samples were centrifuged, collected, and subjected to SDS-PAGE; gels were stained with Coomassie blue. Data were quantified using densitometry and normalized to the syx band in each lane.

Cosedimentation assays

The membrane-binding activity of the syt-1 or chimera$_{1,3}$ was monitored via a cosedimentation assay using an Optima MAX-E tabletop ultracentrifuge (Beckman Coulter) as described previously (Liu et al., 2014). Data were analyzed using Prism software (GraphPad) to determine the Hill coefficients and [cation]1/2 values.

Stopped-flow rapid mixing

Divalent cation regulated interactions be- tween syt constructs and membranes were monitored via FRET using an SX.18MV stopped-flow spectrometer (Applied

Photophysics) as described previously (Hui et al., 2005). Complexes were formed by mixing 44 nM liposomes, 4 M C2AB, and 0.2 mM cation, and were subsequently disassembled by rapid mixing with 2 mM EGTA. Traces were fit using the Applied Photophysics Pro Data SX software package. A single exponential function was used to determine the rate of disassembly, k_{diss}.

Synprint binding assay

Purified synprint (3g) was incubated with 30 g syt-1 or chimera$_{1,3}$ GST-fusion proteins, immobilized on 30 l of glutathione Sepharose beads, as described previously (Chapman et al., 1998) and immunoblotted with anti-T7 tag mouse monoclonal antibody (1:10,000; Novagen) and a goat-anti-mouse HRP secondary antibody (1:10,000; Abcam).

Cell culture and immunostaining

All procedures were performed un- der the guidance of the Animal Care and Use Committee (Protocol M01221-0-06-14) at the University of Wisconsin–Madison. Hippocampal neurons from syt-1 KO mice, of either sex, were obtained at postnatal day 0 as described previously (Liu et al., 2014). The cells were infected at 5 d *in vitro* (DIV) with lentivirus, prepared in HEK293T cells as described previously (Liu et al., 2014), to express syt-1 or chimera$_{1,3}$, and GFP.

Immunocytochemistry was performed at 14 DIV. Cells were stained with anti-syt-1 (1:500; Developmental Studies Hybridoma Bank), anti-synaptophysin (1:1000; Synaptic Systems), and anti-Map2 (1:500; Millipore) antibodies, DAPI, and Alexa Fluor

secondary antibodies (1:500; Life Technologies). Cells were mounted in Fluoromount (Southern Bio- technology Associates) and imaged on an FV1000 upright confocal microscope with a 60x, 1.4 numerical aperture oil-immersion objective (Olympus).

Electrophysiology

At 14–18 DIV, cells were moved to a recording chamber perfused with a bath solution containing the following (in mM): 128 NaCl, 5 KCl, 25 HEPES, 30 D-glucose, 1 MgCl2, and 5 Ca^{2+} or Sr^{2+}, pH 7.4 (adjusted to 300–310 mOsm with D-glucose). To ensure that residual Ca^{2+} did not confound the Sr^{2+} recordings, Milli-Q water was treated with Chelex-100 resin (Bio-Rad) before use in bath solution to remove residual divalent cations. AMPA receptor currents were isolated with 20 M bicuculline (Tocris Bioscience) and 50 M D-APV (Tocris Bioscience). Borosilicate glass pipettes were pulled to a resistance of 3–5 MΩ and filled with an intracellular solution containing 130 mM K-gluconate, 10 mM HEPES, 5 mM Na-phosphocreatine, 2 mM Mg-ATP, 1 mM EGTA, 5 M QX-314 (Tocris Bioscience), and 0.3 mM Na-GTP, pH 7.4. All experiments were conducted at room temperature.

Whole-cell patch-clamp recordings were made with an Axon Multi- Clamp 700b amplifier (Molecular Devices) in voltage-clamp mode, sampled at 10 kHz and filtered at 2 kHz. Typical series resistances were 15 MΩ with 70% of this resistance compensated, and neurons were clamped at 70 mV. Neurons showing significant changes in series resistance over the course of recording were excluded from analysis, as were cells that exhibited a large degree of recurrent excitation that precluded analysis of EPSC kinetics. For measurement of evoked EPSCs, neurons near (within several hundred

microns of) the patched (i.e., postsynaptic) cell were stimulated with a bipolar electrode in theta glass tubing. This electrode was placed directly adjacent to the soma of the presynaptic neuron. In this configuration, EPSCs from individual presynaptic cells are isolated (i.e., moving the stimulating electrode ~10 microns away from the soma of the presynaptic neuron abolished the response). Neurons whose somata made contact with the somata of other neurons were not stimulated, to avoid evoking overlapping EPSCs from multiple presynaptic neurons. Occasional indirect or polysynaptic responses were easily identified by the lack of smooth rise and decay kinetics and were excluded from analysis. Presynaptic neurons were stimulated with 20 V square-wave pulses every 30 s, and the first artifact-free EPSC (typically the first) was used for analysis.

For measurement of paired-pulse facilitation, two EPSCs were evoked (with a 50 ms interstimulus interval) and quantified as the ratio of the second response over the first. Data were analyzed offline in Clampfit (Molecular Devices) and MATLAB (Math-Works) software. Rise and decay times were computed as 20 – 80% of maximum, and cumulative charge transfer functions (computed across 500 ms) were fit with double exponentials to quantify fast and slow components of the charge transfer.

For recordings of mEPSCs, 1 M TTX was added to the bath solution immediately before recording, and no series resistance compensation was used. Sixty seconds of data were analyzed for each cell. mEPSCs were quantified with the Clampfit template matching algorithm and custom-written MATLAB software with a 5 pA threshold.

Hypertonic sucrose was applied to measure the RRP of SVs (Rosenmund and Stevens, 1996; Liu et al., 2014). After patching a neuron, a second pipette containing extracellular solution, with 500 mM sucrose added, was positioned at the edge of the of

field of view under a 40x objective (upstream of solution flow). The sucrose solution was puffed onto patched cells with a Picospritzer III (Parker) such that all boutons contacting a given neuron were stimulated. Sucrose was applied for 10 seconds, yielding a response with distinct fast and slow (steady-state) phases. The fast component of the response was integrated to measure the RRP.

All recordings were made from a minimum of three coverslips each from three independent litters of animals. The number of cells, *N*, is indicated in the figure legends (*N* 10 –20 per condition for each electrophysiology experiment). Statistical significance was assessed with Student's *t*-tests or Mann–Whitney tests as appropriate.

2.3 Results

We first identified syt isoforms that couple Sr^{2+} to fusion, using a well-characterized "standard" *in vitro* membrane fusion assay that utilizes preassembled t-SNARE heterodimers (Fig. 3A; Tucker et al., 2004). Six isoforms were screened: syt-6, syt-7, and syt-9 coupled both Ca^{2+} and Sr^{2+} to fusion; syt-1, syt-2, and syt-3 were efficiently activated by Ca^{+2} but not Sr^{2+} (Fig. 3B-G; Bhalla et al., 2005). Because syt-7 has the slowest membrane disassembly kinetics within this family (Hui et al., 2005) and is apparently absent from SVs (Dean et al., 2012), we performed further analysis of this isoform. Syt-7 was rescreened using a more stringent variant of the fusion assay in which syt must first fold soluble SNAP-25B onto syx to trigger fusion (Fig. 3H; Bhalla et al., 2006). In this "split" t-SNARE fusion assay, Sr^{2+} failed to activate syt-1 (Fig. 1*I*), but both metals activated syt-7 (Fig. 3J). Isothermal titration calorimetry (ITC) confirmed that syt-1 binds one Sr^{2+} ion via its C2B domain (data not shown; Cheng et al., 2004). These

findings might explain why Sr^{2+} fails to efficiently activate syt-1, as mutagenesis studies indicate the C2B domain must bind two metal (Ca^{2+}) ions to trigger exocytosis (Nishiki and Augustine, 2004). Ca^{2+}-ligand mutations in C2B completely disrupt function, whereas analogous mutations in C2A have little effect (Chapman, 2008); hence, our efforts to engineer syt-1 focused on the C2B domain.

In an effort to tune the kinetics of syt-1, we replaced subsets of its metal binding loops with those of syt-7 (Fig. 4A-B). To determine which C2 domain of syt-7 coupled Sr^{2+} to fusion, both C2A and C2B were screened in a standard fusion assay. Since both C2 domains of syt-7 stimulated fusion in response to Sr^{2+} (data not shown), chimeras were constructed by grafting, individually and in combinations, the metal binding loops of either syt-7 C2A or C2B onto syt-1 C2B (Fig. 4A-B). Of these two sets of chimeras, only the proteins that harbored loops from syt-7 C2A, but not C2B (data not shown), responded to Sr^{2+} in the standard fusion assay (Fig. 4C-D). These four constructs, which all contained loop 3, were therefore rescreened in the split t-SNARE fusion assay and only one, chimera$_{1,3}$, efficiently coupled Sr^{2+} to fusion (Fig. 4E-F). The cation (Ca^{2+} or Sr^{2+}) sensitivities were greater for chimera$_{1,3}$ than for syt-1, in terms of both driving fusion (Fig. 4G-H) and binding to membranes (Fig. 5A), consistent with the higher affinity of syt-7 for metals as compared to syt-1 (Bhalla et al., 2005).

Upon binding Ca^{2+}, metal binding loops 1 and 3, from each C2 domain of syt-1, penetrate membranes, with a small contribution from loop 2 (Hui et al., 2011). To monitor penetration, loops 1 and 3, were individually labeled with an environmentally sensitive fluorophore, NBD. In the presence of Ca^{2+}, all labeled loops of syt-1 penetrated membranes. However, Sr^{2+} failed to trigger efficient penetration (Fig. 5B-C).

Importantly, both C2 domains of chimera$_{1,3}$ efficiently penetrated membranes in the presence of either Ca^{2+} or Sr^{2+} (Fig. 5B-C). These results support the emerging view that membrane penetration by syt-1 is a crucial step in Ca^{2+}-triggered membrane fusion (Paddock et al., 2011; Liu et al., 2014) and provide an explanation as to why Sr^{2+} drives synaptic transmission less efficiently than Ca^{2+}. Interestingly, although the C2A domain of chimera$_{1,3}$ was not engineered to bind Sr^{2+}, it efficiently penetrated membranes (Fig. 5C-D); ITC was not possible with this construct. So, either an active C2B domain "pulls" C2A into the bilayer, or C2A is activated via contact with the engineered C2B domain (Bai et al., 2002; Liu et al., 2014).

To determine whether these alterations in syt-1 led to changes in membrane interactions, we performed stopped-flow rapid- mixing experiments. To mimic the decay of Ca^{2+} transients in nerve terminals, sensor*cation*membrane complexes were rapidly mixed with excess chelator. In Ca^{2+}, chimera$_{1,3}$ disassembled much more slowly than syt-1 (Fig. 5D, left), a point we return to below. Similarly, the disassembly rates of chimera$_{1,3}$ were slower in Sr^{2+} than syt-1 (Fig. 5D, right).

To determine whether chimera$_{1,3}$ can change the rate of neurotransmitter release, we expressed it, or syt-1, in dissociated hippocampal neurons derived from syt-1 KO mice. Both proteins were properly localized to nerve terminals, as colocalization (Pearson's correlation coefficient) with synaptophysin did not differ (p>0.1; Fig. 6). The number of synapses (quantified as the number of synaptophysin puncta) also did not differ across conditions (p>0.1; data not shown).

We performed patch clamp recordings of EPSCs in the presence of 5 mM Ca^{2+} or Sr^{2+}. Individual EPSCs were evoked with a bipolar electrode positioned near the

soma of a nearby cell. Approximately 60% of stimulated neurons had monosynaptic connections with the patched (postsynaptic) neuron, and this did not differ across conditions (p>0.1; data not shown). The characteristics of these EPSCs were comparable to what has been found previously in this preparation (Liu et al., 2009, 2014; Yao et al., 2011).

Chimera$_{1,3}$ did not simply rescue rapid evoked release, but exhibited a gain-of-function relative to syt-1. In the presence of Ca^{2+}, chimera$_{1,3}$ increased the total charge transfer without altering the peak current (Fig. 7A; chimera$_{1,3}$ charge, 14.66 1.94 pC; syt-1 charge, 7.12 1.10 pC; p<0.01; N 10–20 per condition). Importantly, in Ca^{2+}, chimera$_{1,3}$ yielded a slower rise of evoked release (Fig. 8A; chimera$_{1,3}$ rise slope, 60.48 16.8 pA/ms; syt-1 rise slope, 132.9 26.7 pA/ms; p<0.05) and a decay time twice as long as that of neurons expressing syt-1 (Fig. 8A; chimera$_{1,3}$ decay time, 32.90 2.12 ms; syt-1 decay time, 14.45 1.49 ms; p<0.01; N 10–20 per condition). When cumulative charge transfers were fit with double exponential functions, we found that EPSC decays of neurons expressing chimera$_{1,3}$ had a significantly larger slow component of release (Fig. 8B; chimera$_{1,3}$ slow charge amplitude, 4.45 0.79 pC; syt-1 slow charge amplitude, 2.09 0.74 pC; p<0.05), and the time constant (τ) of the fast component was significantly lengthened (Fig. 8B; chimera$_{1,3}$ fast charge , 20.1 1.49 ms; syt-1 fast charge , 12.8 1.45 ms; p<0.01). Hence, grafting the loops of the slowest syt isoform, syt-7 (Hui et al., 2005), onto syt-1 slows the kinetics of synaptic transmission.

A key finding was that in Sr^{2+}, chimera$_{1,3}$ significantly increased both the total charge transfer and peak current relative to syt-1 (Fig. 7B; chimera$_{1,3}$ charge, 9.21 1.37 pC; syt-1 charge, 5.94 1.06 pC; p<0.05; chimera$_{1,3}$ amplitude, 262.5 38.5 pA; syt-1

amplitude, 141.0 21.7 pA; $p<0.05$; N 10 –20 per condition). In neurons expressing chimera$_{1,3}$, the rising phase of the EPSC in Sr^{2+} was steeper than in cells expressing syt-1 (Fig. 8A; chimera$_{1,3}$ rise slope, 66.17 13.3 pA/ms; syt-1 rise slope, 35.49 7.76 pA/ms; $p<0.05$). There were no observable differences in the decay phase of EPSCs regulated by chimera$_{1,3}$ and syt-1 in Sr^{2+} (Fig. 8B), presumably because of the slow rate (seconds) at which Sr^{2+} is cleared from nerve terminals (Xu-Friedman and Regehr, 2000; Babai et al., 2014). As such, EPSC decays in Sr^{2+} were not analyzed further. Consistent with previous reports, Sr^{2+} was ineffective at triggering release in syt-1 KO neurons (Fig. 7B; Shin et al., 2003; Babai et al., 2014), indicating that any remaining asynchronous Ca^{2+} sensors do not efficiently sense Sr^{2+}.

It should be noted that the increase in charge transfer could in principal be due to an increase in the size of the readily-releasable pool (RRP) of vesicles (Rosenmund and Stevens, 1996), rather than an effect on the release machinery during the final stages of exocytosis. To address this, we measured the RRP in KO, syt-1, and chimera$_{1,3}$-expressing neurons with hypertonic sucrose. We found that chimera$_{1,3}$ rescued the size of the RRP as efficiently as syt-1 in either Ca^{2+} (Fig. 9A, left panels) or Sr^{2+} (right panels). To the best of our knowledge, these experiments provide the first example of a mutant form of syt-1 that alters the kinetics of functional synaptic transmission (i.e., without impairing the RRP).

Because overexpression of wild-type and mutant forms of syt do not alter Ca^{2+} entry (Wang et al., 2001; Young and Neher, 2009), it is unlikely that our kinetic effects are due to changes in metal influx. Nonetheless, we examined paired-pulse facilitation, a form of short-term plasticity sensitive to changes in presynaptic Ca^{2+} dynamics

(Fioravante and Regehr, 2011). The paired-pulse ratio was similar between neurons expressing syt-1 and chimera$_{1,3}$ (Fig. 9B). Moreover, the ability of chimera$_{1,3}$ to bind synprint, the Ca^{2+} channel domain that mediates interactions with the release machinery (Sheng et al., 1997), was indistinguishable from that of syt-1 (Fig. 9C). Collectively, these results argue against our observed kinetic effects being due to an alteration in the coupling of release machinery to Ca^{2+} channels.

Recordings of "mini" excitatory currents (mEPSCs), reflecting spontaneous release of individual SVs, showed no difference in amplitude or kinetics among conditions (Fig. 10A, C), arguing against a postsynaptic effect. Loss of syt-1 results in an increase in the frequency of mEPSCs, suggesting that syt-1 has a second function as a fusion clamp (DiAntonio and Schwarz, 1994; Chicka et al., 2008; Liu et al., 2014). Interestingly, chimera$_{1,3}$ failed to clamp minis, showing a frequency equivalent to KO (Fig. 10B). Thus, metal binding loops 1 and 3 of syt-1 C2B not only govern the kinetics of evoked release, but also play roles in suppressing spontaneous transmission.

Finally, to explore the effect of slowing neurotransmitter release kinetics on network-level behavior, we recorded (in Ca^{2+}) evoked "persistent reverberation", an *in vitro* model of population-level oscillations (Lau and Bi, 2005). Networks of neurons expressing chimera$_{1,3}$ oscillated at a significantly slower peak frequency during reverberatory episodes, compared to networks of neurons expressing wildtype syt-1 (Fig. 11A-B). The probably of evoking an oscillation, and the duration (~7s) of such episodes, was indistinguishable between groups ($p>.1$). Thus, by slowing the kinetics of synaptic transmission, we slowed the preferred frequency of network-level behavior *in vitro.*

2.4 Discussion

Upon binding Ca^{2+}, syt-1 penetrates membranes that harbor anionic phospholipids (Chapman and Davis, 1998; Chapman, 2008). In a reconstituted system, syt-1 preferentially penetrated t-SNARE- bearing membranes to accelerate fusion (Bai et al., 2004; Chicka et al., 2008). Moreover, the abilities of mutant forms of syt-1 to penetrate membranes was correlated with their abilities to drive synchronous synaptic transmission in cultured neurons (Liu et al., 2014). This latter finding suggests that membrane penetration constitutes an essential step in excitation–secretion coupling. The work presented here provides a more direct demonstration that penetration by syt-1 is a key step in SV exocytosis. Specifically, we used a chemical genetic approach to engineer syt-1 to respond to a non- physiological metal, Sr^{2+}. In the presence of Sr^{2+}, syt-1 binds membranes (Fig. 5A), but fails to penetrate (Fig. 5B-C), and so only weakly triggers exocytosis in neurons (Fig. 7B). In contrast, chimera$_{1,3}$ bound (Fig. 5A) and penetrated membranes (Fig. 5B-C) in response to Sr^{2+}, resulting in robust synchronous neurotransmitter release (Fig. 7B). These results prompt the question as to whether the kinetics of the crucial interaction between syt-1 and membranes affect the time course of synaptic transmission.

EPSC decays are governed by a myriad of presynaptic and postsynaptic mechanisms, including presynaptic action potential waveform (Taschenberger and von Gersdorff, 2000), AMPA receptor desensitization (Wall et al., 2002), and clearance of glutamate from the synaptic cleft (Takahashi et al., 1995). The effects reported here reveal a novel factor that determines the kinetics of transmission, namely, chimera$_{1,3}$

slowed the sensor–membrane disassembly rate upon chelation of Ca^{2+} (Fig. 5D, left) and also slowed the rate at which EPSCs decay (Fig. 7A). Once activated by metal, the chimera "holds onto" membranes longer, thus widening the window in which vesicles can fuse (Fig. 12). It is unlikely that these kinetic changes are the result of changes in Ca^{2+} affinity, as it has been shown that simply increasing the affinity of syt-1 for Ca^{2+} does not alter the time course of transmission (Rhee et al., 2005). Rather, the longer EPSC decays reported here likely reflect longer-lived sensor–membrane complexes that continue to drive release. Thus, we propose that the decay phase of EPSCs are governed, in part, by the dwell time of syt-1–membrane complexes.

Additionally, by slowing the kinetics syt1-membrane disassembly, we slowed the kinetics of synaptic transmission, and thereby slowed the preferred frequency of network-level oscillations (persistent reverberation). This highlights the importance of (seemingly minor) synaptic parameters for modulating population-level activity.

Previous work has shown that syt-1 KO neurons exhibit a significantly enhanced rate of spontaneous "miniature" release (DiAntonio and Schwarz, 1994; Littleton et al., 1994; Liu et al., 2009). This led to the suggestion that during basal (i.e., low Ca^{2+}) conditions, syt-1 reduces the rate of spontaneous fusion by serving as a "clamp," either by inhibiting SNARE assembly directly (Chicka et al., 2008) or by inhibiting a second Ca^{2+} sensor (Xu et al., 2009; Kochubey and Schneggenburger, 2011). Interestingly, while $chimera_{1,3}$ was able to efficiently trigger evoked exocytosis, it failed to rescue this clamping function of syt-1. The mechanism of this clamping function is unclear, because it can be disrupted by mutating either the metal/membrane binding loops (the present work) or the linker connecting the two C2 domains of syt-1 (Liu et al., 2014; Bai et al.,

2016). It should also be noted that spontaneous release appears to involve a somewhat distinct pool of SVs (Kavalali, 2015), so the differential regulation of these two modes of release likely involves numerous other factors.

Finally, during synaptic transmission, chimera$_{1,3}$ restored the total charge transfer in Sr^{2+} (Fig. 7B) to levels comparable to syt-1 in Ca^{2+} (Fig. 7A), demonstrating the functionality of this engineered sensor. Future work will use this chimera as a tool to dissect aspects of syt-1 function from other Ca^{2+} triggered processes in nerve terminals (discussed in further detail in Chapter 4).

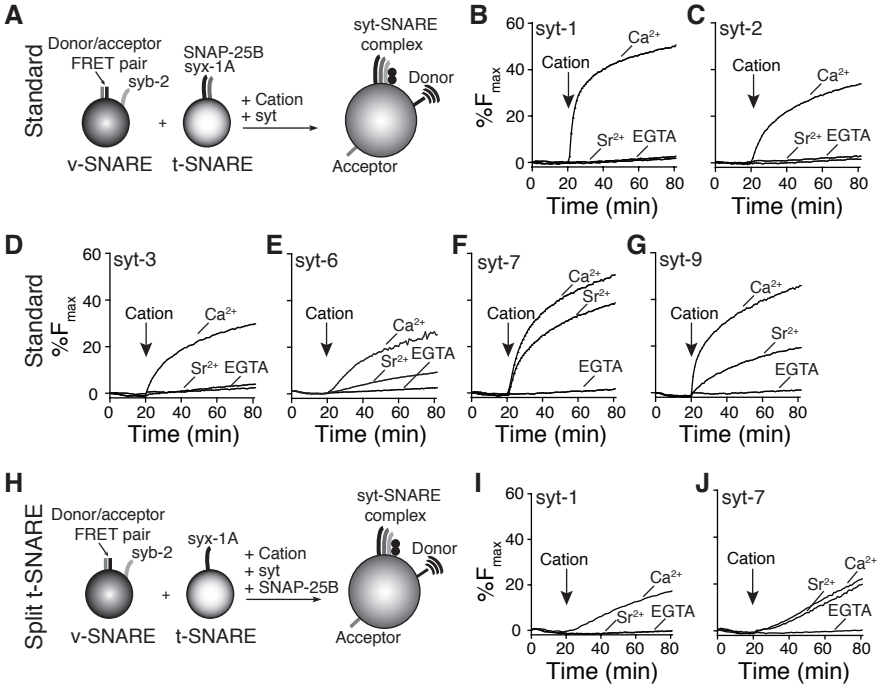

Figure 3. Identification of syt isoforms activated by Sr^{2+}.
(A) Schematic of standard in vitro fusion assay. **(B-G)** Eight isoforms of syt sense Ca^{2+} (Hui et al.,2005), and six of these were screened in a standard in vitro fusion assay to identify isoforms that are activated by Sr^{2+}. Syt-1 **(B)**, syt-2 **(C)**, and syt-3 **(D)** were activated by Ca^{2+} but not Sr^{2+}; in contrast, syt-6 **(E)**, syt-7 **(F)**, and syt-9 **(G)** stimulated fusion in response to either metal.Representative traces are shown. N=3. **(H)** Schematic of the "split" t-SNARE in vitro fusion assays. **(I-J)** Ca^{2+}, but not Sr^{2+},activated syt-1 **(I)**; Syt-7 efficiently facilitated fusion, in the presence of Ca^{2+} or Sr^{2+} **(J)**. Representative traces are shown. N=4.

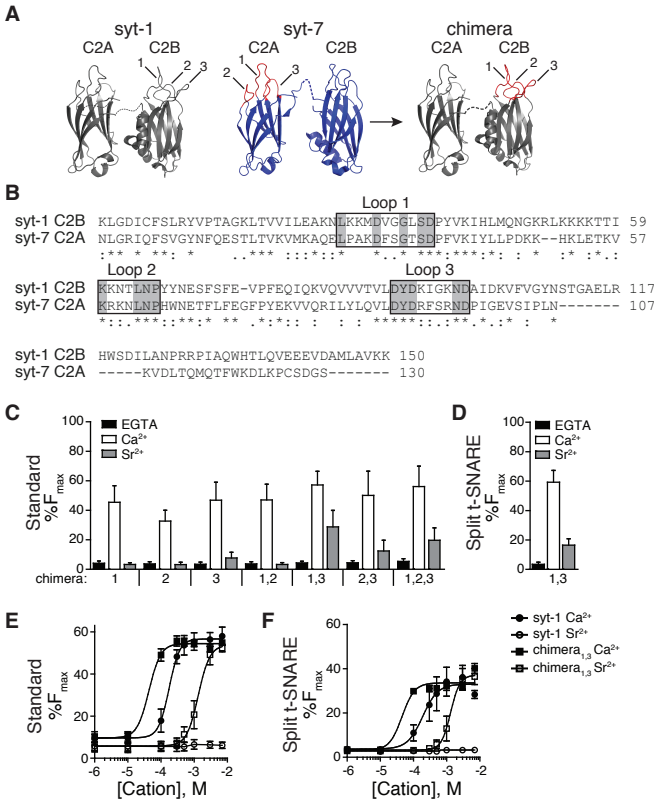

Figure 4. Engineering a Sr2+ activated syt-1/7 chimera. **(A)** Structural models depicting the cytoplasmic domains of syt-1 (gray; C2-domains reoriented from (Fuson et al., 2007)) and -7 (blue; C2A from PDB file 2D8K, C2B from (Xue et al., 2010)); these structures were oriented and connected with a dashed line using a drawing program. The metal binding loops of syt-1 C2B (gray) were replaced with the analogous loops from syt-7 C2A (red). **(B)** Alignment of syt-1 C2B and syt-7 C2A; metal binding loops are boxed; identical residues are highlighted in gray. **(C)** Chimeras were initially screened in the standard in vitro fusion assay. In Ca^{2+}, all seven constructs stimulated fusion; in Sr^{2+}, four constructs stimulated fusion, but chimera1,3 was the most active. **(D)** Chimera1,3 was further analyzed in the split t-SNARE version of the assay. For panels **(C)** and **(D)**, the extent of fusion after 80 min was plotted; N ≥ 3; error bars indicate SEM. **(E-F)** Scatter plots of cation titrations in the standard **(E)** and split t-SNARE **(F)** fusion reactions were carried out using the indicated free [cation] (Ca^{2+} or Sr^{2+}); error bars indicate SEM

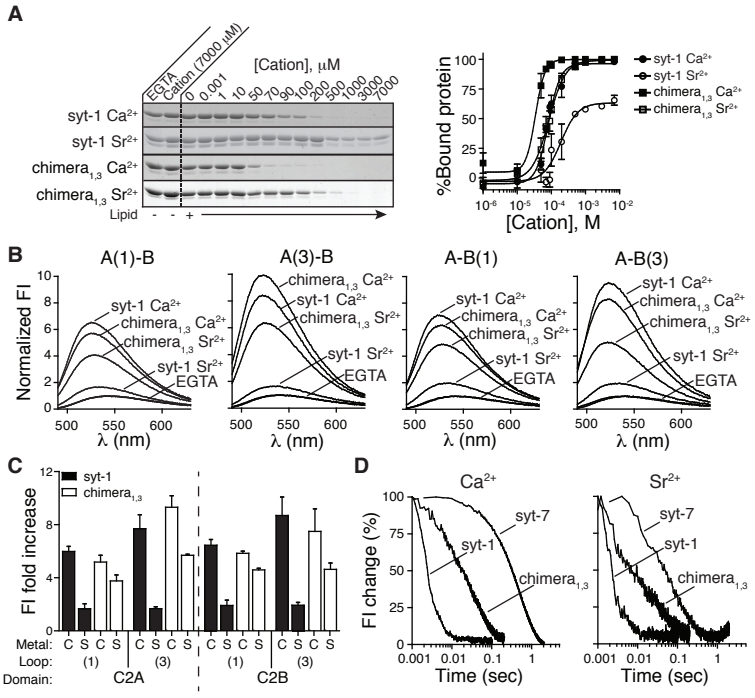

Figure 5. Chimera1,3 has altered membrane binding kinetics. **(A)** Binding of syt-1 and chimera1,3 to liposomes was monitored via co-sedimentation. Representative gels, showing protein depletion from the supernatant as a function of free [metal], are shown (Left). The percentage of bound protein was calculated (Right) and used to determine the [cation]1/2 and Hill coefficient for binding (Table 2). N ≥ 3, error bars and values indicate mean ± SEM. **(B)** Membrane penetration was monitored via an environmentally sensitive fluorophore, NBD, placed in loops 1 or 3 (indicated by brackets) in each C2-domain. Chimera1,3 efficiently penetrated membranes in the presence of Ca^{2+} or Sr^{2+}; Ca^{2+}, but not Sr^{2+}, triggered robust penetration of syt-1. Averaged spectra are shown; N ≥ 4. **(C)** Penetration data were quantified and plotted; Ca^{2+} or Sr^{2+} are denoted C and S, respectively; error bars indicate SEM. **(D)** Disassembly of sensor•cation•membrane complexes upon rapid mixing with EGTA; representative traces are shown (syt-1 kdiss; Ca^{2+} 394 ± 14, Sr^{2+} 327 ± 28 sec-1; syt-7 kdiss: Ca^{2+} 2.72 ± 0.54, Sr^{2+} 14.2 ± 4.5 sec-1; chimera1,3 kdiss: Ca^{2+} 43.3 ± 6.5, Sr^{2+} 41.7 ± 3.7 sec-1; N = 3).

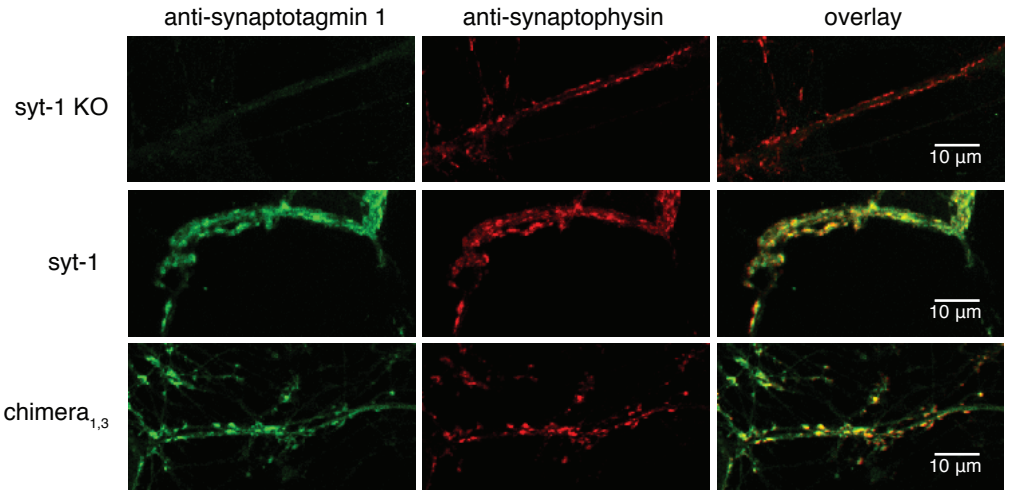

Figure 6. Chimera1,3 properly localizes to nerve terminals.
(A) Immunocytochemistry of cultured syt-1 KO neurons, showing the expression and synaptic localization of chimera1,3 and syt-1. Both proteins (green) colocalize equally well with synaptophysin (red; overlay in yellow). Quantitative colocalization (Pearson's correlation coefficient) of synaptophysin did not differ ($p>0.1$) between syt-1 and chimera1,3.

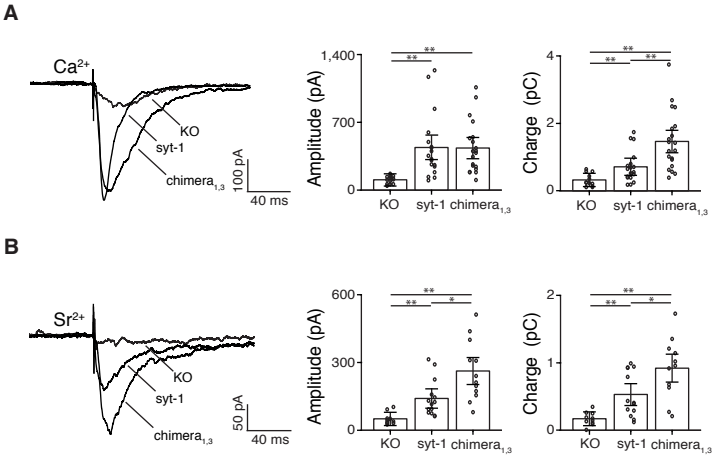

Figure 7. Chimera1,3 efficiently triggers glutamate release in Ca^{2+} or Sr^{2+}. (A) Upper: In Ca^{2+}, chimera1,3 rescued peak amplitude (pA) and increased total charge transfer (pC) relative to syt-1 or KO. **(B)** In Sr^{2+}, chimera1,3 increased charge transfer and amplitude relative to syt-1; KOs showed little release. Shown are averaged traces, N = 10-20 per condition from ≥ 3 independent litters.

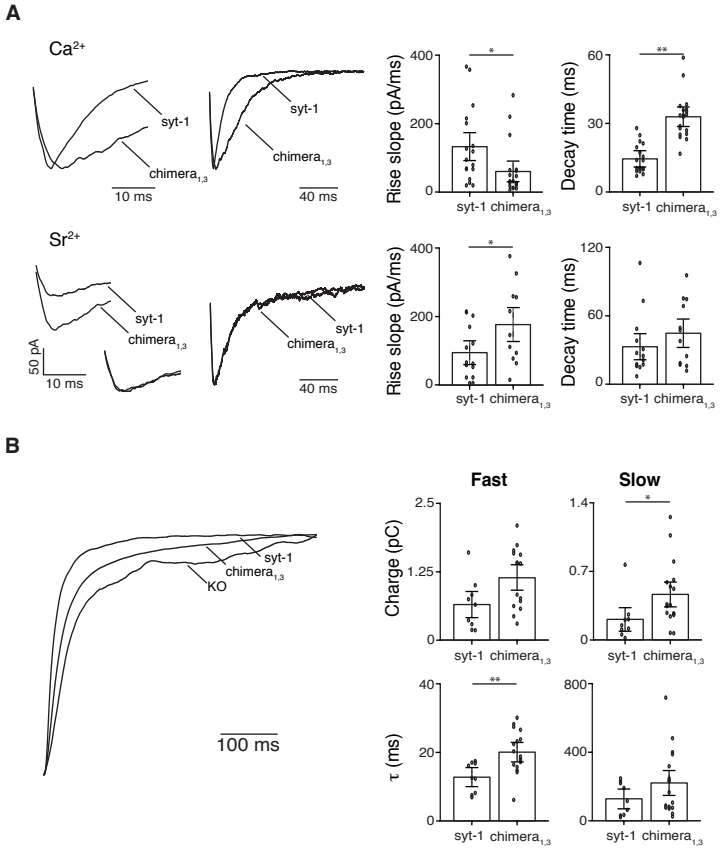

Figure 8. Chimera1,3 alters the kinetics of synaptic transmission. **(A)** Upper: In Ca^{2+}, chimera1,3 EPSCs evinced a slower rise slope (pA/msec) and longer decay time (msec) relative to syt-1. Amplitude-normalized average EPSCs (synchronized to the rising phase) are shown on two different time scales. Lower: In Sr^{2+}, chimera1,3 EPSCs showed a steeper, faster rise slope. No differences in decay kinetics were observed in Sr^{2+}. **(B)** Normalized cumulative charge transfer of data from Figure 5A, computed across 500 msec, in Ca^{2+}. Analysis of synchronous and asynchronous release, in Ca^{2+}, from neurons expressing chimera1,3 or syt-1. Double exponential functions were fit to the cumulative charge of each EPSC, and the amplitude and time constant (τ) of each component was quantified. Expression of chimera1,3 results in an increase in the amplitude of the slow charge component ($p < .05$), a non-significant trend towards an increase in the fast charge component ($p = .086$), and a longer decay τ for the fast component ($p < .01$).

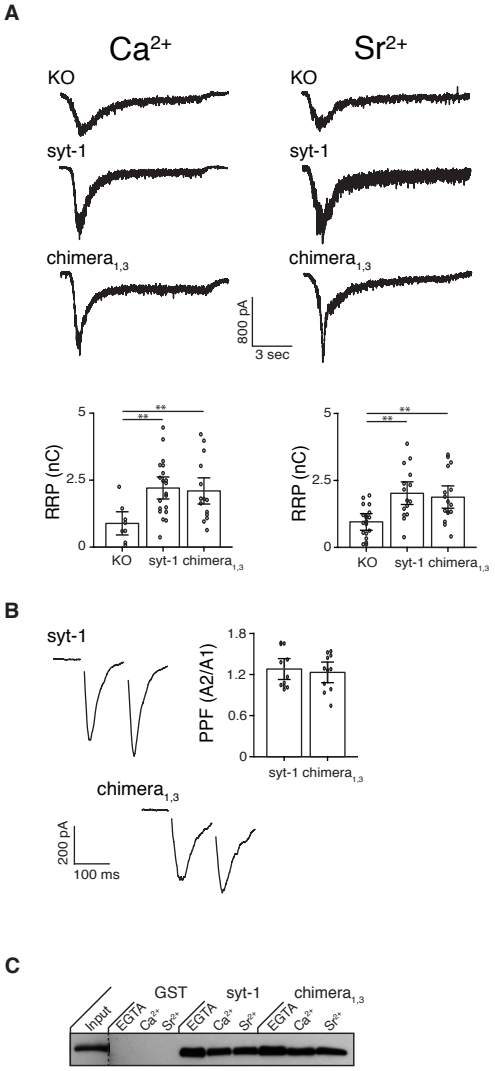

Figure 9. Chimera1,3 rescues the readily-releasable pool of SVs, and exhibits normal paired pulse facilitation and synprint binding activity.

(A) Chimera1,3 and syt-1 yielded equivalent RRPs (nC), as measured using hypertonic sucrose, in Ca^{2+} (Left) and Sr^{2+} (Right). The RRP was reduced in KO neurons in both metals. Representative traces are shown, N = 9-20 per condition from ≥ 3 independent litters. **(B)** Left: Average responses evoked by paired pulses (50 msec interstimulus interval) measured from neurons expressing syt-1 or chimera1,3. Right: paired pulse facilitation (PPF; quantified as the amplitude of the second response over the first) did not differ between conditions. N = 11 per condition. **(C)** Binding of the synprint peptide to syt-1 and chimera1,3 immobilized as GST fusion proteins; a representative immunoblot is shown. No differences were observed. GST was used as a negative control; N = 3.

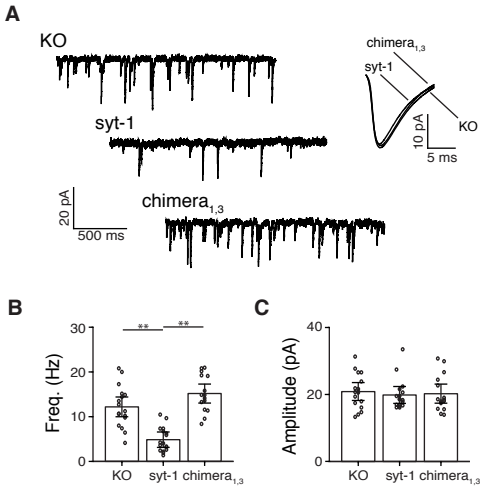

Figure 10. Chimera1,3 fails to clamp spontaneous vesicle exocytosis. (A) Spontaneous mEPSCs recorded from KO, syt-1, and chimera1,3 neurons; averaged mEPSC waveforms for each condition are shown on the right. **(B)** Chimera1,3 failed to clamp the increase in mEPSC frequency characteristic of the KO neurons; WT syt-1 efficiently clamped minis. **(C)** Amplitude of mEPSCs did not differ across conditions. N = 15-20 per condition from ≥ 3 independent litters of animals.

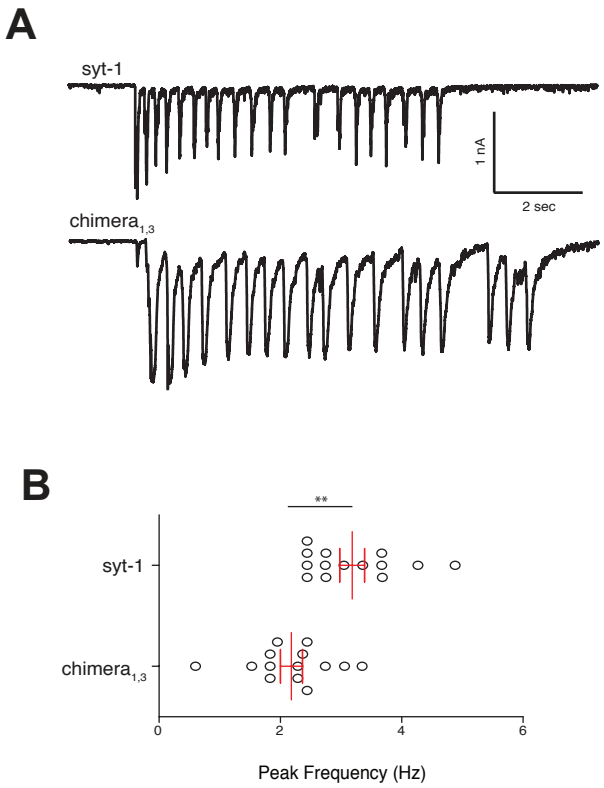

Figure 11. Chimera1,3 alters the frequency characteristics of population-level persistent reverberation. (A) Representative traces are shown. Each deflection represents overlapping EPSCs from a large number of neurons. The duration of oscillations (~7 sec) was unchanged across groups (p>.1). **(B)** Peak frequency of reverbratory episodes. Networks of neurons expressing chimera1,3 oscillated significantly slower.

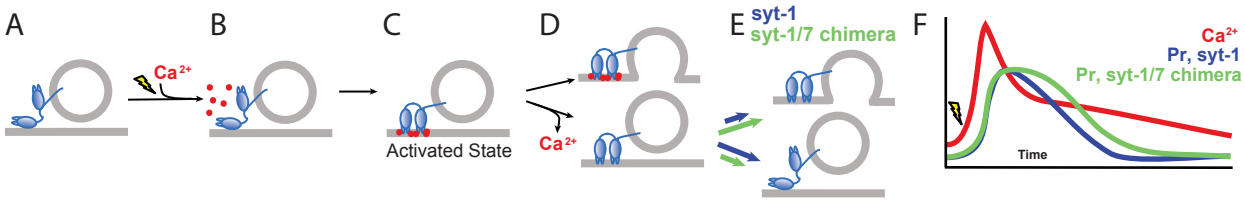

Figure 12. Syt-membrane interactions govern the timecourse of synaptic release. **(A):** Syt (blue) is shown on a synaptic vesicle. After Ca^{2+} influx during an action potential **(B)**, the flexible loops of Syt concurrently bind Ca^{2+} and anionic phospholipids in the plasma membrane **(C)**. This constitutes the activated state of Syt, and is characterized by the parallel orientation of the C2 domains. If this protein*Ca^{2+}*membrane complex stays bound sufficiently long, Syt will trigger synaptic vesicle exocytosis **(D, top)**. If Ca^{2+} dissociates prior to fusion **(D, bottom)**, Syt will either dissociate from the membrane **(E, bottom, blue arrow)** or remain bound and trigger exocytosis **(E, top, blue arrow)**. Chimera1,3 **(E, green arrows)** increases the dwell time syt remains on the membrane, increasing the likelihood that the sensor*membrane complex will trigger release. **(F)** Conceptual timecourse of synaptic release. The release probability (Pr) of terminals harboring Syt (blue) follows the timecourse of the presynaptic Ca^{2+} transient (red). Terminals expressing chimera1,3 (green) exhibit a wider window of high release probability, due to the slower dissociation kinetics of chimera1,3 from membranes.

Chapter 3:

Synaptotagmin 17 Controls Neuronal Development and Physiology Through Multiple Cellular Pathways

3.1 Background and Significance

Syt-17 is the most recently-discovered, and among the least-studied, members of the syt protein family. The 474 amino acid syt-17 (originally termed “B/K protein”, as discussed below) was first isolated from a rat brain cDNA library by Kwon et al. (1996), and recognized as a dual C2 domain protein possessing 36-44% sequence identity to syts 1-5. The protein is comprised of an N-terminal region (discussed below) and (like other syts) two C2 domains connected by a short, flexible linker. Structurally, syt-17 is an atypical syt isoform, insofar as it lacks the hydrophobic transmembrane domain characteristic of all other syts (Fukuda & Mikoshiba, 2001). Nonetheless syt-17 was reported to be associated with membranes in subcellular fractionation experiments, and this association was mediated by a string of cysteine residues near the N-terminus of the protein. Mutation of these seven cysteines (amino acid positions 19, 23, 26, 27, 30, 35, and 36) to alanines disrupted the association of syt-17 with membranes (ibid.). Additionally, the region near the N-terminus of syt-17 contains three putative Protein Kinase A (PKA) phosphorylation sites (starting at amino acids 92, 106, and 114). *In vitro* phosphorylation experiments, and overexpression experiments in the LLC-PK1 kidney cell line, revealed that these sites can indeed be phosphorylated by PKA (Chin et al., 2006).

The expression profile of syt-17 has been assessed at the mRNA and protein level. The original report describing syt-17 (Kwon et al., 1996) found high levels of

expression in brain (including cortex, hippocampus, hypothalamus, and olfactory bulb) and kidney tissues using Northern blotting and *in situ* hybridization (thus the original name for the protein: "B/K protein"). Another study (Chin et al., 2006) using Northern blotting found similar, but not identical results: syt-17 mRNA was detected in brain (cortex, hippocampus, hypothalamus, amygdala, substantia nigra, and pituitary), kidney, and prostate. These results in brain are in broad agreement with mRNA expression reported in the Allen Brain Atlas (http://mouse.brain-map.org/gene/show/74215), in which syt-17 mRNA was found at high levels in the olfactory bulb and piriform cortex, the hippocampus (in the *stratrum pyrmadidale* of the *cornu ammonis* subfields and granule cell layer of the dentate gyrus, consistent with endogenous expression in glutamatergic neurons), the thalamus and hypothalamus, and in a subset of cortical neurons (especially in superficial layers and cingulate cortex). At the protein level, endogenous syt-17 expression was subsequently confirmed in brain by Western blot, with the highest expression observed in hippocampus, and low levels detectible in cerebrum and the olfactory bulbs (Fukuda & Mikoshiba, 2001). Interestingly, this study failed to identify syt-17 protein expression in any non-brain tissues, including kidney (Fig. 2A of Fukuda & Mikoshiba, 2001). This indicates that the term "B/K protein" is a misnomer (hence our use of "syt-17" throughout), and that the protein is exclusively expressed in brain, chiefly in hippocampal neurons. The differences between expression profiles using mRNA and protein is not unusual for syt isoforms, as many laboratories in the field have observed that the presence of syt mRNA is not a consistent predictor of syt protein expression (Li et al., 1995; Chapman lab, unpublished observations; Mikoshiba lab, unpublished observations). This potentially suggests that

expression of many syt isoforms (including syt-17) is regulated at the translational, rather than transcriptional, level. Another study examined syt-17 protein expression exclusively in brain, using a different polyclonal antibody, and found syt-17 expressed in hippocampal neurons (evidently in excitatory cells, though no costain for GABAergic markers was performed), the olfactory bulb, the hypothalamus (in vasopressin-positive cells), and the pituitary (Lee et al., 2001). Subsequent proteomic studies further confirmed the expression of syt-17 protein in hippocampus *in vivo* and cultured neurons (Sharma et al., 2015, and E. Bomba-Warzak, unpublished observations). In sum, all studies to assay for syt-17 expression, regardless of methodology, agree that syt-17 is expressed in hippocampal neurons (apparently in glutamatergic neurons). Evidence for expression in other brain regions is more mixed, but expression is often detected in the hypothalamus and olfactory bulb.

The subcellular localization of syt-17 is a matter of debate. One group reported that overexpressed syt-17 localizes to the trans-golgi network (Fukuda & Mikoshiba), another reported syt-17 is present in the ER and mitochondria (Jang et al., 2004). One study found syt-17 expression in hippocampal neurons is restricted to the soma (Lee et al., 2001). A subsequent study found that in hippocampal neurons, overexpressed syt-17 is exclusively axonal, and largely localized presynaptically (Wong et al., 2015). Yet another study found exogenous syt-17 is expressed throughout the neuron (axonal, dendritic, and somatic compartments) and shows no synaptic localization (Dean et al., 2012). In sum, no consensus exists on the location (or locations) of syt-17 in cells. Heterogeneity in methodology (use neuronal vs. non-neuronal cells, use of unvalidated

antibodies, variability in expression levels of exogenously-expressed fusion proteins, etc.) likely underlies the confusion.

Several studies have implicated (intronic) single-nucleotide polymorphisms of syt-17 in autism-spectrum disorders (Wang et al., 2009; Connolly et al., 2013). Though no function (molecular or cellular) has been described for syt-17, several studies have noted that syt-17 is upregulated following various conditions of stress. Jang et al. (2004) reported an increase of syt-17 expression in rat hippocampus following kainite-induced seizures, and in PC12 cells following pharmacological induction of ER stress (with thapsigardin). Transient ischemia has also been reported to upregulate syt-17 expression in retinal (Ju et al., 2000) and kidney (Lee et al. 2001; Han et al., 2007) cells.

More recently, our laboratory found that syt-17 localized to mobile vesicles in axons, and that these vesicles recycled in a manner more consistent with large dense-core vesicle recycling than synaptic vesicle recycling (Dean et al., 2012). This experiment was conducted using syt-17 tagged with a pHluorin, a pH-sensitive variant of GFP whose fluorescence is quenched at acidic pH (i.e., inside acidified vesicles). Expressing a pHluorin inside a vesicle thus allows a direct readout of exocytosis – fluorescence increases upon fusion of an acidified vesicle with the plasma membrane (thus bringing the pHluorin into contact with the extracellular space at pH 7.4). Thus, the results of Dean et al. (2012) would seem to indicate that some fraction of exogenously-expressed syt-17 exists in the lumen of vesicles which undergo exocytosis. However, we have subsequently determined (D. Ruhl & Joseph Briguglio, Chapman lab, unpublished observations) that the cloning strategy employed in this study was likely to

sort the overexpressed syt-17 to non-physiological compartments (syt-17 localization is discussed further below). At present, the only inference that can be safely be made on syt-17 function is that the protein appears to be upregulated under conditions of ER stress.

In sum, syt-17 is an unusual, membrane-associated syt isoform expressed in neurons (especially hippocampal) and potentially other tissues. No function of syt-17 has been determined, and the subcellular localization is not established, but expression of the protein appears to be upregulated in conditions of ER stress. In the present work, we analyzed syt-17 biochemically, and localize it in primary hippocampal neurons to both the golgi and rab5-positive endosomes. We performed the first characterization of a syt-17 knockout mouse, and found that deletion of syt-17 results in impaired neurite outgrowth, a deficiency in early secretory trafficking, and an ER stress response that results in a global downregulation of protein translation. Additionally, neurons lacking syt-17 show substantial enhancement of glutamatergic synaptic transmission attributable to a pathological accumulation of AMPA-type glutamate receptors on the postsynaptic membrane (presumably the consequence of an endocytic defect). We conclude that syt-17 is a multifunctional regulator of intracellular protein trafficking in excitatory hippocampal neurons, modulating both neural development and synaptic physiology.

3.2 Materials and Methods

Ethics Statement

All experiments were conducted at the University of Wisconsin-Madison, and protocols were reviewed and approved by the Animal Care and Use Committee (assurance # A3368-01). The guidelines set by the NIH *Guide for the Care and Use of Laboratory Animals* handbook were followed in all cases.

Generation of Knockout Mice & Cell Culture

The syt-17 knockout mouse employed in this study was generated from ES cell clone EPD0659_3_A09, acquired from the KOMP repository (www.komp.org), by the Wellcome Trust Sanger Institute (WTSI). WTSI and the Children's Hospital Oakland Research Institute generated the targeting vectors as part of the Knockout Mouse Project (3U01HG004080; methods described in Skarnes et al., 2011).

Primary hippocampal neurons were harvested from newborn (P0) mice and cultured essentially as described (Yeh et al., 2010). All reagents were purchased from Sigma except as indicated below. Briefly, hippocampi (CA subfields) from each pup in a litter were dissected and incubated in 0.25% trypsin-EDTA Corning, 20mM D-Glc, and 25U/mL DNase for 22 minutes. Tissue was washed twice, mechanically dissociated, and plated on poly-D-lysine (Life Technologies) coated glass coverslips in a solution of Dulbecco's Modified Eagle Medium (Gibco) with 10% fetal bovine serum. Once cells attached (<1hr), media was changed to a growth media consisting of Neurobasal-A (GIBCO) supplemented with 2% B27 (GIBCO) and 2mM Glutamax (Invitrogen). Cultures were maintained in a 5% CO2-humidified incubator at 37°C; 1/3 of the media

volume was replaced every three days, as we have found this “feeding” scheme optimal for neuronal health. All other reagents were purchased from Sigma except as indicated below.

Statistics and analysis

Image analysis was performed in ImageJ (Schneider et al., 2012) and MATLAB (Mathworks), and electrophysiology data were analyzed with Clampfit 10.2 (Molecular Devices) except where otherwise noted; statistical analysis was performed in Prism software (GraphPad). Significance was assessed with Students t-test or Mann-Whitney tests, as appropriate.

Cell Culture and Transfection

Most transfections were performed using the Ca^{2+}-phosphate method described in Jiang and Chen (2006) at 3DIV. For experiments imaging fluorescent proteins in young (2-4 DIV) neurons, transfection was performed with an Invitrogen Neon electroporation system. For experiments using VSVG-YFP-2xUVR8, transfections were performed using Lipofectamine LTX at 6DIV (24-36 hours before the experiment) according to the manufacturer’s instructions, as prolonged expression of this probe results in “leak” to the plasma membrane.

Live-Cell Imaging & Analysis

Measurements of axonal outgrowth were performed at 2-4DIV on an Olympus CellTIRF with DIC optics using a 60x Apo N objective. Only cells that were identifiably

stage 3 (extending axon at least 2-3x longer than other neurites), with visible growth cones, whose axons were not growing along processes of other cells, were selected for imaging. Neurons were maintained in their native grown media in an environmentally-controlled chamber with 5% CO2 at 37 degrees; typical imaging duration was 8-12 hours (1 min interval). Outgrowth rate, growth cone area, and spontaneous growth cone collapse were measured offline in MetaMorph software (Molecular Devices).

Live-cell imaging of overexpressed fusion proteins was conducted similarly, at ages indicated in the text. Measurements of ER-to-Golgi trafficking using VSVG-YFP-2xUVR8 were performed on an Olympus IX81 inverted microscope with a Lambda DG-4 light source and an Olympus 60x Plan Apo N objective (z-series collected every 30s for 40min) at 7-8DIV (pilot experiments showed this to be the optimal window for expression). For uncaging, a 300nm fiber-coupled LED (ThorLabs M300F2) was positioned ~.5cm above the cell media, and the sample was illuminated for 10s. Offline, a small ROI was drawn in the cis-golgi (verified by GM130 staining, data not shown, but see Chen et al., 2013) and the timecourse of cargo accumulation was quantified for each cell. Internalization of fluorescently-labelled transferrin-546 (25ug/mL, ThermoFisher) and Thioflavin T (5um, ThermoFisher; Beriault & Werstuck, 2013) was monitored on an upright Olympus FV100 confocal laser-scanning confocal microscope with a 60x LUMFL water immersion objective in an environmentally-controlled chamber.

For Ca^{2+} imaging, 13-15DIV neurons were depolarized with 40mM KCl and loaded with 14.8uM FM-464 (Thermo Scientific) for 10min to label synaptic boutons. Cells were washed with artificial cerebrospinal fluid (ACSF) containing 128mM NaCl, 5mM KCl, 2mM CaCl2, 1mM MgCl2, 30mM Glc, and 25mM HEPES (pH 7.4, mOsm

310). For this wash step, ACSF was supplemented with 1mM ADVASEP-7 (Sigma). Cells were then loaded with 13.6 uM Fluo-5F AM (with 1% Pluronic F-127, Thermo Scientific) for a further 10min, washed, and transferred to a field stimulation chamber. Imaging was performed on an Olympus CellTIRF with a 60X Apo N objective. Imaging fields of view were selected to maximize the number of boutons (visualized by FM4-64) on isolated processes, taking care to avoid glia (identifiable by morphology, kinetics of evoked Ca^{2+} responses, and/or high resting Ca^{2+} signal). Images were acquired 100 Hz with 2x2 pixel binning (482 nm excitation). During imaging, 50uM D-APV (Abcam), 100 um picrotoxin (Tocris), and 10 um CNQX were included in the ACSF. Atypically-large FM-464 puncta (likely representing either endosomes or closely adjacent boutons) were excluded from analysis. Ca^{2+} responses were quantified from individual boutons following a single action potential, converted to $\Delta F/F_0$ (change in fluorescence divided by baseline fluorescence), and the peak of each response was extracted.

Imaging of GluR2-pHluorin (Addgene plasmid #24001) was performed on the same CellTIRF setup as described above, substituting 0.5 μM tetrodotoxin (TTX, Abcam) for APV/CNQX/picrotoxin in the ACSF. Soluble mRuby2 was cotransfected with the pHluorin constructs to visualize dendritic morphology. To determine the surface expression level, cells were alternatively perfused with acidic ACSF (25mM N-morpholino] ethane sulphonic acid substituted for HEPES, pH 5.5) or ACSF with ammonium chloride (50mM NH4Cl and 38mM NaCl). ROIs were selected on dendrites and spines (visible as puncta in during NH4Cl perfusion), and surface expression was calculated as ((pH 7.4 fluorescence – pH 5.5 fluorescence)/(NH4Cl fluorescence – pH

5.5 fluorescence)) x 100 (Gordon et al., 2011). Greater >10 synapses across multiple dendrites were measured for each cell.

Fixed-Cell Imaging & Analysis

Morphological analysis of axon lengths, dendritic arbors, and spine morphology were performed by sparsely-transfecting cells with GFP, fixing the cells in 4% paraformaldehyde at the appropriate DIV (7DIV for axons, 15DIV for dendrites and spines), and immunostaining for the GFP (Abcam). This allowed full reconstruction of transfected cells. For most measurements, immunostaining against MAP2 was also performed to ensure accurate identification of axons and dendrites. Coverslips were imaged on an Olympus FV1000 confocal microscope with a 20x XLUMPlanFL N, 60x PlanApo N, or 100x UApo N objective. Resultant neurite arbors were reconstructed in ImageJ. Sholl analysis was performed according to Ferreria et al. (2014).

To quantify protein translation in WT and KO neurons, the Click-It Plus OPP Protein Synthesis Assay Kit (Thermo Fisher) was used. Coverslips were incubated with 0.5uL/mL OPP reagent for two hours, fixed, and stained. Phalloidin-546 and NuclearMask-405 were included as counterstains.

Electrophysiology

Whole-cell patch-clamp recordings were acquired from 13-16DIV neurons using a MultiClamp 700b amplifier and pClamp software (Molecular Devices). Patch pipettes (3-5 MΩ resistance) were filled with an intracellular solution containing 135mM cesium-methylsulfate, 5mM KCl, 2mM NaCl, 0.2mM EGTA, 10mM HEPES, 10mM Na2-

phosphocreatine, 5mM MgATP, 0.3mM Na2-GTP. 5mM QX-314 was included in the patch pipette for evoked EPSC recordings to prevent depolarization of the postsynaptic neuron. The recording chamber was continually perfused with an ACSF containing 128mM NaCl, 5mM KCl, 2mM CaCl2, 1mM MgCl2, 30mM Glc, 25mM HEPES, 50um APV, and 100 um picrotoxin (pH 7.4, mOsm 310). Postsynaptic (putative pyramidal) neurons were clamped at -70mV. Measurements were aborted if a series resistance >15 MΩ was observed, or if the series resistance changed > 10% during recording.

For evoked EPSC recordings, a bipolar electrode in theta glass was positioned at the soma of a neuron adjacent to the patched cell and a single biphasic pulse was applied. The stimulation voltage (using a Warner A350 stimulus isolator) was set at 5V and gradually increased to ensure the resulting response was unitary. EPSCs that lacked a smooth rising phase (potentially suggesting disynaptic excitation) were excluded from analysis. For measurement of mEPSCs, 0.5 um tetrodotoxin was added to the bath and spontaneous quantal currents were recorded for >3 min. Miniature events were identified using a template-matching algorithm in Clampfit.

For glutamate puffing experiments, neurons were first filled with 0.2% of Alexa 488 Biocytin (ThermoFisher) in intracellular solution through the patch pipette to visualize morphology. Cells that did not exhibit a pyramidal-like morphology, with a clear apical dendrite, were excluded. Subsequently, a second patch pipette containing ACSF with 200 um L-glutamate and 200um Alexa 488 Hydrazide (ThermoFisher) was positioned along the main (apical) dendrite ~60um away from the soma. Fluorescence from the stimulation pipette and membrane current during the patch cell were monitored during approach to ensure minimal leak. Pulses of glutamate were then applied for 5ms

with a Picospritzer III (Parker) as the cell holding voltage was varied from -70 to +40mV in 22mV increments. The ejection of the glutamate/dye was visually monitored during the experiment. The stimulation pipette was moved closer to the dendrite each trial. When the pipette was moved close enough to rupture the cell (and the patch was lost), the previous trial was selected for analysis.

Recombinant proteins and protein purification

cDNA encoding the C2AB domain of rat syt-1 (residues 96–421) was provided by T. C. Südhof (Stanford University); the D374 mutation was corrected by replacement with a glycine. Syt17 was provided by M. Craxton (MRC Laboratory). Syt-1 C2AB, syt17 C2AB and Syt17 C2B were subcloned into pGEX vectors to generate GST-tagged fusion proteins, which were purified as previously described (Evans et al., 2015).

In vitro fusion assays

The following lipids were purchased from Avanti Polar Lipids: 1-palmitoyl-2-oleoyl-*sn*-glycero-3-phosphoethanolamine [phosphatidylethanolamine (PE)]; 1,2-dioleoyl-*sn*-glycero-3-phospho-l-serine [phosphatidylserine (PS)]; 1-palmitoyl-2-oleoyl-*sn*-glycero-3-phosphocholine [phosphatidylcholine (PC)]; 1,2-dipalmitoyl-*sn*-glycero-3-phospho-ethanolamine-*N*-(7-nitro-2–1,3-benzoxadiazol-4-yl) (NBD-PE);*N*-(lissamine rhodamine B sulfonyl)-1,2-dipalmitoyl-*sn*-glycero-3-phosphoethanolamine (rhodamine-PE); and 1,2-dioleoyl-sn-glycero-3-phosphoethanolamine-*N*-(5-dimethylamino-1-naphthalenesulfonyl) (dansyl-PE).*N*,*N*′-dimethyl-*N*-(iodoacetyl)-*N*′-(7-nitrobenz-2-oxa-1,3-diazol-4-yl)ethylenediamine (IANBD-amide) was purchased from Invitrogen.

SNARE-bearing vesicles were prepared as described previously (Chika et al., 2008). Lipid compositions for the vesicles used in the *in vitro* fusion assays: 15% PS, 27% PE, 55% PC, 1.5% NBD-PE, and 1.5% rhodamine-PE for v-SNARE vesicles; 15% PS, 30% PE, and 55% PC for heterodimer t-SNARE vesicles; and 25% PS, 30% PE, and 45% PC for syx-only t-SNARE vesicles. .

Fusion between v-SNARE vesicles and heterodimer, or syx-only t-SNARE, vesicles was monitored using a Synergy HT multidetection microplate reader (Bio-Tek) as described previously (Chika et al., 2008; Liu et al., 2014). For standard assays 1 μm of the indicated syt fragments was used. For the protein titration 0 – 10 μm of syt-1 C2AB or Syt17 C2AB was used. 7 μm soluble SNAP-25B was used in the split t-SNARE assays. During each run, 1 mm final free Ca^{2+} or EGTA was added at 20min, and the reaction was monitored for an additional 120 min. Traces were normalized to the first timepoint and the maximum fluorescence signal, determined from the addition of *n*-dodecyl-β-d-maltoside, to determine the $\%F_{max}$.

ITC

Syt-1 C2AB and syt17 C2AB were dialyzed overnight against 50 mM HEPES-NaOH (pH 7.4), 200 mM NaCl, and 10% glycerol; in order to remove divalent cations, the buffer was pre-treated with Chelex-100 resin (Bio-Rad). Filtered dialysis buffer was used to make all protein and Ca^{2+} dilutions. Samples were degassed before each experiment. Heat of binding was measured by 20 consecutive injections of Ca^{2+} into a sample cell containing the protein of interest. Corrections for heat of dilution were done

by subtracting the signal of Ca^{2+} into buffer. Experiments were performed using a MicroCal iTC_{200} (Malvern Instruments).

3.3 Results

We first characterized recombinant syt-17 using an in vitro fusion assay in which the dual C2 domains (C2AB) of syt-17, Ca^{2+}, and SNAP-25 are added to a mixture containing VAMP2- and Syntaxin-1a-bearing liposomes. This assay has been used extensively to determine the role of syt-1 in membrane fusion (ex, Bhalla et al., 2006). We found that syt-17 did not mediate membrane fusion in vitro with this complement of SNARES/lipids (Fig. 13A-B). It has been noted (Chin et al., 2006) that, of the five putative Ca^{2+} binding aspartic acid residues in syt-1 C2A domain, three are not conserved in syt-17. To assay for Ca^{2+} binding activity, we performed isothermal titration calorimetry on syt-17 C2AB, and found no apparent binding to Ca^{2+} (Fig. 13C). Syt-17 is thus a rather unusual syt isoform, lacking both Ca^{2+} binding to it's C2 domains and a transmembrane domain.

To examine to localization of syt-17 in developing hippocampal neurons, we transfected cells with syt-17 tagged with superecliptic pHluorin in 3 DIV neurons (Fig. 14A, left). Two pools of overexpressed syt-17 were obvious: a large immobile pool in the soma, and smaller puncta that trafficked antero- and retrogradely in neurites (Fig. 14A, right). We observed that the resting fluorescence of syt-17-pHluoin was much higher than pHluorin fusions to other syt isoforms, and noted that the observed fluorescence distribution is unchanged upon addition of 40mM NH4Cl to the imaging media to alkalize intracellular compartments and dequench any pHluorin expressed in

acidified compartments (data not shown). This indicates that syt-17 is not expressed in the lumen of any acidified compartment. The immobile somatic pool of syt-17 subjectively resembled the golgi complex. As such, we performed two-color imaging using syt-17-pHluorin and a mRuby-mannosidase-II to label the golgi (Fig. 14B). The somatic fraction of syt-17 did indeed appear to localize to the golgi. The behavior of the mobile syt-17 puncta in neurites subjectively resembled rab-positive endosomes (Dr. Anjon Audhya, unpublished observation). We thus coexpressed syt-17-mRuby with rab5-GFP (Fig 14C) or rab7-GFP (data not shown). Close to 100% of small syt-17 puncta colocalized with rab5-GFP. We have found that overexpression of syt isoforms can induce spurious localization results, as some syts can “spillover” to non-physiological compartments when dramatically overexpressed (Chapman lab, unpublished observations). As such, we repeated this localization using syt-17 overexpressed at very low levels (using lentivirus instead of sparse transfection) with a Halo-tag instead of a pHluorin tag (permitting the use of extremely bright Janelia-Fluor dyes, thus allowing us to localize the protein in low-expressing cells). The same pattern of localization was observed (data not shown). Finally, all experiments were performed in parallel using constructs with the pHluorin tag on both the N- and C-termini of the protein, no differences were observed (data not shown), increasing our confidence that the fusion protein is not missorted. Syt-17 is thus expressed in two compartments – one pool in the golgi, and one on early endosomes.

To determine the role of syt-17 in neuronal cells, we obtained a recently-generated syt-17 knockout mouse (KOMP, 3U01HG004080, allele diagram in Fig. 15A). Successful knockout was confirmed with RTPCR of brain and kidney tissue obtained

from P15 mice (Fig. 15B). We noticed, anecdotally, that modulating levels of syt-17 in cells seemed to affect neurite morphology. We therefore performed long-term differential interference contrast (DIC) imaging of neurite outgrowth in an environmentally-controlled chamber (37deg, 5% CO2) at 2-3 days in vitro (DIV; Fig 16A).

Cultured hippocampal neurons stereotypically progress through several distinct stages in their initial development (Dotti et al., 1988): at stage one no neurites are evident, only filopodia and flattened lamellipodia extend from the soma; at stage two several neurites are visible and growing slowly, but there is no obvious polarization into axonal and dendritic domains; at stage three the neuron has polarized and possesses a clear axon (or occasionally >1 axon) that is growing substantially faster than other processes. Syt-17 KO neurons show no difference in outgrowth rate at stage two (Fig. 16B, left, $p>.1$). However syt-17 KO stage three neurons showed a substantially slower rate of axonal outgrowth (Fig. 16B, right, $p=.006$), extending axons approximately half as fast as WT neurons. Further, while knockout neurons exhibited a similar number of primary neurites (Fig. 16C; $p>.1$), their growth cones were less stable – we observed a higher rate of spontaneous growth cone collapse in KO neurons (Fig. 16D, $p=.004$). When we monitored growth cones at higher (100x) magnification, we observed that axonal growth cones in syt-17 knockouts were significantly smaller (Fig. 16E, $p=.03$). Phenomenologically, this appeared to manifest as a lack of prominent lammelipodia in KO neurons. Syt-17 knockout neurons thus exhibit multiple deficits in axonal outgrowth: their axons extend more slowly, and their axonal growth cones collapse more often (thereby affording less time for growth).

To assay morphology in more mature cells, we sparsely transfected neurons with GFP at 3DIV. Consistent with the observed early outgrowth deficits, syt-17 KO neurons exhibit shorter axons when measured at 7DIV (Fig. 17A-B, $p<.001$). To determine if this stunted morphology was specific to axons, we examined dendrite morphology at 14DIV, and found the dendritic arbors of syt-17 KO neurons were stunted and less complex (by Sholl analysis, Ferreria et al., 2014; Fig. 18A-B), and average dendritic length was shorter (Fig. 18C, $p<.001$). We overexpressed syt-17 in WT neurons, and found that overexpression increased axon length (Fig. 19A, $p=.003$). Interestingly, the overexpression phenotype was specific to axons, as overexpression of syt-17 has no effect on dendritic morphology (Fig. 19B-C, $p>.1$).

The fact that much of syt-17 localizes to the golgi prompted us to wonder if the stunted neurite morphology could be due to an alteration in secretory trafficking. We assayed for alterations in trafficking of an exogenously expressed cargo from the endoplasmic reticulum (ER) to the early golgi (Hirschberg et al., 1998). We used VSVG-YFP-2xUVR8 (Chen et al., 2013). The UVR8 domain on this probe forms aggregates in basal conditions, and these aggregates accumulate in the ER (Fig. 20A, left; also see Chen et al., 2013). Upon illumination with 300nm light, UVR8 undergoes a conformational change that disrupts this aggregation (Wu et al., 2012), and individual probes become diffuse in the ER (Chen et al., 2013, and Fig. 20A, second column). The disaggregated probe can then move through the secretory pathway, and can be observed accumulating in the golgi (Fig. 20A, right). To determine if trafficking in the early secretory pathway is perturbed in syt-17 KO, we monitored the timecourse of VSVG-YFP-2xUVR8 accumulation in the early golgi after disaggregating the probe with

a pulse of 300nm light. In neurons lacking syt-17, the probe accumulates more slowly in the golgi following uncaging (Fig. 20B-C, p=.03), indicating that the kinetics of early secretory trafficking are slowed in the KO.

A dysfunction in trafficking from ER to golgi would be predicted to produce a stress response in the ER. Indeed, earlier reports noted that syt-17 expression is upregulated in ER stress states (ex., Ju et al., 2000). Accumulation of proteins in the ER that cannot be efficiently trafficked to the golgi triggers the Unfolded Protein Response (UPR, reviewed in Oslowski & Urano, 2011 and Lindholm et al., 2017). The fluorescent small molecule Thioflavin T can be used to directly probe for such ER stress in live cells, as the cell permeant probe will bind to aggregated and misfolded proteins accumulating in the ER during UPR states (Beriault & Werstuck, 2013). We incubated 7DIV WT and syt-17 KO neurons with Thioflavin T for 30m and measured somatic fluorescence with confocal LSM (a far-red impermeant plasma membrane dye, ThermoFisher, was included as a counterstain and used to trace somata). Fluorescence intensity was significantly increased in the KO (Fig. 21A-B, p<.001), and KO neurons often exhibited bright somatic puncta rarely observed in WT neurons. This indicates that syt-17 KO neurons, under basal conditions, operate under conditions of ER stress.

Under UPR conditions, to avoid apoptosis secondary to pathological protein accumulation, protein translation is globally (or near-globally) downregulated (Lindholm et al., 2017). To probe depressed for protein translation in syt-17 KO, we used a tagged puromycin (OPP), which binds to translating proteins as they emerge from the ribosome (this approach is derived from the FUNCAT method, which has been used extensively to study protein translation in neurons and other primary cells; Dietrich et al., 2010; Hsu

et al., 2015; Kos et al., 2016). These OPP-tagged proteins accumulate in the cytosol, and the OPP can be subsequently conjugated to a fluorophore. Following tagging, cytosolic fluorescence thus provides a readout proportional to the total amount of protein translated during the incubation period (Dietrich et al., 2010). We incubated WT & KO neurons in OPP for two hours, with the addition of either 100ng/uL BDNF (which is known to upregulate translation in neurons, ex., Inamura et al., 2005) or 40uM cycloheximide (which inhibits protein synthesis at the translocation step, Schneider-Poetsch et al., 2010). Cells were then fixed/permeablized, pocolyl azide-Alexa 647 was conjugated to the OPP, and coverslips were incubated with phalloidin and NuclearMask dyes as counterstains (Fig 22A, insets). As expected, in both genotypes BDNF increased, and cycleheximide abolished, labelling intensity (Fig. 22B, $p<.001$ in both genotypes), indicating that this approach can indeed be used as a readout of newly-synthesized protein. We detected a significant reduction (by ~30%) of labelling intensity in knockout neurons (Fig. 22B, $p<.001$), indicating that (in basal conditions) syt-17 knockout neurons exhibit depressed protein translation. The defect in secretory trafficking and depressed protein translation provide a plausible explanation for the outgrowth defects observed in syt-17 knockout neurons (see discussion below).

We also examined synaptic physiology in neurons lacking syt-17. Cultured hippocampal neurons (14 DIV) were patch clamped, and adjacent neurons were stimulated with brief square-wave voltage pulses to stimulate neurotransmitter release. AMPA-mediated currents were isolated pharmacologically. We found a dramatic and unexpected upregulation of evoked EPSCs in neurons lacking syt-17, the amplitude of AMPA-mediated responses was approximately doubled in KO neurons (Fig. 23A-B,

p=.003). The kinetics of evoked responses were unchanged, as rise (Fig. 23C, p>.1) and decay (23D, p>.1) times were unaltered in the KO.

Such an upregulation of evoked excitatory neurotransmission could be attributable to several possible mechanisms. The increased EPSC amplitude could be due to augmented presynaptic release secondary to alterations in Ca^{2+} signaling (i.e., an increase in Ca^{2+} influx in the KO increasing release probability). To probe for alter presynaptic Ca^{2+} influx, we depolarized neurons with 40mM KCl in the presence of the fluorescent stryl dye FM-464, and washed the cells following a 10m incubation to allow endocytosis of the dye. Following the wash, fluorescent puncta (in axons) delineate boutons that have undergone exo-/endocytosis during dye application. Neurons were then loaded with 13.6 uM Fluo-5F-AM cell permeant Ca^{2+} dye at 37 deg and subject to a final wash. This dye has a K_d of 2.3uM, is therefore unlikely to saturate during presynaptic Ca^{2+} influx, and so is ideal to probe for differences between genotypes. Neurons were loaded into a field stimulation chamber (Warner) and imaged on an Olympus CellTIRF at 60x. Responses of individual axonal boutons to single action potentials were monitored, converted to deltaF/F, averaged, and compared across genotypes. No significant difference in Ca^{2+} influx was observed (Fig. 24A-B).

Alternatively, the increase in synaptic response could be secondary to an increase in the per-neuron density of synapses in syt-17 KO neuron (without any functional change in the synapses themselves). To assay for synaptic density, we fixed 14 DIV neurons, immunostained for vGlut (a presynaptic marker) and PSD-95 (a postsynaptic marker), and quantified the density of colocalized puncta (i.e., those positive for both markers) along dendrites (Fig. 25A). No increase was evident in syt-17

KO, and indeed we observed a slight (non-significant) trend towards *fewer* synapses per unit dendrite in syt-17 KO (Fig. 25B, p=.06). This indicates that the augmented EPSCs observed in syt-17 KO are not due to an upregulation in the number of synapses.

We next measured the response of postsynaptic neurons to the spontaneous release of individual synaptic vesicles, so-called “miniature” release (Fig. 26A). We found that the amplitude of quantal synaptic currents was significantly increased in syt-17 KO neurons (Fig. 26B, p=.006). The frequency of spontaneous release (Fig. 26C, p>.1) was unaltered, as was the rise (Fig. 26D, p>.1) and decay (Fig. 26E, p>.1) kinetics of the response to quantal events. Such an augmentation of quantal response amplitude is generally interpreted to indicate an increase in postsynaptic receptor activity or surface expression (ex., Willaims and Featherstone, 2014), although it is possible such a change could occur with a presynaptic locus if, for example, the average synaptic vesicle contained more neurotransmitter in KO neurons than WT.

To confirm a postsynaptic locus for the elevated EPSCs, we bypassed the presynapse entirely, and directly stimulated postsynaptic neurons with brief pulses of glutamate applied with a Picospritzer (Parker). Neurons were patched and filled with Alexa-488-biocytin to visualize dendritic morphology. Only neurons with an obvious pyramidal-like morphology (possessing an elliptical soma, visible dendritic spines, a clear main/apical dendrite, and some number of small basal dendrites) were stimulated. A patch pipette containing 200uM L-glutamate and Alexa-488-hydrazide was positioned ~60um from the soma of the patched neuron, along the main dendrite. Fluorescence in the stimulus pipette and membrane voltage of the patch neuron were both monitored

during approach to ensure glutamate was not leaking from the pipette. Brief (5ms) pulses of glutamate were then applied to the dendrite as the holding voltage was varied from -70 to +40 mV. On each subsequent trial, the stimulating pipette was moved slightly (<1um) closer to the target dendrite, and the last trial before the cell was ruptured was selected for analysis. We find that that postsynaptic AMPA-receptor response to applied glutamate was significantly increased in syt-17 KO neurons at all holding voltages (except near 0mV, the AMPAR reversal potential; Fig. 27A-B). Importantly, the magnitude of the increased sensitivity to glutamate in syt-17 KO matched the magnitude of the increased EPSC amplitude evoked by presynaptic release (an approximate doubling at a holding potential of -70 mV in both cases).

The most obvious mechanism for this increase postsynaptic sensitivity to glutamate is an increase in the number of AMPA-type glutamate receptors on the postsynaptic surface. The total expression level of AMPA-type glutamate receptors has often been found to be an imperfect predictor of surface receptor expression levels (ex., Hayashi & Huganir), therefore it is preferable to determine what fraction of total glutamate receptor protein is expressed on the postsynaptic membrane. To assay for surface glutamate receptor fraction, we expressed GluR2-pHluorin in WT and syt-17 KO neuron, with a soluble mRuby3 to visualize dendritic morphology. pHluorin is pH-sensitive variant of GFP, whose fluorescence is quenched in acidic environments (i.e., inside acidified vesicles). In this case, the pHluorin is fused to the extracellular N-terminus of GluR2, an AMPA receptor subunit. The pHluorin is thus exposed to the extracellular space (and fluorescing at pH 7.4) if the exogenously expressed receptor is inserted in the postsynaptic membrane, and the pHluorin is quenched if the receptor is

internal. The surface expression of the GluR2-pHluorin can be determined by alternatively perfusing cells with an acidic (pH 5.5) bath solution (thus temporarily quenching the surface fraction), and a bath solution containing 40mM ammonium chloride (which penetrates and alkalizes all cellular compartments, illuminating all pHluorin molecules). This approach has been widely employed to assay surface expression of glutamate receptors in neurons (Kopec et al., 2006; Gong & Di Camilli, 2008). Using this method, we find that syt-17 knockout neurons express a larger fraction of GluR2 on their surface (Fig 27C, p=.01). This indicates that the increase in excitatory neurotransmission in syt-17 knockout neurons is attributable to an increase in the surface expression of AMPA-type glutamate receptors in the knockout.

A pathological accumulation of glutamate receptors on the cell surface could be due to an upregulation in the exocytosis of these receptors, or a downregulation of constitutive receptor endocytosis. Given our finding that syt-17 in neurites localizes to rab5-positive early endosomes, and the fact that these endosomes mediate endocytosis of AMPA-type glutamate receptors (Brown et al., 2005; reviewed in Hirling, 2009), we judged a defect in endocytosis more likely. We therefore incubated live neurons in Alexa-546-tagged Transferrin T for 30 min. Transferrin T binds to the Transferrin receptor on the cell surface, which subsequently undergoes clathrin-mediated endocytosis and is sorted to early endosomal compartments (Liu et al., 2016). Internalized Transferrin T can therefore be used to assay for constitutive endocytosis. After Transferrin T incubation and subsequent washes, clear internalized puncta were visible in both WT and KO. We measured the average somatic intensity of the

Transferrin-546 signal and found it was significantly reduced in neurons lacking syt-17, confirming a defect in constitutive endocytosis in the knockout (Fig. 27D, p=.05).

Finally, an increase in GluR2 expression on the plasma membrane has been shown to alter dendritic spine morphology. Passafaro et al. (2003) showed that genetic upregulation of GluR2 in dendrites results in an increase in the length of dendritic spines, and resulted in a large fraction of spines with a filopodia-like appearance (as opposed to classic mushroom-type spines). The authors posit that upregulation of synaptic GluR2 effectively pushes spines into a growth state, and propose this to be a mechanism for spine enlargement during LTP (i.e., insertion of GluR2-containing into the postsynaptic membrane during synaptic potentiation triggers a pro-growth signaling cascade that promotes LTP; ibid.). We examined dendritic spine morphology in syt-17 knockout neurons sparsely expressing GFP (Fig. 28A). Consistent with the observed upregulation in GluR surface expression, dendritic spines in syt-17 knockout neurons were significantly longer than those of wildtype neurons (Fig. 28B, p<.001), and exhibited a filopodia-like morphology reminiscent of Passafaro et al. (2003).

3.4 Discussion

While a subset of synaptotagmin isoforms have been well-characterized, most have no known function in neurons. Syt-17 in particular has received scant attention. In this study, we localized syt-17 to the golgi and early endosomes of hippocampal neurons. We showed that loss of syt-17 results in impaired ER-to-golgi trafficking and an ER stress response that downregulates protein translation. We propose that the

observed defects in neurite outgrowth we observe in knockout neurons is a result of these alterations in secretory traffic. Disruption of secretory trafficking and downregulation of translation secondary to ER stress in neurons have both been shown to impair neurite outgrowth (ex., Aridor & Fish, 2009; Oñate et al., 2015; Prashberger et al., 2017). At present, we are unable to determine the relative importance of these two factors for neurite outgrowth in syt-17 KO (an additive effect would not be surprising).

Additionally, we find that syt-17 knockout neurons exhibit a dramatic upregulation of EPSC amplitudes. After ruling out several other possibilities, we show that this phenotype has a postsynaptic locus, and is attributable to accumulation of excess AMPA-type glutamate receptors on the dendritic surface. This accumulation seems to alter dendritic spine morphology in a manner similar to previous reports, although we cannot rule out the possibility that this alteration in dendritic spines is actually somehow due to the observed dysfunction in the secretory pathway. We further observed that syt-17 knockout neurons exhibit a deficiency in constitutive endocytosis. Because the pool of syt-17 that is expressed at/near synapses localizes with early endosomes, and endocytosis of surface AMPA-type receptors is mediated by these early endosomes (Hirling, 2009), we argue that the accumulation of excess glutamate receptors on the dendrites of syt-17 knockout neurons is due to a deficiency in rab5-dependent early endosomal trafficking.

The picture that emerges is one in which syt-17 plays two functions in cells: mediating efficient protein trafficking in the early secretory pathway, and maintaining early endosomal trafficking. Dysregulation of either of these processes has profound effects on the normal development and physiology of neurons.

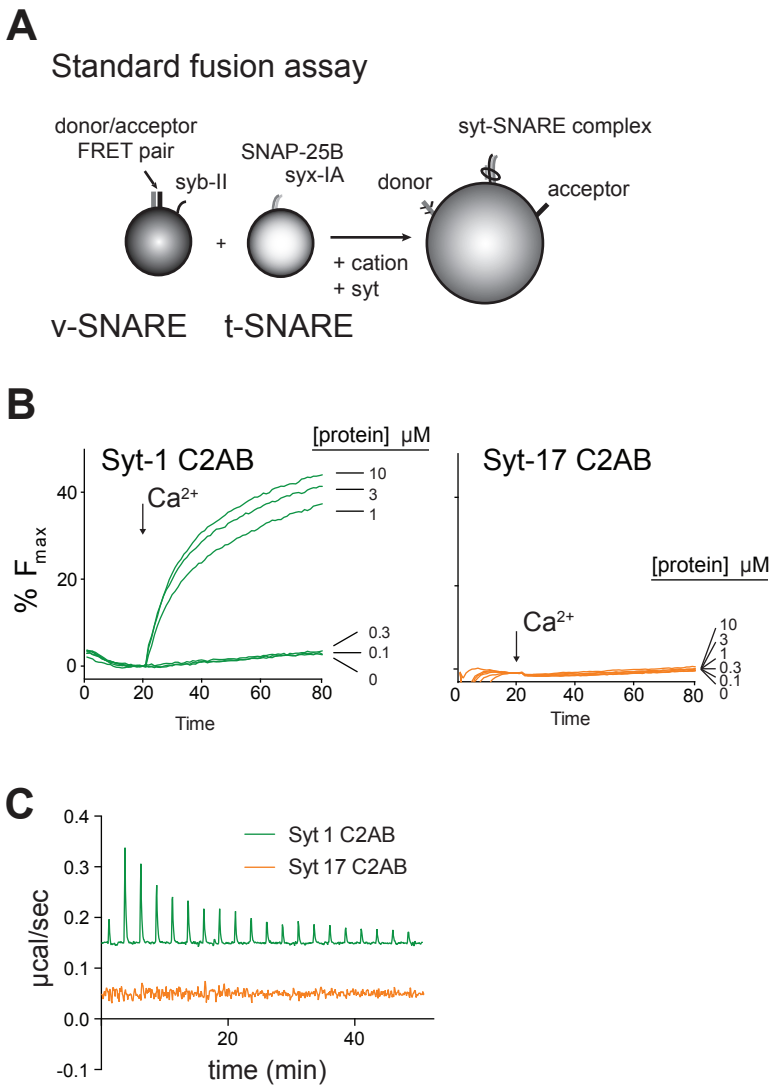

Figure 13. Syt-17 does not drive fusion in response to, or bind, Ca^{2+} **(A)** Schematic of standard in vitro fusion assay. **(B)** Syt-1 and syt-17 protein titration in the standard fusion assay. Syt-17, in contrast to syt-1, is unable to stimulate fusion at all protein concentrations tested **(C)** ITC analysis of Ca^{2+} binding to the isolated C2AB domains of syt-1 and syt-17 shows that syt-17 does not bind Ca^{2+}.

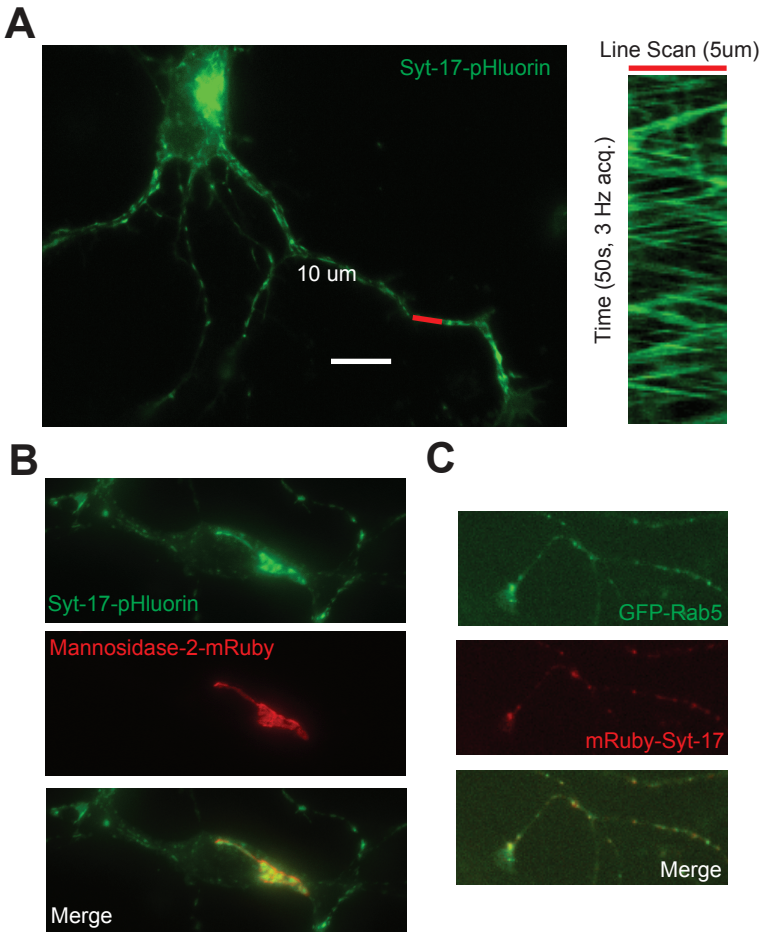

Figure 14. Syt-17 localizes to golgi and early endosomes in hippocampal neurons. (A) Left: 3 DIV neuron expressing syt-17-pHluorin. Note the large somatic fraction and smaller, dispersed puncta. Right: Linescan of region indicated in red. Syt-17-pHluorin puncta are highly moble and traffic bidirectionally. **(B)** Syt-17-pHluorin coexpresses with the golgi marker mannosidase-2-mRuby demonstrates somatic golgi colocalization. **(C)** mRuby-syt-17 coexpressed with GFP-Rab5 demonstrates colocalization with early endosomes in neurite and near growth cones.

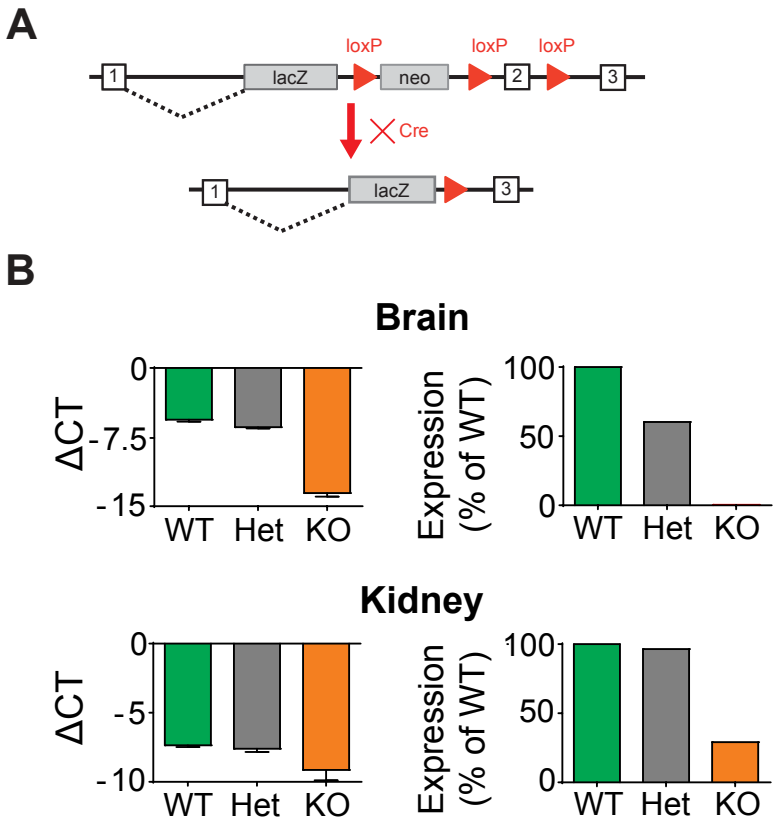

Figure 15. Allele diagram and validation of a syt-17 knockout mouse model. (A) Schematic of the genetic strategy. Intron 2 and the floxed Neo cassette were excised by performing a cross with a germline-expressing Cre mouse, resulting in nonsense-mediated degredation of the transcript. **(B)** RT-PCR validation of the knockout in brain and kidney tissue harvested from young (15 day postnatal) mice.

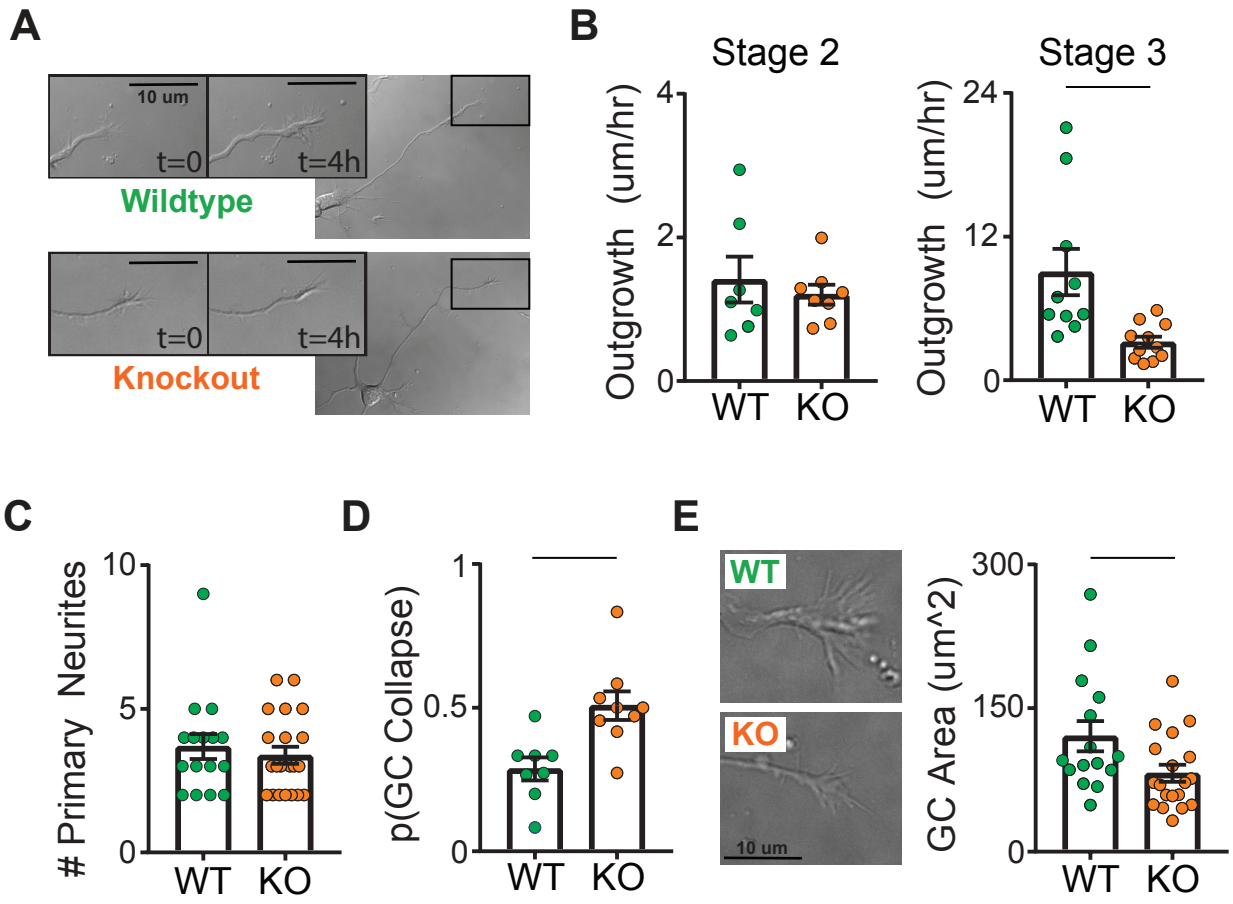

Figure 16. Syt-17 is needed for axonal outgrowth and growth cone stability.
(A) Time-lapse DIC images of stage 3 neurons from wildtype (top) and syt-17 knockout (bottom) animals. **(B)** Neurite outgrowth at stage 2 (left) is normal in the KO, while at stage three developing axons extend at a slower rate (p=.006). **(C)** The number of primary neurites per neuron does not differ between genotypes. **(D)** The probability of spontaneous axonal growth cone collapse was higher in syt-17 KO (p=.004).
(E) Axonal growth cones were significantly smaller in neurons lacking syt-17 (p=.03).

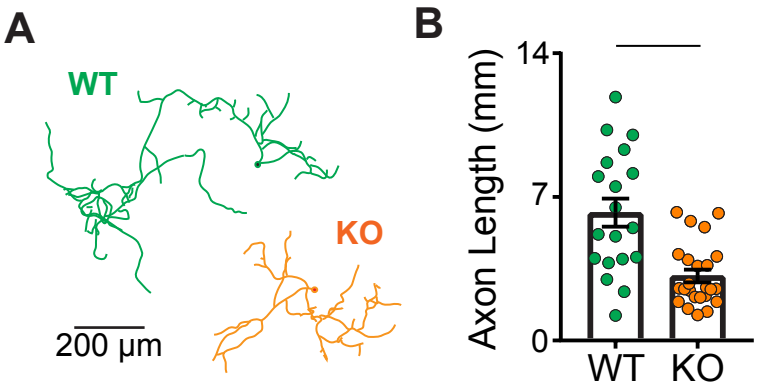

Figure 17. Shorter axons in syt-17 knockout neurons.
(A) Neural morphology was visualized by sparse transfection with GFP, and resultant axons were semi-manually traced.
(B) Average axon length was significantly reduced in syt-17 KO neurons ($p<.001$).

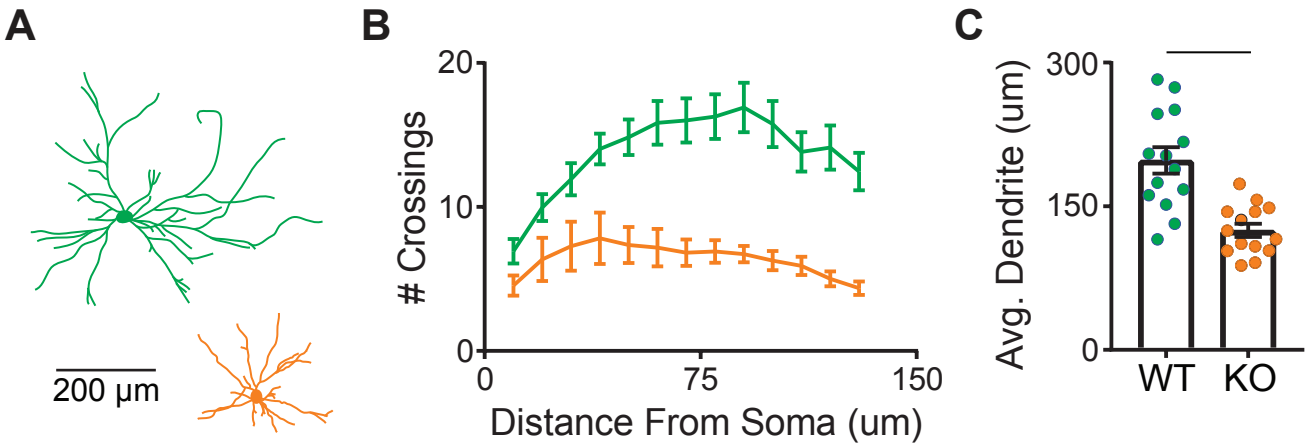

Figure 18. Knockout of syt-17 results in stunted dendritic arbors in mature neurons. **(A)** Neuron morphology was visualized with sparse transfection of GFP, and dendritic arbors were semi-manually reconstructed based on the presence of dendritic spines and positive MAP-2 immunostaining. **(B)** Sholl analysis demonstrating less dendritic branching complexity in neurons lacking syt-17. **(C)** The average primary dendrite length was significantly shorter in syt-17 knockout neurons ($p<.001$).

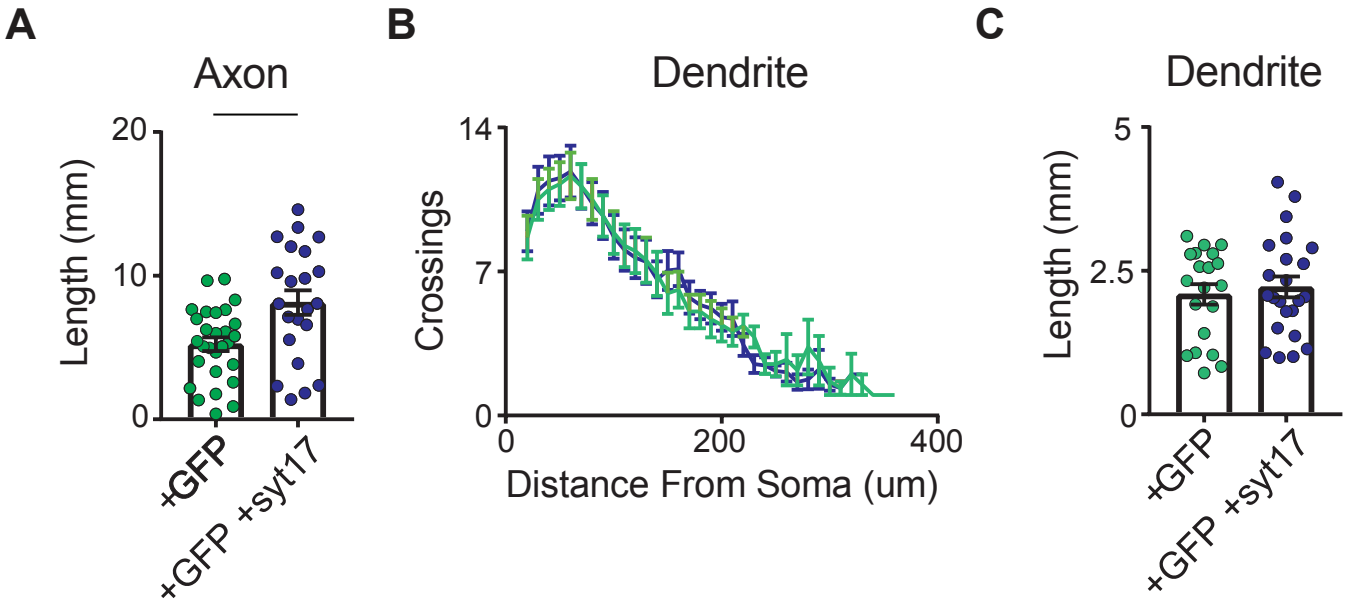

Figure 19. Overexpression of syt-17 selectively increases axon length.
Wildype neurons were sparsely transfected (at 3DIV) with GFP to visualize morphology, with and without overexpression of syt-17. **(A)** Neurons overexpressing syt-17 exhibit significantly longer axons at 7 DIV (p=.003). **(B)** At 14 DIV, dendrites of neurons overexpressing syt-17 showed an unchanged branching complexity, assayed by Sholl analysis. **(C)** The total dendritic lengh of 14 DIV neurons overexpressing syt-17 was unaltered relative to control neurons (p>.1).

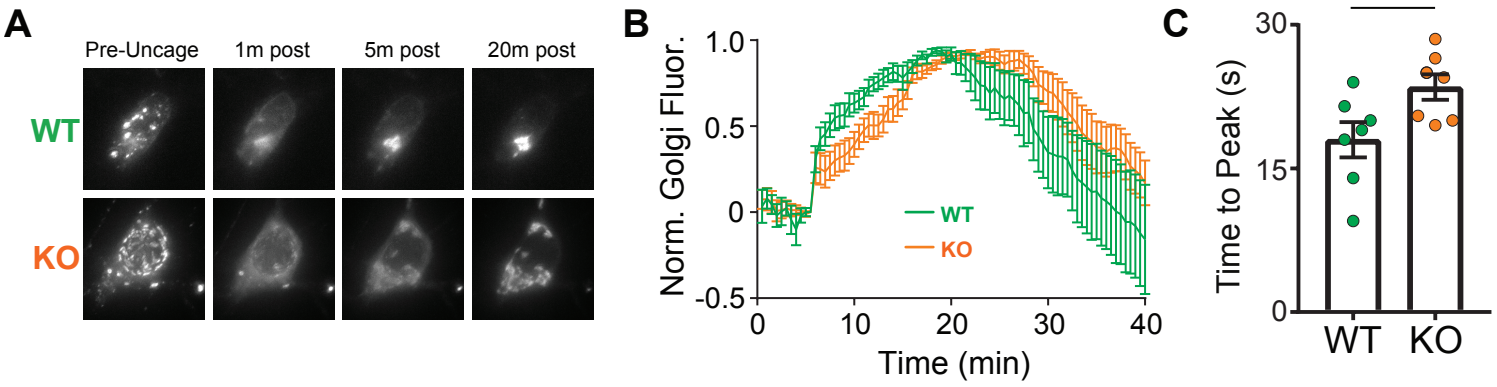

Figure 20: Knockout of syt-17 slows trafficking in the early secretory pathway.
(A) VSVG-YFP-2xUVR8 aggregates in the endoplasmic reticulum in the dark (left). Upon 300 nm uncaging, the protein disaggregates, diffuses through theER, and accumulates in the golgi (right). (B) Timecourse of golgi fluorescence quantified for each cell. In knockout neurons (red) the cargo accumulates more slowly. (C) Syt-17 knockouts exhibit a slower time to peak golgi fluorescence. N=7 neurons per genotype from two preparations.

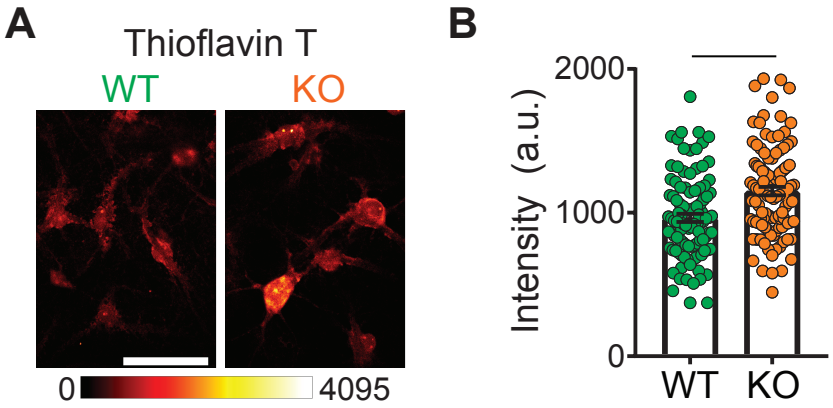

Figure 21. ER stress in syt-17 KO neurons.
(A) Live cells were incubated with Thioflavin T for 30m to label unfolded protein aggregates in the ER lumen. Knockout neurons often exhibited bright puncta rarely observed in WT neurons. Scale bar = 50 um. **(B)** Average somatic intensity of Thioflavin T labeling was higher in neurons lacking syt-17 ($p<.001$).

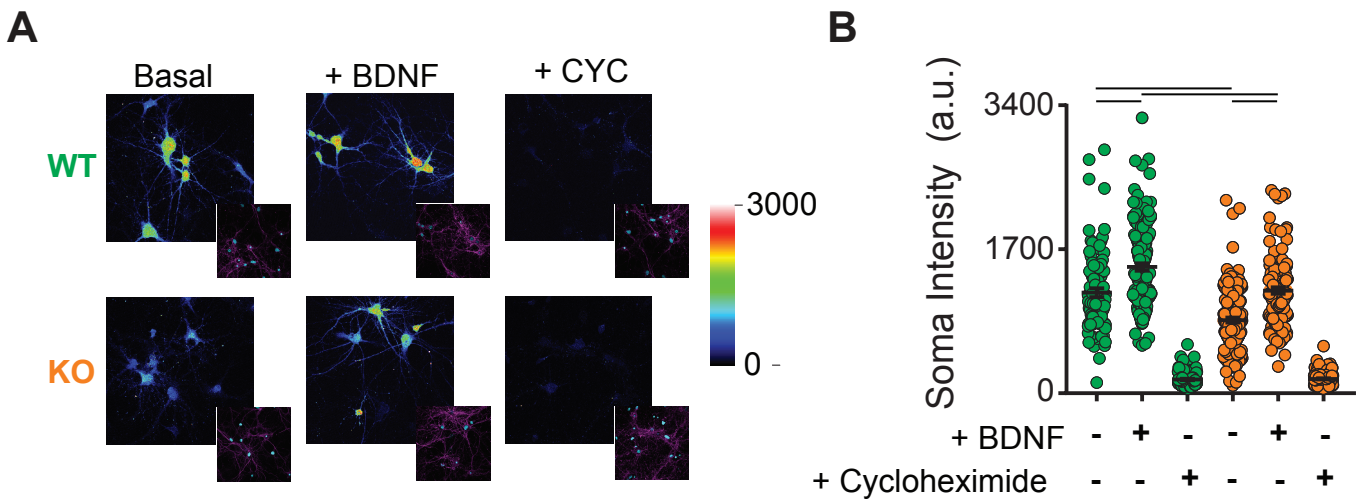

Figure 22: Impaired protein translation in syt-17 KO.
(A) Neurons were incubated for two hours in 2mM O-propargyl-puromycin (OPP) to label newly-translated proteins, with or without addition of 100ng/mL BDNF or 40uM cycloheximide. Post-fixation, Alexa Fluor picolyl azide was used to fluorescently tag OPP-labeled transcripts. Fluorescence intensity, visualized with confocal microscopy, provides an index of the quantiy of protein translation during the incubation period. Inset images depict phalloidin and NuclearMask counterstains. **(B)** Average somatic labelling is quantified across cells. Syt-17 KO neurons exhibit less labelled, newly-translated, protein in basal conditions ($p<.001$) and in response to BDNF stimulation ($p<.001$). Treatment with the protein synthesis inhibitor cycloheximide abolished labelling in both genotypes. N = 93-156 neurons per condition from three independent preparations.

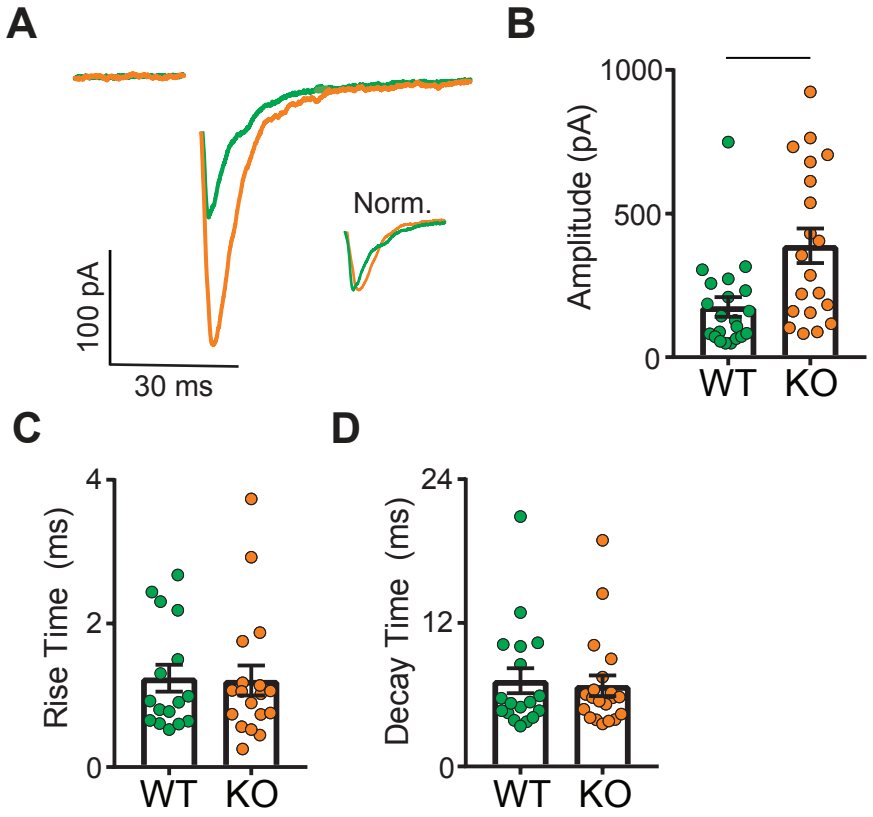

Figure 23. Neurons lacking syt-17 exhibit enhanced synaptic transmission. (A) Cultured hippocampal neurons were patch clamped (13-16 DIV), and individual adjacent neurons were stimulated to evoke excitatory (AMPA-mediated) postsynaptic currents (EPSCs). **(B)** Syt-17 knockout neurons exhibit significantly higher EPSC amplitudes (p=.003). Evoked EPSC kinetics were unaltered, as EPSC **(C)** rise times and **(D)** decay times did not differ between genotypes (p>.1).

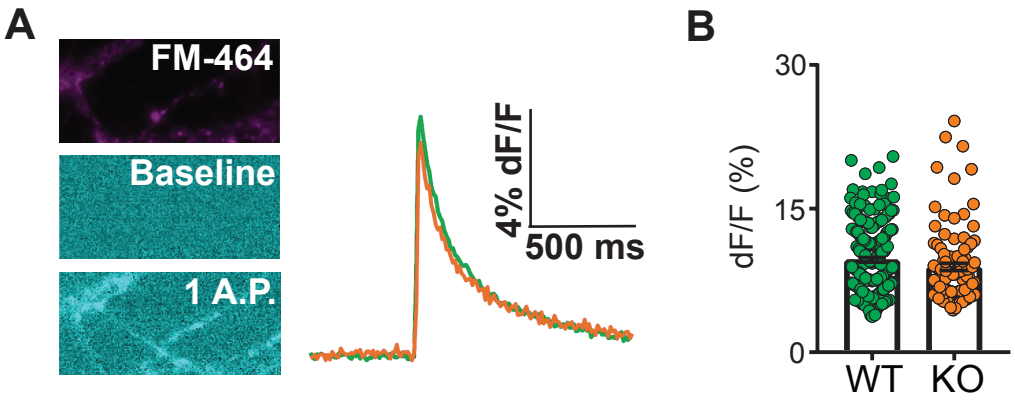

Figure 24. Presynaptic Ca^{2+} influx is unaltered in syt-17 KO boutons. **(A)** Boutons were labelled by pre-loading with FM-464 dye (left, top). Following loading with Fluo-5F Ca^{2+} dye, single action potentials were evoked with a field stimulation chamber (left, middle/bottom). Average Fluo-5F fluorescence change was quantified from individual boutons (right). **(B)** No significant difference in peak response was observed between genotypes (p=.09).

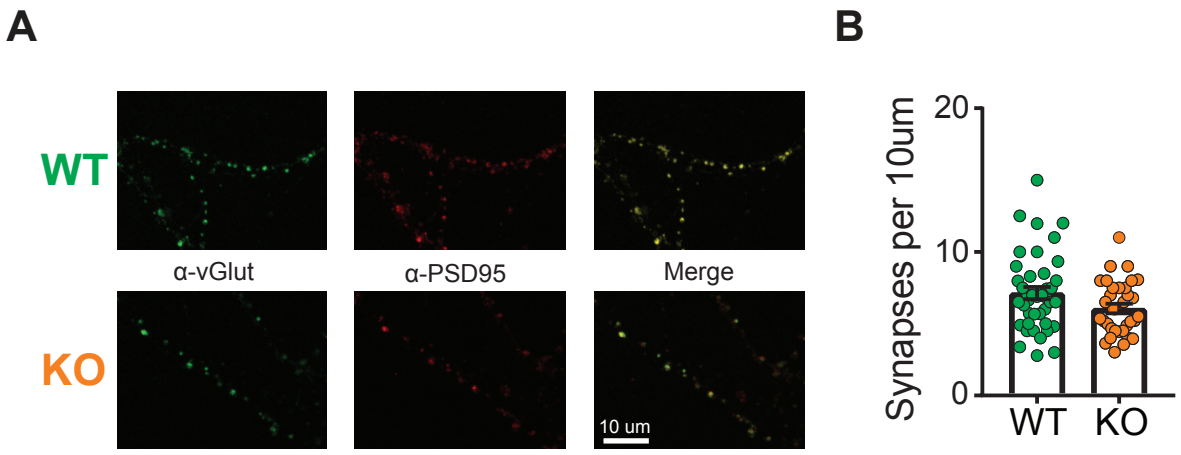

Figure 25. No increase in synapse number in syt-17 KO neurons.
(A) Neurons (14DIV) were fixed and immunostained for vGlut and PSD-95. **(B)** The number of synapses (defined as puncta positive for both pre- and postsynaptic markers) per unit dendrite did not significantly differ between groups (though a non-significant trend towards fewer synapses in the KO was noted, p=.06).

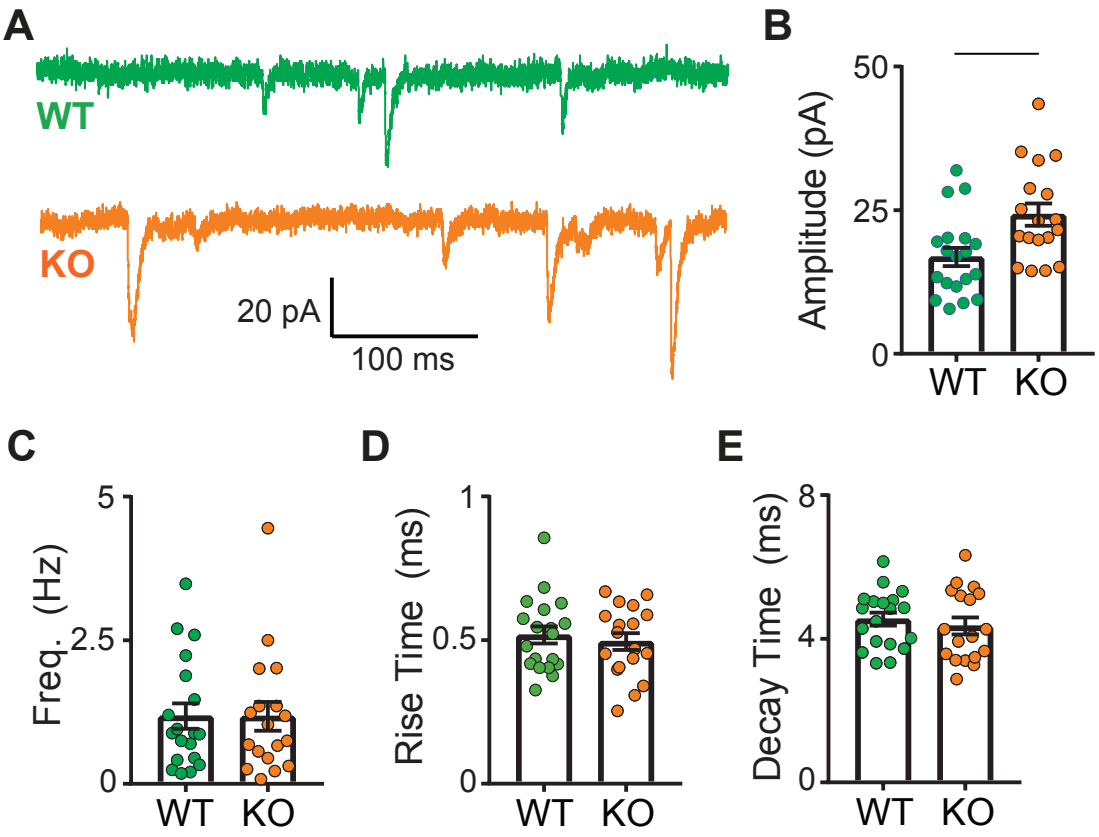

Figure 26. Syt-17 KOs exhibit larger amplitude quantal synaptic currents. **(A)** Whole-cell patch clamp recordings were made from 14-17 DIV hippocampal neurons in the presence of TTX to block action potentials and AP-V and picrotoxin to isolate AMPAR currents. **(B)** The average amplitude of spontaneous mEPSCs was significantly larger in syt-17 KO neurons (p=.006). No alteration was detected in **(C)** presynaptic release frequency, **(D)** average mEPSC rise time, or **(E)** average mEPSC decay time (all p>.1).

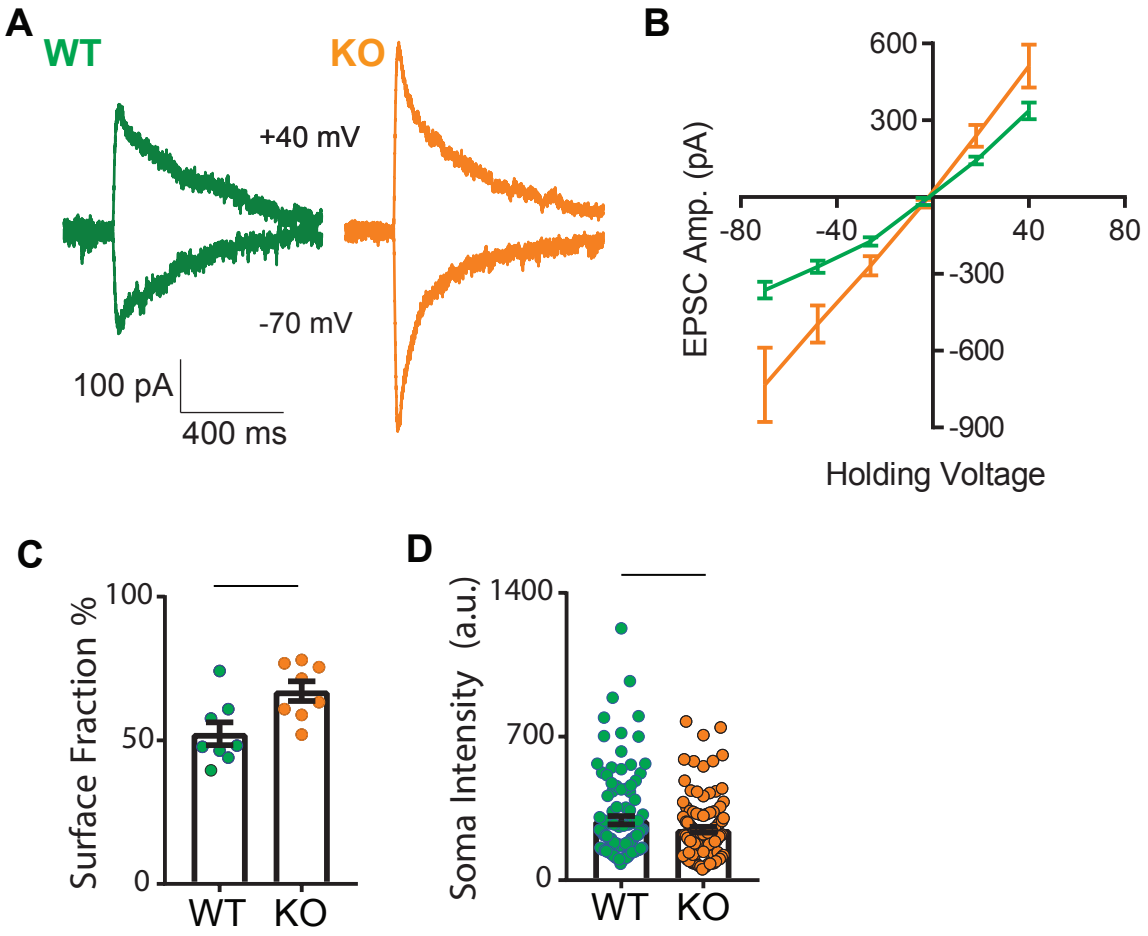

Figure 27. Increased glutamate receptor surface expression in syt-17 knockouts. **(A)** A stimulation pipette containing 200uM L-glutamate was positioned directly adjacent to the apical dendrite of patched neurons, and glutamate was pressure applied (5 ms pulse) as the holding voltage was varied. **(B)** I-V plot showing observed current as a function of holding voltage - the amplitude of postsynaptic responses in syt-17 KO neurons was uniformly increased. (C) Surface expression of GluR2-pHluorin is increased in syt-17 KO (p=.01). (D) Average somatic Transferrin-546 intensity post-incubation is reduced in syt-17 KO (p=.05), demonstrating impaired endocytosis.

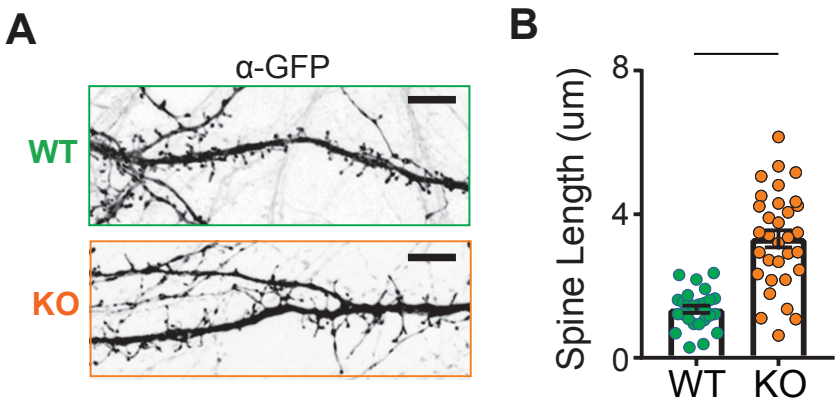

Figure 28. Syt-17 KOs exhibit altered dendritic spine morphology. **(A)** Neurons were transfected at 3 DIV with soluble GFP to visualize neuronal morphology. The dendritic spines of neurons lacking syt-17 more closely resemble filopodia than mature mushroom-type spines. **(B)** The average length of dendritic spines was significantly longer in syt-17 KO neurons ($p<.001$).

Chapter 4:

Perspectives and Future Directions

In my graduate work, I split my time between mechanistic characterization of syt-1, the best-studied synaptotagmin, and characterizing the knockout phenotype of syt-17, among the least-studied synaptotagmins.

Synaptotagmin 1

As described in Chapter 1 of this dissertation, syt-1 plays a myriad of functions in central synapses, and is implicated at essentially every stage of the synaptic vesicle cycle. Notably, every step of the synaptic vesicle cycle is regulated by Ca^{2+}. In light of this fact, the value of a variant of syt-1 that has been engineered to respond to a non-physiological ligand like Sr^{2+} becomes immediately apparent. $Chimera_{1,3}$ can be used to dissociate the role of syt-1 from other Ca^{2+}-dependent processes in the synapse. For example, our lab has employed elaborate genetic strategies to dissociate syt-1's role in exocytosis from it's putative role in endocytosis (Yao et al., 2012). An attractive alternative approach would be to replace native syt-1 with $chimera_{1,3}$, and monitor endocytosis in the presence of Sr^{2+}. If syt-1 is indeed serving as a Ca^{2+} sensor for endocytosis, Sr^{2+} should support SV endocytosis only if $chimera_{1,3}$ (but not WT syt-1) is expressed. Similarly, our lab has argued (Chika et al., 2008) that syt-1 serves as a clamp for spontaneous release, while others have argued it is in fact a Ca^{2+} sensor for spontaneous release (Xu et al., 2009). If syt-1 is a sensor for spontaneous release, then substitution of wildtype syt-1 with $chimera_{1,3}$ should confer a steep Sr^{2+}-dependence on miniature release.

Finally, we observed that slowing the kinetics of synaptic transmission slows the kinetics of population level oscillations *in vitro*. This is a rather artificial system (cultured excitatory neurons), it would be interesting to see if a similar relationship between network-level oscillation frequency and synaptic kinetics exists in an intact neuron circuit, via AAV transgene expression.

Synaptotagmin 17

Given that the work presented herein is the first phenotypic characterization of syt-17, it is not surprising that there are many areas open to exploration in the future. I address some of the possibilities (a subset of which we are actively pursuing) below.

We found syt-17 to be localized to the golgi complex, where it mediates ER-to-golgi trafficking. Presumably this would require that syt-17 be present on the early golgi. This subjectively appeared to be the case, but it was not possible to distinguish early, middle, and late golgi in neural somata with light microscopy in our hands (data not shown). A previous report (Fukuda & Mikoshiba, 2001) reported that syt-17 localizes to the *trans*-golgi, based on colocalization with TGN38 following treatment with Brefeldin A (which redistributes early golgi proteins to the ER). It is possible cell-type specific differences in syt-17 function explain this apparent discrepancy (we used primary hippocampal neurons, in which endogenous syt-17 is expressed [Sharma et al., 2015], while Fukuda & Mikoshiba used PC12 cells, in which endogenous expression of syt-17 has not been determined). It is equally possible that syt-17 is expressed in multiple subcompartments of the golgi complex. Future localization with super-resolution approaches is necessary to resolve this question.

Perhaps the most pressing future direction is to determine the molecular mechanism by which syt-17 exerts its effects. Herein I have delineated the cellular mechanisms of the phenotype observed in syt-17 knockout neurons, but we have yet to determine the molecular mechanism of syt-17 action, either at the golgi or at early endosomes. Given that the protein in question is a synaptotagmin, and SNARE function is essential both within the golgi and for endosomal trafficking, it is tempting to wonder whether syt-17 may act on SNARE isoforms particular (Malsam & Sollner, 2011) to the golgi (such as syntaxin 5) or early endosomes (such as syntaxin 16). Immunoprecipitation experiments currently underway in our laboratory aim to address exactly this question.

The fact that overexpression of syt-17 selectively increases the length of axons (by ~40%) but not dendrites raises the question of whether modulating syt-17 expression levels or function might have the potential to augment regeneration of damaged axons. Identifying genes whose expression modulates axonal growth in cultured cells, and subsequently up- or downregulating those genes in *in vivo* models of axonal (typically spinal) injury, has proven to be a fruitful approach in the field of axon regeneration (ex., Blackmore et al., 2010). In collaboration with the lab of Murray Blackmore at Marquette University and the University of North Carolina Viral Vector Core, we are currently conducting experiments overexpressing syt-17 in the motor cortex of mice that have undergone controlled spinal injury, to determine if syt-17 overexpression can accelerate the rate of axonal regeneration *in vivo*. Results are expected early next year.

We report here that syt-17 plays a role in accelerating protein trafficking from the ER to the golgi. However, as discussed earlier in this dissertation, it is established that syt-17 is not ubiquitously expressed, but selectively expressed in certain cell types in brain. Syt-17 is thus clearly not an essential component of the secretory pathway in most cells, but its function in secretory trafficking is specific to neurons. Indeed, a consensus has emerged that secretory trafficking is quite specialized in neuronal cells. In addition to secretory trafficking within the soma, neurons possess a molecularly-distinct protein translation/processing machinery specialized for local synthesis in dendrites (reviewed in Holt & Schuman, 2013). Evidence exists for another related specialized secretory pathway in axons (reviewed in Rangaraju et al., 2017), but this has been the subject of less study. Here I will note that I anecdotally observed syt-17 expression colocalized with remote mannosidase-II puncta at apparent “golgi outposts” (Holt & Schuman, 2013) in neuronal dendrites, intermingled with more mobile endosomal puncta. Whether syt-17 exerts any similar modulatory effect on local protein secretion remains to be determined. Further, how secretory trafficking *in the soma* of neurons differs from that of other cell types is an area ripe for future study.

Several previous studies (Ju et al., 2000; Jang et al., 2004; Han et al., 2007) have reported an upregulation of syt-17 expression under conditions known to produce an ER stress response. Our findings provide a potential explanation for these reports: under conditions of ER stress, expression of syt-17 (which we find accelerates the rate of trafficking from ER to golgi) is upregulated as a compensatory mechanism, alleviating the accumulation of unprocessed proteins in the ER. On this account, upregulated syt-17 expression would be *part of* the neuronal Unfolded Protein Response. However this

account is speculative, and further work is needed to determine the specific factors upregulating syt-17 expression under UPR conditions.

In a similar vein, genetic deletion of syt-17 produces an ER stress response, as traffic into the golgi is disrupted. Given that neuronal ER stress is a common observation in many neurological disorders (Lindholm et al., 2017), it will be interesting to explore whether modulating syt-17 function has potential therapeutic value in diseases characterized by a UPR. Interestingly, activation of the UPR in neurons *not* undergoing ER stress has been proposed as a potential therapeutic too to improve axonal regrowth following injury (Oñate et al., 2015). I hope the work I presented here is the first of many studies into the roles of syt-17 in neurons, and further that some of the potential therapeutic avenues I described above will be explored.

In sum, the present dissertation highlight the diversity of the synaptotagmin family of proteins. The canonical syt, syt-1, triggers neurotransmitter release through a mechanism dependent on penetration of the presynaptic plasma membrane by the Ca^{2+}-binding loops. The lifetime of this syt*Ca^{2+}*membrane complex controls the decay kinetics of synaptic transmission, setting the window of high release probability following an action potential. The newest (and arguably strangest) member of the syt family, syt-17, plays two roles in neurons – control of trafficking in the early secretory pathway, and endosomal recycling of receptors to the postsynaptic membrane – and disruptions of these functions leads to perturbations neurite outgrowth and synaptic transmission. Still, only a minority of syt isoforms have been assigned any specific function, clearly more work remains to be done.

References

Aridor, M., & Fish, K. N. (2009). Selective targeting of er exit sites supports axon development. *Traffic*, *10*(11), 1669–1684. https://doi.org/10.1111/j.1600-0854.2009.00974.x

Arthur, C. P., Dean, C., & Pagratis, M. (2010). Loss of synaptotagmin IV results in a reduction in synaptic vesicles and a distortion of the golgi struture in in cultured hippocampal neurons. *Neuroscience*, *167*(1), 135–142. https://doi.org/10.1016/j.neuroscience.2010.01.056

Babai, N., Kochubey, O., Keller, D., & Schneggenburger, R. (2014). An alien divalent ion reveals a major role for Ca^{2+} buffering in controlling slow transmitter release. *The Journal of Neuroscience : The Official Journal of the Society for Neuroscience*, *34*(38), 12622–35. https://doi.org/10.1523/JNEUROSCI.1990-14.2014

Bacaj, T., Wu, D., Yang, X., Morishita, W., Zhou, P., Xu, W., … Su, T. C. (2013). Article Synaptotagmin-1 and Synaptotagmin-7 Trigger Synchronous and Asynchronous Phases of Neurotransmitter Release. *Neuron*, *80*, 947–959. https://doi.org/10.1016/j.neuron.2013.10.026

Bai, H., Xue, R., Bao, H., Zhang, L., Yethiraj, A., Cui, Q., & Chapman, E. R. (2016). Different states of synaptotagmin regulate evoked versus spontaneous release. *Nature Communications*, *7*, 1–9. https://doi.org/10.1038/ncomms10971

Bai, J., Tucker, W. C., & Chapman, E. R. (2004). PIP2 increases the speed of response of synaptotagmin and steers its membrane-penetration activity toward the plasma membrane. *Nature Structural and Molecular Biology*, *11*(1), 36–44. https://doi.org/10.1038/nsmb709

Bai, J., Wang, P., & Chapman, E. R. (2002). C2A activates a cryptic Ca(2+)-triggered membrane penetration activity within the C2B domain of synaptotagmin I. *Proceedings of the National Academy of Sciences of the United States of America*, *99*(3), 1665–70. https://doi.org/10.1073/pnas.032541099

Beriault, D. R., & Werstuck, G. H. (2013). Detection and quantification of endoplasmic reticulum stress in living cells using the fluorescent compound, Thioflavin T. *Biochimica et Biophysica Acta (BBA) - Molecular Cell Research*, *1833*(10), 2293–2301. https://doi.org/10.1016/j.bbamcr.2013.05.020

Bhalla, A., Chicka, M. C., Tucker, W. C., & Chapman, E. R. (2006). Ca(2+)-synaptotagmin directly regulates t-SNARE function during reconstituted membrane fusion. *Nature Structural & Molecular Biology*, *13*(4), 323–30. https://doi.org/10.1038/nsmb1076

Bhalla, A., Chicka, M. C., & Chapman, E. R. (2008). Analysis of the synaptotagmin family during reconstituted membrane fusion: Uncovering a class of inhibitory isoforms. *Journal of Biological Chemistry*, *283*(31), 21799–21807. https://doi.org/10.1074/jbc.M709628200

Bhalla, A., Tucker, W. C., & Chapman, E. R. (2005). Synaptotagmin Isoforms Couple Distinct Ranges of Ca2+, Ba2+, and Sr2+ Concentration to SNARE-mediated Membrane Fusion. *Molecular Biology of the Cell*, *16*, 4755–4764. https://doi.org/10.1091/mbc.E05

Blackmore, M. G., Moore, D. L., Smith, R. P., Goldberg, J. L., Bixby, J. L., & Lemmon, V. P. (2010). High content screening of cortical neurons identifies novel regulators of axon growth. *Molecular and Cellular Neuroscience*, *44*(1), 43–54. https://doi.org/10.1016/j.mcn.2010.02.002

Bouhours, B., Gjoni, E., Kochubey, O., & Schneggenburger, R. (2017). Synaptotagmin2 (Syt2) drives fast release redundantly with Syt1 at the output synapses of Parvalbumin-expressing inhibitory neurons. *The Journal of Neuroscience*, *2*. https://doi.org/10.1523/JNEUROSCI.3736-16.2017

Brose, N., Petrenko, A. G., Südhof, T. C., Jahn, R., & Sudhof, T. C. (2011). Synaptotagmin : A Calcium Sensor on the Synaptic Vesicle Surface. *Science*, *256*(5059), 1021–1025.

Brown, T. C., Tran, I. C., Backos, D. S., & Esteban, J. A. (2005). NMDA receptor-dependent activation of the small GTPase Rab5 drives the removal of synaptic AMPA receptors during hippocampal LTD. *Neuron*, *45*(1), 81–94. https://doi.org/10.1016/j.neuron.2004.12.023

Burgalossi, A., Jung, S., Meyer, G., Jockusch, W. J., Jahn, O., Taschenberger, H., … Rhee, J.-S. (2010). SNARE protein recycling by αSNAP and βSNAP supports synaptic vesicle priming. *Neuron*, *68*(3), 473–87. Retrieved from http://dx.doi.org/10.1016/j.neuron.2010.09.019

Cao, P., Maximov, A., & Südhof, T. C. (2011). Activity-dependent IGF-1 exocytosis is controlled by the Ca(2+)-sensor synaptotagmin-10. *Cell*, *145*(2), 300–11. https://doi.org/10.1016/j.cell.2011.03.034

Cao, P., Yang, X., & Su, T. C. (2013). Complexin Activates Exocytosis of Distinct Secretory Vesicles Controlled by Different Synaptotagmins. *The Journal of Neuroscience*, *33*(4), 1714–1727. https://doi.org/10.1523/JNEUROSCI.4087-12.2013

Chapman, E. R. (2008). How does synaptotagmin trigger neurotransmitter release? *Annual Review of Biochemistry*, *77*, 615–41. https://doi.org/10.1146/annurev.biochem.77.062005.101135

Chapman, E. R., & Davis, A. F. (1998). Direct Interaction of a Ca 2 + -binding Loop of Synaptotagmin with Lipid Bilayers. *Journal of Biological Chemistry*, *273*(22), 13995–14001. https://doi.org/10.1074/jbc.273.22.13995

Chapman, E. R., Desai, R. C., Davis, A. F., & Tornehl, C. K. (1998). Delineation of the oligomerization, AP-2 binding, and synprint binding region of the C2B domain of synaptotagmin. *Journal of Biological Chemistry*, *273*(49), 32966–32972. https://doi.org/10.1074/jbc.273.49.32966

Chen, C., Arai, I., Satterfield, R., Young, S. M., Chen, C., Arai, I., … Jonas, P. (2017). Synaptotagmin 2 Is the Fast Ca 2 + Sensor at a Central Inhibitory Synapse Article Synaptotagmin 2 Is the Fast Ca 2 + Sensor at a Central Inhibitory Synapse. *Cell Reports*, *18*(3), 723–736. https://doi.org/10.1016/j.celrep.2016.12.067

Chen, D., Gibson, E. S., & Kennedy, M. J. (2013). A light-triggered protein secretion system. *Journal of Cell Biology*, *201*(4), 631–640. https://doi.org/10.1083/jcb.201210119

Chen, Y. A., Scheller, R. H., & Medical, H. H. (2001). Snare-Mediated Membrane Fusion. *Nature Reviews Molecular Cell Biology*, *2*(February), 98–106.

Cheng, Y., Sequeira, S. M., Malinina, L., Tereshko, V., Söllner, T. H., & Patel, D. J. (2004). Crystallographic identification of Ca2+ and Sr2+ coordination sites in synaptotagmin I C2B domain. *Protein Science*, *13*, 2665–2672. https://doi.org/10.1110/ps.04832604.cium

Chicka, M. C., Hui, E., Liu, H., & Chapman, E. R. (2008). Synaptotagmin arrests the SNARE complex before triggering fast, efficient membrane fusion in response to Ca2+. *Nature Structural & Molecular Biology*, *15*(8), 827–35. https://doi.org/10.1038/nsmb.1463

Chin, H., Choi, S.-H., Jang, Y.-S., Cho, S.-M., Kim, H.-S., Lee, J.-H., … Kwon, O.-J. (2006). Protein kinase A-dependent phosphorylation of B/K protein. *Experimental & Molecular Medicine*, *38*(2), 144–152. https://doi.org/10.1038/emm.2006.18

Connolly, J. J., Glessner, J. T., & Hakonarson, H. (2013). A Genome-Wide Association Study of Autism Incorporating Autism Diagnostic Interview-Revised, Autism Diagnostic Observation Schedule, and Social Responsiveness Scale. *Child Development*, *84*(1), 17–33. https://doi.org/10.1111/j.1467-8624.2012.01838.x

Craxton, M. (2010). A manual collection of Syt, Esyt, Rph3a, Rph3al, Doc2, and Dblc2 genes from 46 metazoan genomes -an open access resource for neuroscience and evolutionary biology. *BMC Genomics*, *11*, 37. https://doi.org/10.1186/1471-2164-11-37

Dean, C., Dunning, F. M., Liu, H., Bomba-Warczak, E., Martens, H., Bharat, V., … Chapman, E. R. (2012). Axonal and dendritic synaptotagmin isoforms revealed by a pHluorin-syt functional screen. *Molecular Biology of the Cell*, *23*(9), 1715–27. https://doi.org/10.1091/mbc.E11-08-0707

Dean, C., Liu, H., Dunning, F. M., Chang, P. Y., Jackson, M. B., & Chapman, E. R. (2009). Synaptotagmin-IV modulates synaptic function and long-term potentiation by regulating BDNF release. *Nature Neuroscience*, *12*(6), 767–76. https://doi.org/10.1038/nn.2315

Di Wu, Hu, Q., Yan, Z., Chen, W., Yan, C., Huang, X., … Shi, Y. (2012). Structural basis of ultraviolet-B perception by UVR8. *Nature*, *484*(7393), 214–219. https://doi.org/10.1038/nature10931

DiAntonio, A., & Schwarz, T. L. (1994). The effect on synaptic physiology of synaptotagmin mutations in drosophila. *Neuron*, *12*(4), 909–920. https://doi.org/10.1016/0896-6273(94)90342-5

Dieterich, D. C., Hodas, J. J. L., Gouzer, G., Shadrin, I. Y., Ngo, J. T., Triller, A., … Schuman, E. M. (2010). In situ visualization and dynamics of newly synthesized proteins in rat hippocampal neurons. *Nature Neuroscience*, *13*(7), 897–905. https://doi.org/10.1038/nn.2580

Dotti, C. G., Sullivan, C. a, & Banker, G. a. (1988). The establishment of polarity by hippocampal neurons in culture. *The Journal of Neuroscience : The Official Journal of the Society for Neuroscience*, *8*(4), 1454–1468. https://doi.org/10.1016/0012-1606(89)90269-8

Du, C., Wang, Y., Zhang, F., Yan, S., Guan, Y., Gong, X., … Zhang, C. X. (2017). Synaptotagmin-11 inhibits cytokine secretion and phagocytosis in microglia. *Glia*, *6*, 1656–1667. https://doi.org/10.1002/glia.23186

Evans, C. S., Ruhl, D. A., & Chapman, E. R. (2015). An Engineered Metal Sensor Tunes the Kinetics of Synaptic Transmission. *Journal of Neuroscience*, *35*(34), 11769–11779. https://doi.org/10.1523/JNEUROSCI.1694-15.2015

Ferreria, T. A., Blackman, A. V, Oyrer, J., Jayabal, S., Chung, A. J., Watt, A. J., … van Meyel, D. J. (2014). Neuronal morphometry directly from bitmap images. *Nature Methods*, *11*(10), 982–984. https://doi.org/10.1038/nmeth.3102

Fioravante, D., & Regehr, W. G. (2011). Short-term forms of presynaptic plasticity. *Current Opinion in Neurobiology*, *21*(2), 269–74. https://doi.org/10.1016/j.conb.2011.02.003

Fukuda, M., & Mikoshiba, K. (2001). The N-terminal cysteine cluster is essential for membrane targeting of B/K protein. *The Biochemical Journal*, *360*(Pt 2), 441–8. https://doi.org/10.1042/0264-6021:3600441

Fuson, K. L., Montes, M., Robert, J. J., & Sutton, R. B. (2007). Structure of human synaptotagmin 1 C2AB in the absence of Ca2+ reveals a novel domain association. *Biochemistry*, *46*(45), 13041–8. https://doi.org/10.1021/bi701651k

Geppert, M., Goda, Y., Hammer, R. E., Li, C., Rosahl, T. W., Stevens, C. F., & Südhof, T. C. (1994). Synaptotagmin I: a major Ca2+ sensor for transmitter release at a central synapse. *Cell*, *79*(4), 717–27. Retrieved from http://www.ncbi.nlm.nih.gov/pubmed/7954835

Goda, Y., & Stevens, C. F. (1994). Two components of transmitter release at a central synapse. *Proceedings of the National Academy of Sciences of the United States of America*, *91*(26), 12942–6. https://doi.org/10.1073/pnas.91.26.12942

Gong, L.-W., & De Camilli, P. (2008). Regulation of postsynaptic AMPA responses by synaptojanin 1. *Proceedings of the National Academy of Sciences of the United States of America*, *105*(45), 17561–6. https://doi.org/10.1073/pnas.0809221105

Gordon, S. L., Leube, R. E., & Cousin, M. a. (2011). Synaptophysin is required for synaptobrevin retrieval during synaptic vesicle endocytosis. *The Journal of Neuroscience : The Official Journal of the Society for Neuroscience*, *31*(39), 14032–6. https://doi.org/10.1523/JNEUROSCI.3162-11.2011

Han, K. H., Lee, U. Y., Jang, Y. S., Cho, Y. M., Jang, Y. M., Hwang, I. A., … Kwon, O. J. (2007). Differential regulation of B/K protein expression in proximal and distal tubules of rat kidneys with ischemia-reperfusion injury. *Am J Physiol Renal Physiol*, *292*(1), F100-6. https://doi.org/00009.2006 [pii]\r10.1152/ajprenal.00009.2006

Hayashi, T., & Huganir, R. L. (2004). Tyrosine Phosphorylation and Regulation of the AMPA Receptor by Src Family Tyrosine Kinases. *Journal of Neuroscience*, *24*(27), 6152–6160. https://doi.org/10.1523/JNEUROSCI.0799-04.2004

Hirling, H. (2009). Endosomal trafficking of AMPA-type glutamate receptors. *Neuroscience*, *158*(1), 36–44. https://doi.org/10.1016/j.neuroscience.2008.02.057

Hirschberg, K., Miller, C. M., Ellenberg, J., Presley, J. F., Siggia, E. D., Phair, R. D., & Lippincott-Schwartz, J. (1998). Kinetic analysis of secretory protein traffic and characterization of Golgi to plasma membrane transport intermediates in living cells. *Journal of Cell Biology*, *143*(6), 1485–1503. https://doi.org/10.1083/jcb.143.6.1485

Holt, C. E., & Schuman, E. M. (2013). The central dogma decentralized: New perspectives on RNA function and local translation in neurons. *Neuron*, *80*(3), 648–657. https://doi.org/10.1016/j.neuron.2013.10.036

Hsu, W. L., Chung, H. W., Wu, C. Y., Wu, H. I., Lee, Y. T., Chen, E. C., … Chang, Y. C. (2015). Glutamate stimulates local protein synthesis in the axons of rat cortical neurons by activating ??-amino-3-hydroxy-5-methyl-4-isoxazolepropionic acid (AMPA) receptors and metabotropic glutamate receptors. *Journal of Biological Chemistry*, *290*(34), 20748–20760. https://doi.org/10.1074/jbc.M115.638023

Hui, E., Bai, J., Wang, P., Sugimori, M., Llinas, R. R., & Chapman, E. R. (2005). Three distinct kinetic groupings of the synaptotagmin family: candidate sensors for rapid and delayed exocytosis. *Proceedings of the National Academy of Sciences of the United States of America*, *102*(14), 5210–4. https://doi.org/10.1073/pnas.0500941102

Hui, E., Gaffaney, J. D., Wang, Z., Johnson, C. P., Evans, C. S., & Chapman, E. R. (2011). Mechanism and function of synaptotagmin-mediated membrane apposition. *Nature Structural & Molecular Biology*, *18*(7), 813–21. https://doi.org/10.1038/nsmb.2075

Inamura, N., Nawa, H., & Takei, N. (2005). Enhancement of translation elongation in neurons by brain-derived neurotrophic factor: Implications for mammalian target of rapamycin signaling. *Journal of Neurochemistry*, *95*(5), 1438–1445. https://doi.org/10.1111/j.1471-4159.2005.03466.x

Jackman, S. L., Turecek, J., Belinsky, J. E., & Regehr, W. G. (2016). The calcium sensor synaptotagmin 7 is required for synaptic facilitation. *Nature*, *529*(7584), 88–91. https://doi.org/10.1038/nature16507

Jackson, M. B., & Chapman, E. R. (2006). Fusion pores and fusion machines in Ca2+-triggered exocytosis. *Annual Review of Biophysics and Biomolecular Structure*, *35*, 135–60. https://doi.org/10.1146/annurev.biophys.35.040405.101958

Jang, Y. S., Lee, M. Y., Choi, S. H., Kim, M. Y., Chin, H., Jeong, S. W., … Kwon, O. J. (2004). Expression of B/K protein in the hippocampus of kainate-induced rat seizure model. *Brain Research*, *999*(2), 203–211. https://doi.org/10.1016/j.brainres.2003.11.047

Jiang, C., Chen, G. (2006). Hi Ca2+-phosphate transfection efficiency in low-density neuronal cultures. Nat Protoc, 1, 695-700.

Ju, W. K., Choi, S. H., Kwon, J. S., Kwon, O. J., Lee, M. Y., Oh, S. J., … Chun, M. H. (2000). Expression of brain/kidney protein in Müller cells of rat retina following transient ischemia. *Neuroscience Letters*, *293*(1), 53–6. Retrieved from http://www.ncbi.nlm.nih.gov/pubmed/11065136

Kaeser-Woo, Y. J., Younts, T. J., Yang, X., Zhou, P., Wu, D., Castillo, P. E., & Südhof, T. C. (2013). Synaptotagmin-12 phosphorylation by cAMP-dependent protein kinase is essential for hippocampal mossy fiber LTP. *The Journal of Neuroscience : The Official Journal of the Society for Neuroscience*, *33*(23), 9769–80. https://doi.org/10.1523/JNEUROSCI.5814-12.2013

Kaeser, P. S., & Regehr, W. G. (2014). Molecular Mechanisms for Synchronous, Asynchronous, and Spontaneous Neurotransmitter Release. *Annual Review of Physiology*, *76*, 333.63. https://doi.org/10.1146/annurev-physiol-021113-170338

Kavalali, E. T. (2015). The mechanisms and functions of spontaneous neurotransmitter release. *Nature Reviews Neuroscience*, *16*(1), 5–16. https://doi.org/10.1038/nrn3875

Kochubey, O., Babai, N., Kochubey, O., Babai, N., & Schneggenburger, R. (2016). A Synaptotagmin Isoform Switch during the Development of an Identified CNS Synapse Article A Synaptotagmin Isoform Switch during the Development of an Identified CNS Synapse. *Neuron*, 984–999. https://doi.org/10.1016/j.neuron.2016.04.038

Kochubey, O., & Schneggenburger, R. (2011). Synaptotagmin increases the dynamic range of synapses by driving Ca^2+-evoked release and by clamping a near-linear remaining Ca^2+ sensor. *Neuron*, *69*(4), 736–48. https://doi.org/10.1016/j.neuron.2011.01.013

Kopec, C. D. (2006). Glutamate Receptor Exocytosis and Spine Enlargement during Chemically Induced Long-Term Potentiation. *Journal of Neuroscience*, *26*(7), 2000–2009. https://doi.org/10.1523/JNEUROSCI.3918-05.2006

Kos, A., Wanke, K. A., Gioio, A., Martens, G. J., Kaplan, B. B., & Aschrafi, A. (2016). Monitoring mRNA Translation in Neuronal Processes Using Fluorescent Non-Canonical Amino Acid Tagging. *Journal of Histochemistry & Cytochemistry*, *64*(5), 323–333. https://doi.org/10.1369/0022155416641604

Kwon, O. J., Gainer, H., Wray, S., & Chin, H. M. (1996). Identification Of a Novel Protein Containing 2 C2 Domains Selectively Expressed In the Rat-Brain and Kidney. *FEBS Letters*, *378*(2), 135–139.

Lai, Y., Lou, X., Diao, J., & Shin, Y. K. (2015). Molecular origins of synaptotagmin 1 activities on vesicle docking and fusion pore opening. *Scientific Reports*, *5*, 38–40. https://doi.org/10.1038/srep09267

Lau, P.-M., & Bi, G.-Q. (2005). Synaptic mechanisms of persistent reverberatory activity in neuronal networks. *Proceedings of the National Academy of Sciences of the United States of America*, *102*(29), 10333–8. https://doi.org/10.1073/pnas.0500717102

Lee, M. Y., Choi, S. H., Shin, S. L., Chin, H., & Kwon, O. J. (2001). Distribution of B/K protein in rat brain. *Cell and Tissue Research*, *303*(1), 47–56. https://doi.org/10.1007/s004410000221

Li, C., Ullrich, B., Zhang, J. Z., Anderson, R. G. W., Brose, N., & Südhof, T. C. (1995). Ca2+-dependent and -independent activities of neural and non-neural synaptotagmins. *Nature*. https://doi.org/10.1038/375594a0

Li, C., Ullrich, B., Zhang, J. Z., Anderson, R. G. W., Brose, N., & Südhof, T. C. (1995). Ca2+-dependent and -independent activities of neural and non-neural synaptotagmins. *Nature*. https://doi.org/10.1038/375594a0

Li, H., Liu, K., Lei, R., Li, Q., Wang, X. X., Wu, Q., … Li, H. (2016). Transferrin Receptor Controls AMPA Receptor Trafficking Efficiency and Synaptic Plasticity. *Scientific Reports*, *6*(February), 1–14. https://doi.org/10.1038/srep21019

Lindholm, D., Korhonen, L., Eriksson, O., & Kõks, S. (2017). Recent Insights into the Role of Unfolded Protein Response in ER Stress in Health and Disease. *Frontiers in Cell and Developmental Biology*, *5*(May), 1–16. https://doi.org/10.3389/fcell.2017.00048

Littleton, J. T., Stern, M., Perin, M., & Bellen, H. J. (1994). Calcium dependence of neurotransmitter release and rate of spontaneous vesicle fusions are altered in Drosophila synaptotagmin mutants. *Proceedings of the National Academy of Sciences of the United States of America*, *91*(23), 10888–92. Retrieved from http://www.pubmedcentral.nih.gov/articlerender.fcgi?artid=45131&tool=pmcentrez&rendertype=abstract

Liu, H., Bai, H., Hui, E., Yang, L., Evans, C. S., Wang, Z., … Chapman, E. R. (2014). Synaptotagmin 7 functions as a Ca 2 + -sensor for synaptic vesicle replenishment. *eLIFE*, *3*(e01524), 1–18. https://doi.org/10.7554/eLife.01524

Liu, H., Bai, H., Xue, R., Takahashi, H., Edwardson, J. M., & Chapman, E. R. (2014). Linker mutations reveal the complexity of synaptotagmin 1 action during synaptic transmission. *Nature Neuroscience*, *17*(5), 670–7. https://doi.org/10.1038/nn.3681

Liu, H., Dean, C., Arthur, C. P., Dong, M., & Chapman, E. R. (2009). Autapses and networks of hippocampal neurons exhibit distinct synaptic transmission phenotypes in the absence of synaptotagmin I. *The Journal of Neuroscience : The Official Journal of the Society for Neuroscience*, *29*(23), 7395–403. https://doi.org/10.1523/JNEUROSCI.1341-09.2009

Lou, F., & Sudhof, T. C. (2017). Synaptotagmin-7-Mediated Asynchronous Release Boosts High-Fidelity Synchronous Transmission at a Central Synapse. *Neuron*, *94*, 826–839. https://doi.org/10.1016/j.neuron.2017.04.020

Luo, F., Bacaj, T., & Südhof, T. C. (2015). Synaptotagmin-7 Is Essential for Ca2+-Triggered Delayed Asynchronous Release But Not for Ca2+-Dependent Vesicle Priming in Retinal Ribbon Synapses. *The Journal of Neuroscience : The Official Journal of the Society for Neuroscience*, *35*(31), 11024–33. https://doi.org/10.1523/JNEUROSCI.0759-15.2015

Mackler, J. M., Drummond, J. A., Loewen, C. A., Robinson, I. M., & Reist, N. E. (2002). The C2B Ca2+-binding motif of synaptotagmin is required for synaptic transmission in vivo. *Nature*, *418*(6895), 340–344. https://doi.org/10.1038/nature00846

Malsam, J., & Söllner, T. H. (2011). Organization of SNAREs within the Golgi stack. *Cold Spring Harbor Perspectives in Biology*, *3*(10), 1–17. https://doi.org/10.1101/cshperspect.a005249

Martinez, I., Chakrabarti, S., Hellevik, T., Morehead, J., Fowler, K., Andrews, N. W., … Biol, N. W. A. J. C. (2000). Synaptotagmin VII Regulates Ca2+-dependent Exocytosis of Lysosomes in Fibroblasts. *The Journal of Cell Biology*, *148*(6), 1141–1149.

Matthew, W. D., Tsavaler, L., & Reichardt, L. F. (1981). Identification of a Synaptic Vesicle-Specific Membrane Protein with a Wide Distribution in Neuronal and Neurosecretory Tissue. *The Journal of Cell Biology*, *91*, 257–69.

Maximov, A., Lao, Y., Li, H., Chen, X., Rizo, J., Sørensen, J. B., & Su, T. C. (2008). Genetic analysis of synaptotagmin-7 function in synaptic vesicle exocytosis. *Proceedings of the National Academy of Sciences*, *105*(10), 3986–3991.

Maximov, A., Shin, O., & Liu, X. (2007). Synaptotagmin-12, a synaptic vesicle phosphoprotein that modulates spontaneous neurotransmitter release. *The Journal of Cell Biology*, *176*(1), 113–124. https://doi.org/10.1083/jcb.200607021

Mohrmann, R., de Wit, H., Connell, E., Pinheiro, P. S., Leese, C., Bruns, D., … Sorensen, J. B. (2013). Synaptotagmin Interaction with SNAP-25 Governs Vesicle Docking, Priming, and Fusion Triggering. *Journal of Neuroscience*, *33*(36), 14417–14430. https://doi.org/10.1523/JNEUROSCI.1236-13.2013

Nagy, G., Kim, J. H., Pang, Z. P., Matti, U., Rettig, J., Su, T. C., & Sørensen, J. B. (2006). Different Effects on Fast Exocytosis Induced by Synaptotagmin 1 and 2 Isoforms and Abundance But Not but Not by Phosphorylation. *The Journal of Neuroscience*, *26*(2), 632–643. https://doi.org/10.1523/JNEUROSCI.2589-05.2006

Newport, J., & Dunphy, W. (1992). Characterization of the membrane binding and fusion events during nuclear envelope assembly using purified components. *Journal of Cell Biology*, *116*(2), 295–306. https://doi.org/10.1091/mbc.E10

Nicoll, R. A. (2017). A Brief History of Long-Term Potentiation. *Neuron*, *93*(2), 281–290. https://doi.org/10.1016/j.neuron.2016.12.015

Nishiki, T., & Augustine, G. J. (2004). Dual roles of the C2B domain of synaptotagmin I in synchronizing Ca2+-dependent neurotransmitter release. *The Journal of Neuroscience : The Official Journal of the Society for Neuroscience*, *24*(39), 8542–50. https://doi.org/10.1523/JNEUROSCI.2545-04.2004

Oñate, M., Catenaccio, A., Martínez, G., Armentano, D., Parsons, G., Kerr, B., … Court, F. A. (2016). Activation of the unfolded protein response promotes axonal regeneration after peripheral nerve injury. *Scientific Reports*, *6*(February), 1–14. https://doi.org/10.1038/srep21709

Oslowski, C. M., & Urano, F. (2011). *Measuring ER stress and the unfolded protein response using mammalian tissue culture system*. *Methods in Enzymology* (1st ed., Vol. 490). Elsevier Inc. https://doi.org/10.1016/B978-0-12-385114-7.00004-0

Padamsey, Z., Mcguinness, L., Bardo, S. J., Hedegaard, A., Hart, M. L., Emptage, N. J., … Emptage, N. J. (2017). Activity-Dependent Exocytosis of Lysosomes Regulates the Structural Plasticity of Dendritic Article Activity-Dependent Exocytosis of Lysosomes Regulates the Structural Plasticity of Dendritic Spines. *Neuron*, *93*(1), 132–146. https://doi.org/10.1016/j.neuron.2016.11.013

Paddock, B. E., Wang, Z., Biela, L. M., Chen, K., Getzy, M. D., Striegel, A., … Reist, N. E. (2011). Membrane Penetration by Synaptotagmin Is Required for Coupling Calcium Binding to Vesicle Fusion In Vivo. *Journal of Neuroscience*, *31*(6), 2248–2257. https://doi.org/10.1523/JNEUROSCI.3153-09.2011

Pang, Z. P., Melicoff, E., Padgett, D., Liu, Y., Teich, A. F., Dickey, B. F., … Su, T. C. (2006). Synaptotagmin-2 Is Essential for Survival and Contributes to Ca 2+ Triggering of Neurotransmitter Release in Central and Neuromuscular Synapses. *The Jounal of Neuroscience*, *26*(52), 13493–13504. https://doi.org/10.1523/JNEUROSCI.3519-06.2006

Passafaro, M., Nakagawa, T., Sala, C., & Sheng, M. (2003). Induction of dendritic spines by an extracellular domain of AMPA receptor subunit GluR2. *Nature*, *424*(6949), 677–681. https://doi.org/10.1038/nature01781

Perin, M., Fried, V. A., Mignery, G. A., Jahn, R., & Sudhof, T. C. (1990). Phospholipid binding by a synaptic vesicle protein homologous to the regulatory region of protein kinase C. *Nature*, *345*, 260–3.

Poskanzer, K. E., Marek, K. W., Sweeny, S. T., & David, G. W. (2003). Synaptotagmin I is necessary for compensatory synaptic vesicle endocytosis in vivo. *Nature*, *426*(December), 559–563. https://doi.org/10.1038/nature02157.1.

Praschberger, R., Lowe, S. A., Malintan, N. T., Giachello, C. N. G., Patel, N., Houlden, H., … Jepson, J. E. C. (2017). Mutations in Membrin/GOSR2 Reveal Stringent Secretory Pathway Demands of Dendritic Growth and Synaptic Integrity. *Cell Reports*, *21*(1), 97–109. https://doi.org/10.1016/j.celrep.2017.09.004

Rangaraju, V., tom Dieck, S., & Schuman, E. M. (2017). Local translation in neuronal compartments: how local is local? *EMBO Reports*, *18*(5), 693–711. https://doi.org/10.15252/embr.201744045

Rhee, J.-S., Li, L. Y., Shin, O.-H., Rah, J.-C., Rizo, J., Südhof, T. C., & Rosenmund, C. (2005). Augmenting neurotransmitter release by enhancing the apparent Ca2+ affinity of synaptotagmin 1. *Proceedings of the National Academy of Sciences of the United States of America*, *102*(51), 18664–9. https://doi.org/10.1073/pnas.0509153102

Rosenmund, C., & Stevens, C. F. (1996). Definition of the readily releasable pool of vesicles at hippocampal synapses. *Neuron*, *16*(6), 1197–207. Retrieved from http://www.ncbi.nlm.nih.gov/pubmed/8663996

Rumpel, E., & Behrends, J. C. (1999). Sr2+ -dependent asynchronous evoked transmission at rat striatal inhibitory synapses in vitro. *The Journal of Physiology*, *514*(2), 447–458. https://doi.org/10.1111/j.1469-7793.1999.447ae.x

Schneider-Poetsch, T., Ju, J., Eyler, D. E., Dang, Y., Bhat, S., Merrick, W. C., … Liu, J. O. (2010). Inhibition of eukaryotic translation elongation by cycloheximide and lactimidomycin. *Nature Chemical Biology*, *6*(3), 209–217. https://doi.org/10.1038/nchembio.304

Schneider, C. A., Rasband, W. S., & Eliceiri, K. W. (2012). NIH Image to ImageJ: 25 years of image analysis. *Nature Methods*, *9*(7), 671–675. https://doi.org/10.1038/nmeth.2089

Sharma, K., Schmitt, S., Bergner, C. G., Tyanova, S., Kannaiyan, N., Manrique-Hoyos, N., … Simons, M. (2015). Cell type- and brain region-resolved mouse brain proteome. *Nature Neuroscience*, *18*(12), 1819–1831. https://doi.org/10.1038/nn.4160

Sheng, Z. H., Yokoyama, C. T., & Catterall, W. A. (1997). Interaction of the synprint site of N-type Ca2+ channels with the C2B domain of synaptotagmin I. *Proceedings of the National Academy of Sciences*, *94*(10), 5405–5410. https://doi.org/10.1073/pnas.94.10.5405

Shin, O.-H., Rhee, J.-S., Tang, J., Sugita, S., Rosenmund, C., & Südhof, T. C. (2003). Sr2+ binding to the Ca2+ binding site of the synaptotagmin 1 C2B domain triggers fast exocytosis without stimulating SNARE interactions. *Neuron*, *37*(1), 99–108. Retrieved from http://www.ncbi.nlm.nih.gov/pubmed/12526776

Skarnes, W. C., Rosen, B., West, A. P., Koutsourakis, M., Bushell, W., Iyer, V., … Bradley, A. (2011). A conditional knockout resource for the genome-wide study of mouse gene function. *Nature*, *474*(7351), 337–344. https://doi.org/10.1038/nature10163

Sommeijer, J., & Levelt, C. N. (2012). Synaptotagmin-2 Is a Reliable Marker for Parvalbumin Positive Inhibitory Boutons in the Mouse Visual Cortex. *PLOS One*, *7*(4), 1–12. https://doi.org/10.1371/journal.pone.0035323

Steinha, C., Mittelsteadt, T., Seifert, G., Alva, E., Becker, A. J., & Schoch, S. (2009). Differential mRNA Expression Patterns of the Synaptotagmin Gene Family in the Rodent Brain. *The Journal of Comparative Neurology*, *528*(October 2008), 514–528. https://doi.org/10.1002/cne.21908

Takahashi, M., Kovalchuk, Y., & Attwell, D. (1995). Pre- and postsynaptic determinants of EPSC waveform at cerebellar climbing fiber and parallel fiber to Purkinje cell synapses. *Journal of Neuroscience*, *15*(8), 5693–5702.

Taschenberger, H., & von Gersdorff, H. (2000). Fine-tuning an auditory synapse for speed and fidelity: developmental changes in presynaptic waveform, EPSC kinetics, and synaptic plasticity. *The Journal of Neuroscience : The Official Journal of the Society for Neuroscience*, *20*(24), 9162–9173. https://doi.org/20/24/9162 [pii]

Trimbuch, T., & Rosenmund, C. (2016). Should I stop or should I go? The role of complexin in neurotransmitter release. *Nature Reviews Neuroscience*, *17*(2), 118–125. https://doi.org/10.1038/nrn.2015.16

Tucker, W. C., Weber, T., & Chapman, E. R. (2004). Reconstitution of Ca2+-regulated membrane fusion by synaptotagmin and SNAREs. *Science*, *304*(5669), 435–8. https://doi.org/10.1126/science.1097196

Turecek, J., Jackman, S. L., & Regehr, W. G. (2017). Synaptotagmin 7 confers frequency invariance onto specialized depressing synapses. *Nature*, *551*, 503–6. https://doi.org/10.1038/nature24474

Wall, M. J., Robert, A., Howe, J. R., & Usowicz, M. M. (2002). The speeding of EPSC kinetics during maturation of a central synapse. *European Journal of Neuroscience*, *15*(5), 785–797. https://doi.org/10.1046/j.1460-9568.2002.01910.x

Wang, C. T., Grishanin, R., Earles, C. a, Chang, P. Y., Martin, T. F., Chapman, E. R., & Jackson, M. B. (2001). Synaptotagmin modulation of fusion pore kinetics in regulated exocytosis of dense-core vesicles. *Science*, *294*(5544), 1111–5. https://doi.org/10.1126/science.1064002

Wang, C., Wang, Y., Hu, M., Chai, Z., Wu, Q., Huang, R., … Zhou, Z. (2016). Synaptotagmin-11 inhibits clathrin-mediated and bulk endocytosis. *EMBO Reports*, *17*(1), 47–63.

Wang, K., Zhang, H., Ma, D., Bucan, M., Glessner, J. T., Abrahams, B. S., … Hakonarson, H. (2009). Common genetic variants on 5p14.1 associate with autism spectrum disorders. *Nature*, *459*(7246), 528–533. https://doi.org/10.1038/nature07999

Weber, J. P., Toft-bertelsen, T. L., Mohrmann, R., & Delgado-, I. (2014). Synaptotagmin-7 Is an Asynchronous Calcium Sensor for Synaptic Transmission in Neurons Expressing SNAP-23. *PLOS One*, *9*(11), 1–22. https://doi.org/10.1371/journal.pone.0114033

Wen, H., Linhoff, M. W., Mcginley, M. J., Li, G., Corson, G. M., Mandel, G., & Brehm, P. (2010). Distinct roles for two synaptotagmin isoforms in synchronous and asynchronous transmitter release at zebra fi sh neuromuscular junction. *Proceedings of the National Academy of Sciences*, *107*(31), 13906–11. https://doi.org/10.1073/pnas.1008598107/-/DCSupplemental.www.pnas.org/cgi/doi/10.1073/pnas.1008598107

Williams, L. E., & Featherstone, D. E. (2014). Regulation of Hippocampal Synaptic Strength by Glial xCT. *Journal of Neuroscience*, *34*(48), 16093–16102. https://doi.org/10.1523/JNEUROSCI.1267-14.2014

Wong, Y., Lee, C., Xie, W., Cui, B., & Poo, M. (2015). Activity-dependent BDNF release via endocytic pathways is regulated by synaptotagmin-6 and complexin. *Proceedings of the National Academy of Sciences*, 4475–4484. https://doi.org/10.1073/pnas.1511830112

Xu-Friedman, M., & Regehr, W. G. (2000). Probing fundamental aspects of synaptic transmission with strontium. *The Journal of Neuroscience : The Official Journal of the Society for Neuroscience*, *20*(12), 4414–22. Retrieved from http://www.ncbi.nlm.nih.gov/pubmed/10844010

Xu, J., Mashimo, T., & Su, T. C. (2007). Synaptotagmin-1, -2, and -9: Ca2+ Sensor for Fast Release that Specify Distinct Presynaptic Properties in Subsets of Neurons. *Neuron*, *54*, 567–581. https://doi.org/10.1016/j.neuron.2007.05.004

Xu, J., Pang, Z. P., Shin, O.-H., & Südhof, T. C. (2009). Synaptotagmin-1 functions as a Ca2+ sensor for spontaneous release. *Nature Neuroscience*, *12*(6), 759–66. https://doi.org/10.1038/nn.2320

Xue, M., Craig, T. K., Shin, O.-H., Li, L., Brautigam, C. a, Tomchick, D. R., … Rizo, J. (2010). Structural and mutational analysis of functional differentiation between

synaptotagmins-1 and -7. *PloS One*, *5*(9), 1–12. https://doi.org/10.1371/journal.pone.0012544

Yao, J., Gaffaney, J. D., Kwon, S. E., & Chapman, E. R. (2011). Doc2 is a Ca2+ sensor required for asynchronous neurotransmitter release. *Cell*, *147*(3), 666–77. https://doi.org/10.1016/j.cell.2011.09.046

Yao, J., Gaffaney, J. D., Kwon, S. E., & Chapman, E. R. (2011). Doc2 is a Ca 2+ sensor required for asynchronous neurotransmitter release. *Cell*, *147*(3), 666–677. https://doi.org/10.1016/j.cell.2011.09.046

Yao, J., Kwon, S. E., Gaffaney, J. D., Dunning, F. M., & Chapman, E. R. (2012). Uncoupling the roles of synaptotagmin i during endo-and exocytosis of synaptic vesicles. *Nature Neuroscience*, *15*(2), 243–249. https://doi.org/10.1038/nn.3013

Yeh, F. L., Dong, M., Yao, J., Tepp, W. H., Lin, G., Johnson, E. A., & Chapman, E. R. (2010). SV2 mediates entry of tetanus neurotoxin into central neurons. *PLoS Pathogens*, *6*(11). https://doi.org/10.1371/journal.ppat.1001207

Yeo, H., Mo, J., Lee, D., Han, S., Hong, S., Koh, M. J., … Lee, H. W. (2012). Developmental expression and subcellular distribution of synaptotagmin 11 in rat hippocampus. *Neuroscience*, *225*, 35–43. https://doi.org/10.1016/j.neuroscience.2012.08.062

Young, S. M., & Neher, E. (2009). Synaptotagmin has an essential function in synaptic vesicle positioning for synchronous release in addition to its role as a calcium sensor. *Neuron*, *63*(4), 482–96. https://doi.org/10.1016/j.neuron.2009.07.028

Zhang, X., Kim-Miller, M. J., Fukuda, M., Kowalchyk, J. a, & Martin, T. F. (2002). Ca 2+ -dependent synaptotagmin binding to SNAP-25 is essential for Ca 2+ -triggered exocytosis. *Neuron*, *34*(4), 599–611. https://doi.org/10.1016/S0896-6273(02)00671-2